REACTOR MATERIALS

A Quarterly Technical Progress Review

Prepared for DIVISION OF TECHNICAL INFORMATION, U. S. ATOMIC ENERGY COMMISSION,
by BATTELLE MEMORIAL INSTITUTE, COLUMBUS LABORATORIES

RECEIVED
APR 6 1970
THE JOHN CRERAR LIBRARY

Spring 1970

● VOLUME 13

● NUMBER 1

Nuclear Science Abstracts

The U. S. Atomic Energy Commission, Division of Technical Information, publishes *Nuclear Science Abstracts (NSA)*, a semimonthly journal containing abstracts of the literature of nuclear science and engineering.

NSA covers (1) research reports of the U. S. Atomic Energy Commission and its contractors; (2) research reports of government agencies, universities, and industrial research organizations on a worldwide basis; and (3) translations, patents, books, and articles appearing in technical and scientific journals.

Complete indexes covering subject, author, source, and report number are included in each issue. These indexes are cumulated and sold separately.

Availability of NSA

SALE *NSA* is available on subscription from the Superintendent of Documents, U. S. Government Printing Office, Washington, D. C. 20402, at $42.00 per year for the semimonthly abstract issues and $38.00 per year for the cumulated-index issues. Subscriptions are postpaid within the United States, Canada, Mexico, and all Central and South American countries, except Argentina, Brazil, Guyana, French Guiana, Surinam, and British Honduras. Subscribers in these Central and South American countries, and in all other countries throughout the world, should remit $52.50 per year for subscriptions to semimonthly abstract issues and $47.50 per year for the cumulated-index issues. The single-copy price for the abstract issues is $1.75 postpaid, with this exception: Add one-fourth of $1.75 for mailing to the countries to which the $52.50 subscription rate applies.

EXCHANGE *NSA* is also available on an exchange basis to universities, research institutions, industrial firms, and publishers of scientific information. Inquiries should be directed to the Division of Technical Information Extension, U. S. Atomic Energy Commission, P. O. Box 62, Oak Ridge, Tennessee 37830.

REACTOR MATERIALS

Vol. 13, No. 1 Spring 1970

Contents

Metallurgy of Common Cladding Materials (Section I)	Light Metals	1
	Zirconium and Zirconium Alloys	1
	Stainless Steels	7
	Superalloys	9
	Ferritic Steels	10
Metallurgy of Refractory Metals (Section II)	Tungsten and Rhenium Metal and Alloys	14
	Properties and Metallurgy of Niobium and Tantalum Alloys	15
	Properties of Chromium	16
	Literature Review	17
Diffusion Studies (Section III)	Solid-State Diffusion	18
	Diffusion of Gases in Solids	19
Radiation Effects in Structural Materials (Section IV)	Zirconium and Zirconium Alloys	21
	Stainless Steels and Superalloys	23
	Pressure-Vessel Steels	30
	Effects of Radiation on Miscellaneous Materials	31
	Basic Mechanisms of Radiation Damage in Nonfuel Materials	32
Nonfueled Refractories (Section V)	Transition-Metal Carbides	39
	Silicon Carbide	39
	Cermets	40
	Zirconium Dioxide	40
Concrete (Section VI)	Creep of Concrete	42
	Radioactivity in Concretes	42
Corrosion of Base-Metal Alloys in Aqueous and Gaseous Media (Section VII)	Corrosion of Zirconium Alloys	44
	Corrosion of Stainless Steels	44
	Corrosion of Nickel Alloys	45
	Corrosion of Magnesium Alloys	45
	Corrosion of Copper Alloys	46
Corrosion of Refractory Metals in Aqueous and Gaseous Media (Section VIII)	Corrosion of Uncoated Refractory Metals	47
	Protection of Refractory Metals by Coating	47

Corrosion by Liquid Metals and Fused Salts (Section IX)

Sodium 49
Corrosion in Rankine-Cycle Space Power Systems 53
Corrosion by Lithium 54
Corrosion by Lead–Bismuth Alloys . . . 54
Corrosion by Molten Uranium Alloys . . . 55
Liquid-Metal Corrosion Mechanisms . . . 55
Corrosion by Fused Salts 56

Cladding Behavior in Loss-of-Coolant Accidents (Section X) 59

Superintendent of Documents, U. S. Government Printing Office, Washington, D. C. 20402, $2.50 per year

Reactor Materials

is one of a series of nuclear science and technology progress reviews being published under the auspices of the USAEC Division of Technical Information. About 35 specialists from the staff of the Columbus Laboratories of Battelle Memorial Institute prepare topical reviews periodically from worldwide literature. *Reactor Materials* covers properties, behavior, and fabrication processes of materials applicable to nuclear reactor components and associated equipment.

The authors and editors attempt to combine the highlights of significant new developments into a concise summary for both management and the technical specialist. Generally, enough of the results are presented to define the research and summarize the findings. For readers desiring more detailed information on any particular topic, the coverage is documented by references at the end of each section.

This issue marks the start of our 13th year of publication. Unfortunately, we are at the same time faced with a significantly reduced budget. Continuity will be maintained, but the specific subjects covered will vary from issue to issue. The previous issue dealt with fuel and fertile materials, moderator and control materials, and special fabrication techniques. This issue treats properties, corrosion, and radiation effects in cladding and structural materials.

E. M. Simons
D. L. Keller

BATTELLE MEMORIAL INSTITUTE
COLUMBUS LABORATORIES

Issued quarterly by the U. S. Atomic Energy Commission. Use of funds for printing this publication approved by the Director of the Bureau of the Budget on May 12, 1969.

TECHNICAL PROGRESS REVIEWS

The United States Atomic Energy Commission publishes the Technical Progress Reviews to meet the needs of industry and government for concise summaries of current nuclear developments. Each journal digests and evaluates the latest findings in a specific area of nuclear technology and science. *Nuclear Safety* is a bimonthly journal; the other three are quarterly journals.

Isotopes and Radiation Technology
P. S. Baker, A. F. Rupp, and associates
Isotopes Information Center, Oak Ridge National Laboratory

Nuclear Safety
Wm. B. Cottrell, W. H. Jordan, J. P. Blakely, and associates
Nuclear Safety Information Center, Oak Ridge National Laboratory

Reactor Technology

Reactor Materials (Publication will be discontinued with Vol. 13, No. 3)
E. M. Simons and associates
Battelle Memorial Institute, Columbus Laboratories

All are available from the U. S. Government Printing Office. See the back cover for ordering instructions.

The views expressed in this publication do not necessarily represent those of the United States Atomic Energy Commission, its divisions or offices, or of any Commission advisory committee or contractor.

Availability of Reports Cited in This Review

United States Atomic Energy Commission (USAEC) reports are available at USAEC depository libraries and are sold by the Clearinghouse for Federal Scientific and Technical Information (CFSTI), National Bureau of Standards, U. S. Department of Commerce, Springfield, Va. 22151. All reports sold by CFSTI are $3.00 for printed copy and $0.65 for microfiche. Each separately bound part of a report is priced as a separate report. Some reports may not be available because of their preliminary nature; however, the information contained in them will generally be found in later progress or topical reports on the subject.

Other U. S. Government agency reports identified in this journal generally are available from CFSTI.

Private-organization reports should be requested from the originator.

United Kingdom Atomic Energy Authority (UKAEA) and Atomic Energy of Canada Limited (AECL) reports are available at USAEC depository libraries. UKAEA reports are sold by Her Majesty's Stationery Office, London; AECL reports are sold by the Scientific Document Distribution Office, Atomic Energy of Canada Limited, Chalk River, Ontario, Canada. UKAEA and AECL reports issued after March 1, 1967, are sold by CFSTI to purchasers in the United States and its territories.

Section

I

Reactor Materials

Metallurgy of Common Cladding Materials

By M. Kangilaski

LIGHT METALS

In a study of the effect of cyclic thermal treatments on the structural stability of an Al–3 Mg alloy,[1] tubular specimens were subjected to thermal fatigue tests and thermal treatments at 420°C for times up to 5000 hr. The alloy proved to have good stability, and its tensile properties at room temperature and 400°C were found to be unaffected by the thermal cycling.

A two-part summary report[2] on the mechanical properties of Al–Al_2O_3 dispersions has been issued by Euratom. The report discusses the effects of fabrication variables and Al_2O_3 content on the tensile and creep properties of the material at temperatures up to 600°C.

A French patent[3] has been issued for a fuel-element can that is composed of a magnesium alloy containing 0.15 to 0.8 (preferably 0.5) wt.% zirconium and 1 to 5 (preferably 1.3 to 1.7) wt.% lead, the remainder being magnesium. The creep resistance of the alloy may be improved by adding zinc or cerium in an amount less than 0.5 wt.%. Traces of manganese in the range 100 to 200 ppM by weight may be added to improve the elastic properties of the alloy. The can may be provided with an outer layer consisting of a highly corrosion-resistant magnesium alloy containing about 0.5 wt.% zirconium.

Soviet investigators have issued a volume[4] on binary, ternary, and quaternary phase diagrams. Of special interest to reactor developers are the diagrams that are based on aluminum, magnesium, and zirconium. Most of these new phase diagrams involve rare-earth metals.

ZIRCONIUM AND ZIRCONIUM ALLOYS

A study was made[5] to delineate the dislocation mechanisms that control prismatic slip in hexagonal close packed (hcp) zirconium at low temperatures. Specimens were single crystals of zirconium containing approximately 150 ppM of interstitial impurities so the results could be compared with those reported in the literature for both higher and lower impurity concentrations. The thermal component of the critical shear stress, τ^*, and the activation volume, v^*, were measured. A single, thermally activated dislocation process was found to control the initiation of prismatic slip at temperatures below 450°K. At low temperatures, τ^* is intermediate to values reported for higher and lower impurity levels, confirming the operation of an impurity-controlled mechanism. The variation of τ^* with concentration, the temperature dependence of τ^*, the stress dependence of activation energy, and the stress dependence of v^* are all in agreement with Fleischer's theory of strengthening by the interaction of dislocations with tetragonal lattice distortions caused by interstitial atoms.

The habit planes of zirconium hydride platelets in zirconium were studied[6] using zirconium single crystals. In agreement with previous findings, it was found that hydrides lie primarily in the $\{10\bar{1}0\}$ habit planes. However, it was determined that the secondary habit plane of zirconium hydride in zirconium is $\{10\bar{1}7\}$.

The yielding characteristics of the two-phase Zr–H alloys were investigated.[7] Discontinuous yielding was observed in fine-grained (0.006 mm) pure zirconium at room temperature, the upper yield strength and magnitude of yield drop being higher for material pulled transverse to the rolling direction (as contrasted to parallel). Progressive increases in hydrogen content resulted in decreases in the upper yield strength. Air cooling of specimens from the hydriding temperature was found to be more effective than furnace cooling in lowering the upper yield strength (for equivalent hydrogen contents). This finding was attributed to a larger number of small hydride precipitates resulting from air cooling and a smaller number of large hydride particles resulting from furnace cooling because of the lower cooling rate. The hydride particles are believed to reduce the upper yield strength by acting as preferential nucleation centers for preyield plastic regions.

The solubility of carbon in beta zirconium, as determined by workers at Ames Laboratory,[8] is given in Table I-1.

Table I-1 Solubility of Carbon in Beta Zirconium[8]

Temperature °C	Carbon concentration, ppM
1180	400
1320	700
1390	1000
1780	3000
>1800	7500

Two different types of burst tests were utilized[9] on Zircaloy-2 tubes with an outside diameter of 0.53 in. and a wall thickness of 31 mils. In one test (method A), the tube is burst by forcing liquid into it with compressed air. In the other test (method B), the possibilities of storing elastic energy in the fluid were minimized and a rod was placed inside the tube to prevent it from bending during the burst test. It was found that method B yielded circumferential ductilities that were almost twice those obtained by method A. The improved ductilities are attributed mainly to the elimination of bending in method B. Bending causes inhomogeneous deformation and consequent localized failure. With homogeneous deformation, high ductilities are obtained because the strain-hardening capacity of the material around the whole circumference is utilized.

Tensile specimens from many lots of Zircaloy tubing were found[10] to deform to cross-sectional shapes that are polyhedral rather than circular. The formation of a noncircular cross section seems to result from a circumferential variation in plastic properties, which probably stems from differences in texture. X-ray diffraction intensities from (0001), $\{10\bar{1}0\}$, $\{11\bar{2}0\}$, and $\{10\bar{1}1\}$ planes parallel to the tubing surface were measured around the entire circumference of various tubes. If the tube deformed to a circular cross section, then the diffraction intensity varied less than 5% around the whole circumference. Greater intensity variations were obtained for all tubes that developed noncircular cross sections during deformation.

The crack growth rate in Zircaloy-2 was found[11] to follow the power law

$$da/dN = C_1 (\Delta K)^n$$

where da/dN = crack growth rate, in./cycle

ΔK = stress-intensity factor range, lb/in.$^{3/2}$, where K depends on the applied stress field and flaw size

C_1, n = constants for a given material and operating conditions

The room-temperature crack-propagation rates in variously treated specimens of Zircaloy-2 are compared in Fig. I-1. Note that the rate of crack propagation is lowest for annealed material and is increased by cold work. Hydrogen seems to have little effect, except at very large ranges of the stress-intensity factor K.

It has been found at Bettis[12] that some redistribution of alloying elements occurs in Zircaloy-2 when it is cooled slowly from the alpha-plus-beta and beta regions. Tin was found to concentrate in the alpha grains formed during cooling. The grain boundaries were found to be depleted in tin and enriched in iron, chromium, and nickel.

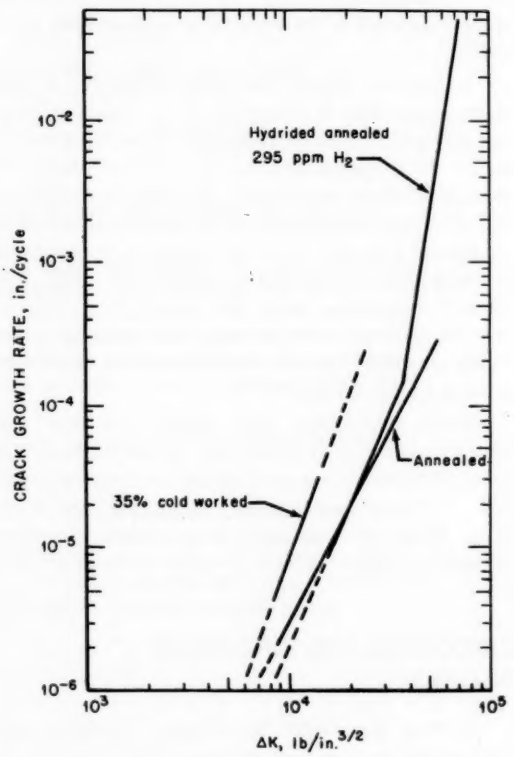

Fig. I-1 Rate of crack growth in Zircaloy-2 at room temperature.[11]

Increasing the amount of hydrogen or hydride in Zircaloy-2 leads to a decrease in its ductility, which normally becomes drastic at some elevated hydrogen content. Transmission-electron-microscope (TEM) observations of cracks in thin foils of Zircaloy-2 containing hydride particles showed[13] that the fracture process is one of linking up satellite cracks in the hydride phase in front of the tip of the main crack. Semiquantitative observations of the width of the zone of high stress and strain in front of a crack were made on a partly cracked tube of hydrided Zircaloy-2. When the tube was stressed so that the crack was opened up slightly, the shape of the zone of high stress and strain was what might be expected from normal fracture-mechanics concepts. Furthermore, its width was found to correspond to the zone where the hydride platelets were cracked. The observations corroborate the idea that the hydrogen-induced drop in ductility occurs when the distance between the hydride particles equals the range of strain that is critical for cracking of the hydride in front of an advancing crack.

The effects of hydrogen and stress-oriented hydrides on the tensile properties of Zircaloy-2 with varying texture were investigated in India.[14] Tensile specimens were prepared from flattened Zircaloy-2 tubes and from extruded rods. All the specimens had a grain size of 15 μ and were hydrided to 250 ppM hydrogen. Their room-temperature tensile properties are given in Table I-2. Stress orientation is accompanied by reductions in ductility and tensile strength. This loss is drastic for samples that have a high basal-pole density along the stress axis, which suggests that stress activates those habit planes that are favorably oriented. Reduction in ductility in all samples after stress orientation (irrespective of texture) shows that hydrides precipitate on many habit planes. After stress orientation, only those habit planes that are favorably oriented come into prominence. Hence the possibility of a single invariable habit plane in all kinds of samples under all conditions is not confirmed. Microscopic observations on fracture specimens suggest that intragranular hydrides may be playing a minor role in reducing the ductility.

The kinetics of hydride precipitation in Zircaloy-2 during aging were investigated by the Japanese[15] using a resistometric method. Two distinct stages were found in the process of hydride precipitation. During the first stage the precipitates grew in the form of platelets whose dimensions were small in comparison with their spacing. The second stage consisted of thickening of the hydride precipitates that had grown during the first stage.

A comprehensive report on the current state of the art of zirconium alloys has been issued by the Canadians.[16] This report discusses the corrosion behavior, mechanical properties, and effects of irradiation

Table I-2 Tensile Properties of As-Received and Hydrided Zircaloy-2 Tubing[14]

Specimen	Treatment	Yield strength (0.2% offset), ksi	Ultimate tensile strength, ksi	Total elongation, %
Tubing, circumferential	As received	65	85	28
	Hydrided*	62.5	78	19.5
	Hydrided and stress oriented	54.5	62	12.5
Tubing, longitudinal	As received	61	78	26
	Hydrided	59.2	77.5	18.4
	Hydrided and stress oriented	59.0	71.0	14.4
Rod, longitudinal	As received	65.5	74.4	24
	Hydrided	62.8	71.0	17.5
	Hydrided and stress oriented	59.5	70.0	15.6
Rod, transverse	As received	67	77	20
	Hydrided	54.6	59.0	12.5
	Hydrided and stress oriented	37.25	39	4.4

*Hydrogen content for all samples was maintained around 250 ppM.

on those properties. The alloys discussed include: Zr–2.5 Nb, Ozhennite 0.5, Zr–1 Nb, and Zr–3 Nb–1 Sn. The discussion centers around water-reactor applications at 300°C, although some mention is made of properties in 400°C steam. Attempts are presently under way at Chalk River to develop zirconium-base alloys for pressure-tube application at 450°C which will have higher strength than the presently used Zr–2.5 Nb (Ref. 17). Both solid solution and precipitation hardening are utilized to obtain the maximum increase in strength. Figure I-2 illustrates the increased

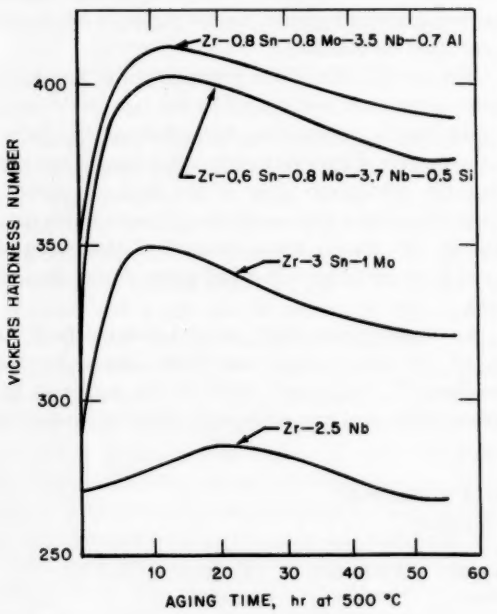

Fig. I-2 Age hardening of beta-quenched complex zirconium alloys.[17]

hardness that can be achieved by using various alloying additions. Some preliminary results of creep and tensile tests are presented in Fig. I-3 and Table I-3, respectively. It appears that an alloy which will undergo limited creep for a stress of 10 to 12 ksi at 450°C can be developed, but this alloy will have a neutron-capture cross section that is about 10% higher than that of Zircaloy-2. The alloy additions that will be used will probably fall in the following ranges, by wt.%: 2 to 4 Sn, 0.5 to 1.5 Mo, 0.5 to 2.0 Nb, 0.5 to 1.5 Al, and 0.5 Si. Most of these alloys showed rapid overaging when the quenched material was aged at 550°C. However, only limited overaging occurred as a result of aging at

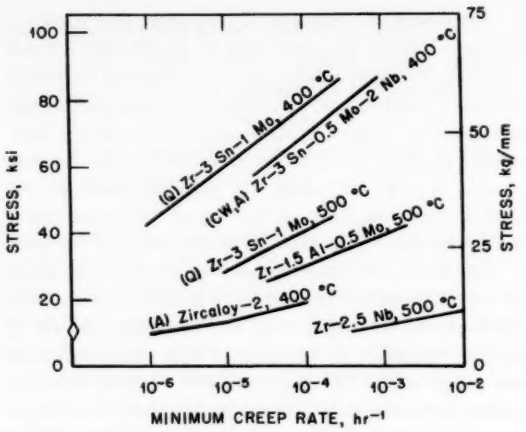

Fig. I-3 Stress dependence of minimum creep rates for complex zirconium alloys.[17] Q = quenched and aged; CW = cold worked; A = annealed; ◇ = target at 450°C.

450°C. The improved properties of the Zr–3 Sn–1 Mo are attributed to (1) solution-hardening effects of tin, (2) precipitation-hardening effects of $ZrMo_2$ and Zr_4Sn, and (3) the martensitic structure.

The $\beta \rightarrow \alpha$ transformation in Zr–V alloys was studied by the Germans[18] using hardness measurements, metallography, and X-ray diffraction. They found that the martensitic transformation is suppressed when the amount of vanadium exceeds about 3 wt.%. However, when the alloy content is higher, the beta phase cannot be quenched completely, and some beta transforms to the metastable omega-prime phase. This omega-prime phase decomposes during subsequent aging into $\alpha + ZrV_2$, and the retained beta phase transforms to the "aged" omega phase.

The effect of chromium content on the hardness of Zr–Cr alloys following aging at various temperatures has been studied in Canada.[19] As can be seen in Fig. I-4, the hardness increases with chromium content for all of the aging temperatures. The terminal solubility of hydrogen in Zr–2 at.% Cr–0.16 at.% Fe in the 250 to 415°C temperature range was found by the British[20] to be about the same as in Zircaloys.

A U. S. patent[21] has been issued for a zirconium-base alloy having a high resistance to hydrogen absorption and low susceptibility to hydrogen embrittlement. The alloy consists essentially of zirconium with 1.5 to 1.7 at.% copper and 0.35 to 0.55 at.% iron. Additional improvement in corrosion resistance of the alloy can be achieved by treating, working, and fabricating it at temperatures below 765°C.

Table I-3 Tensile Properties of Complex Zirconium Alloys[17]

Alloy, wt.%	Condition	Test temp., °C	Yield strength (0.2% offset), ksi	Ultimate strength, ksi	Uniform elongation, %	Total elongation, %	Reduction in area, %
Zr–3 Sn–0.4 Mo	24 hr at 500°C*	20	129.9	149.3	4.8	11	46
		400	90.0	103.0	3.9	11.4	56
Zr–3 Sn–0.4 Mo	24 hr at 500°C†	20	144.2	164.2	4.0	5	12
		400	104.5	116.4	2.4	9	53
Zr–2 Nb–1 V	24 hr at 400°C*	20	134.3	154.6	3	5.4	18
		400	92.5	104.2	2.2	11.2	67
	24 hr at 500°C†	20	140.3				
		400	97.0	107.8	2.4	12	73
Zr–1.5 Al–0.5 Mo	‡	20	123	147	2	10	58
		400	91	119	2	10	72
Zr–3 Sn–0.5 Mo–2 Nb	24 hr at 500°	20	128	138		12	
		400	82	90		12	
Zr–3 Sn–0.8 Mo–3.5 Nb–0.7 Al	6 hr at 525°C	20	220	220		1	
		400	133	143		1	
Zr–3 Sn–0.8 Mo–3.7 Nb–0.7 Si	6 hr at 525°C	20	212	224		1	
		450	136	144		1	
Zr–2.5 Nb	24 hr at 500°C	20	113	120	4	10	25
		400	73	81	3		
Zircaloy-2	15% cold-worked	20	71.3	86.2	8.3	13	
		400	40.6	44	1.8	9.5	

*Quenched from 950°C.
†Quenched from 1050°C.
‡Quenched from 900°C.

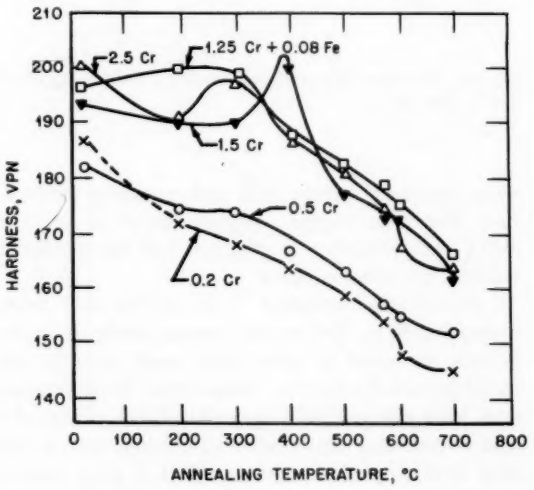

Fig. I-4 Response of Zr–Cr alloys to heat-treatment.[19] All alloys were cold worked 20% and annealed for 30 min at indicated temperature.

A British patent[22] has been issued for a method of treating a zirconium alloy containing 0.5 to 5 wt.% niobium, 0.005 to 1 wt.% beryllium, and optionally one or more of the elements Sn, Cu, Fe, Cr, Mo, V, W, Ta, Ni, Y, Sb, and Te, with a total alloying addition of no more than 10 wt.%. The alloy is suitable for use in reactor structural materials that are exposed to pressurized water, boiling water, or CO_2. The treatment consists of heating at ~50°C below the upper critical temperature for 15 min to 2 hr, quenching to produce a fine-grained martensitic structure, cold working 15 to 30%, aging at 500 to 600°C for 10 to 30 hr, and further cold working.

Factors affecting the strength of Zr–Nb alloys have been investigated by the British.[23] The effects of oxygen content, niobium content, and cold work on tensile strength are illustrated in Figs. I-5 to I-7. Aging studies were performed on the material at temperatures ranging from 300 to 450°C. It was found that maximum hardness was obtained by annealing at 350°C to precipitate a phase containing niobium. Minimum creep rates at 300°C, shown in Fig. I-8 illustrate the superior creep resistance of Zr–2.5 Nb over Zircaloy-2, especially at high stresses. Some

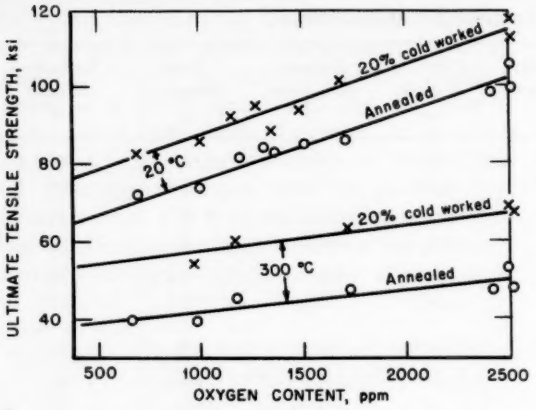

Fig. I-5 Effect of oxygen content on tensile strength of Zr–2.6 Nb alloy[23] at 20 and 300°C.

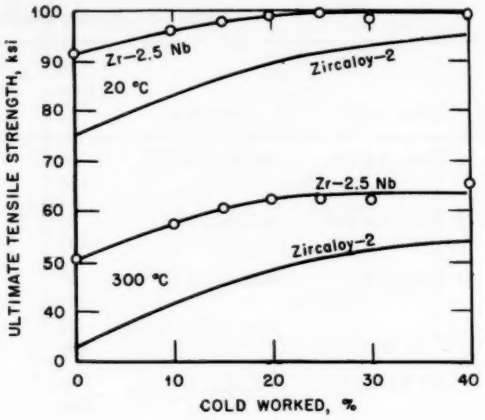

Fig. I-7 Effect of cold work on tensile strength of Zr–2.5 Nb and Zircaloy-2 at 20 and 300°C (Ref. 23).

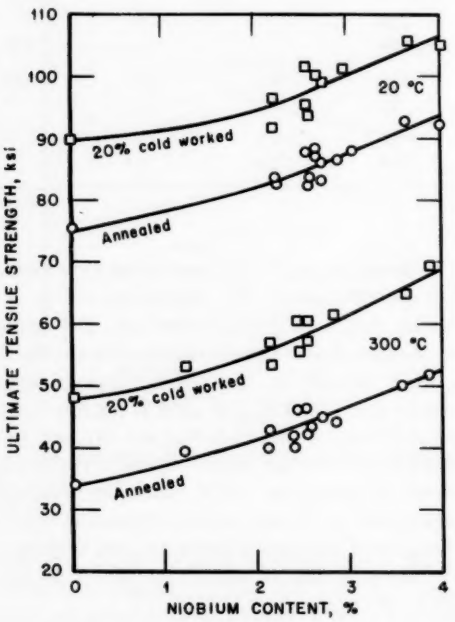

Fig. I-6 Effect of niobium content on tensile strength of Zr–Nb alloys (corrected to 1500 ppM oxygen) at 20 and 300°C (Ref. 23).

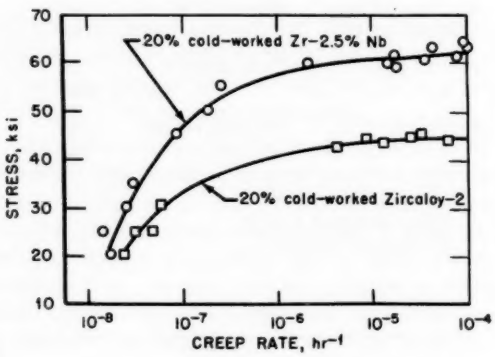

Fig. I-8 Minimum creep rates of Zircaloy-2 and Zr–2.5 Nb at 300°C (Ref. 23).

stress-rupture properties of Zr–2.5 Nb pressure tubes at 300 and 400°C, determined by Battelle–Northwest,[24] are summarized in Fig. I-9.

Figure I-10 shows the results of a Canadian investigation[25] of the stress-rupture properties of Zr–2.5 Nb pressure tubes. Rupture ductility increased with increasing rupture time and increasing temperature. The stress to give a rupture life of 30 years at 300°C was predicted as 49.2 ksi, and the predicted strain at fracture was 21%.

At Battelle–Northwest,[26] Zr–2.5 Nb alloy tubes were fatigued in the tension–tension mode by cyclic internal pressures to cause axial crack growth and unstable fractures at room temperature. Pressure-cycle rates were 400 and 3000 cycles/hr. Tubes in both the cold-worked and heat-treated conditions, before and after hydriding (200 to 300 ppM H_2), were investigated. From short-length (less than or equal to tube-wall thickness) defects, fatigue-crack initiation and growth occurred at nominal peak hoop stresses equal to or less than the estimated endurance limit (about

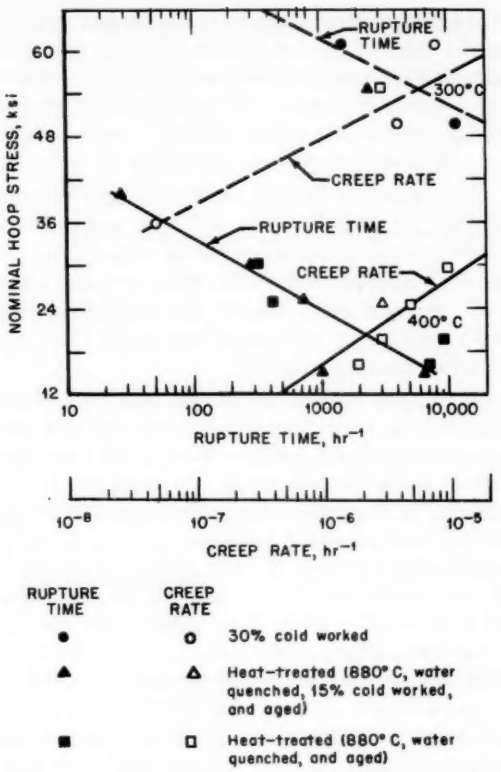

Fig. I-9 Creep-rupture data for Zr–2.5 Nb alloy pressure tubing.[24]

25 ksi). Fatigue cracks that initiated at the outer-diameter surface had a semicircular crack front. The number of stress cycles required to initiate fatigue cracking at the surface was inversely proportional to the square of the surface-defect length.

Neutron irradiation at an estimated flux of 10^{12} neutrons/(cm^2)(sec) and a fluence estimated at 10^{20} neutrons/cm^2 appeared to have little or no effect on the crack-propagation characteristics of Zr–2.5 Nb alloy tubing in the 30% cold-worked condition. When 30% cold-worked tubing is hydrided (200 to 300 ppM) and irradiated, the fracture toughness appears to decrease by about 50% or more. More data, particularly at higher fluxes and fluences, are needed to verify and quantify neutron-irradiation effects.

STAINLESS STEELS

Two articles from the United Kingdom[27,28] discuss the tensile and impact properties of stainless steels, with emphasis on the austenitics and some coverage of duplex stainless steels. Quantitative effects of various strengthening mechanisms such as grain size, twinning frequency, delta ferrite content, and solid-solution strengthening by both interstitial and substitutional solutes are described. The effects of martensite in the initial structure and that formed during straining on the tensile properties of the steel are treated. The martensitic transformation is especially important in governing impact properties at lower temperatures.

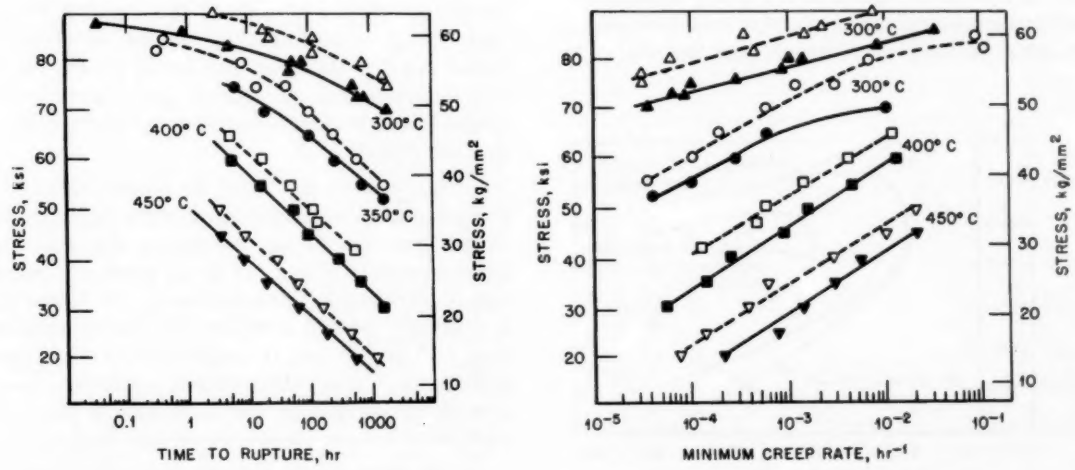

Fig. I-10 Creep-rupture properties[25] of Zr–2.5 Nb alloy extruded, heat-treated at 880°C, water quenched, cold drawn as indicated, and aged 24 hr at 500°C. Open points: cold drawn 10.9% in one pass; closed points: cold drawn 15.9% in three passes.

To study the effect of test temperature and strair rate on the fracture mode of 304 stainless steel, workers at Argonne[29] ran tensile tests at 22, 450, 550, 650, and 750°C at strain rates of 1, 10, 100, and 1000%/min. It was found that fracture occurs transgranularly at all strain rates up to 100%/min and at temperatures below 550°C. At these strain rates, evidence of intergranular fracture begins to appear at about 550°C, and at 750°C the fracture is completely intergranular. At the highest strain rate of 1000%/min, evidence of intergranular fracture does not appear until 650°C, and at 750°C the fracture is entirely intergranular. In all cases a true uniform strain of 15% was obtained at the transition from transgranular to intergranular fracture.

The effects of carbon additions on the creep-rupture characteristics of 304 and 316 stainless steels were investigated by the Japanese.[30] They found that the maximum 1000-hr creep strength for 316 stainless steel at 600°C was obtained with a carbon content of 0.3 wt.%. Maximum hardening on heating in the range 450 to 1150°C occurred in steels with about 0.2 wt.% carbon. The presence of molybdenum in both 304 and 316 stainless steels enhanced the strengthening effects. The peak creep-rupture strength is associated with solid-solution strengthening and precipitation of the carbide particles.

In a study by Westinghouse,[31] the response of different heats of 316 stainless steel to carbide precipitation was investigated. Figure I-11 illustrates a typical time–temperature–precipitation diagram for a specific heat of material. Significant variations in carbide-precipitation behavior were found to exist from lot to lot. Small amounts of cold work decreased the aging time necessary to precipitate $M_{23}C_6$ but had no effect on the types of precipitates formed. The products of aging appear to be dependent on the solution temperature and time before aging. If the solution temperature is high, then $M_{23}C_6$ and intermetallic compounds are more likely to form on subsequent aging.

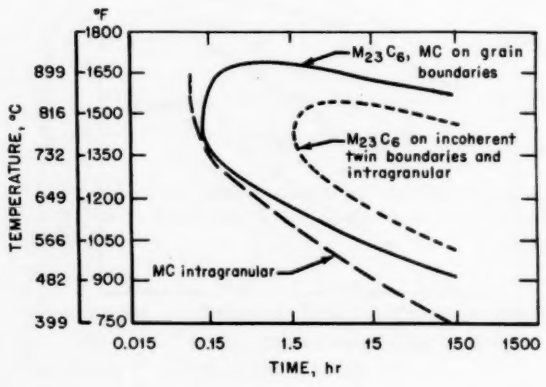

Fig. I-11 Time–temperature–precipitation diagram for 316 stainless steel.[31]

The American Society for Testing and Materials (ASTM) has issued a report[32] that evaluates the tensile, creep, and rupture properties of 304, 316, 321, and 347 stainless steels. This report provides statistically averaged data where all the material variables like composition, fabrication, and amount of cold work have been separated out.

In fatigue testing of stainless steel at elevated temperatures, it has been found[33] that the hold time between cycles (time specimen is held at the prescribed strain) has a marked effect on fatigue life. For example, for 0.3% plastic-strain cycling at 650°C, 304 stainless steel withstood five times as many cycles to failure with a hold time of 1 min as with a hold time of 30 min. The adverse effect of long hold time on fatigue life is believed to result from creep of the material during the holding period. In fact, a plot of the tensile stress against total hold time (number of cycles to failure × length of hold time) yields a curve that essentially coincides with the steady-state stress-rupture curve for the same stainless steel at the same temperature.

A new relation for predicting fatigue life at elevated temperature has been developed by workers at General Electric.[34] The Berling–Conway relation shows a straight line when plastic-strain range is plotted against N_f/f, where N_f is the number of cycles to failure and f is the strain rate during testing. Figure I-12 illustrates that the relation gives a good fit for fatigue life of 304 stainless steel at room temperature, 425, and 650°C.

It has been found[35] that the fatigue life of 316 stainless steel at elevated temperatures is dependent on oxygen pressure. As can be seen in Fig. I-13, the high-temperature fatigue life is not sensitive to either high or low oxygen pressures. However, the fatigue life is drastically reduced as the oxygen pressure increases from 10^{-4} to 10^{-1} torr. It is suggested that this oxygen dependence occurs when fatigue cracks are being covered by oxygen at the same rate as they are produced.

Cyclic-strain fatigue tests have been performed by Westinghouse[36] on 12-mil-wall 316-stainless-steel tubing in air at 650°C. Preliminary results indicate that the fatigue life of this tubing is about an order of

magnitude lower than the fatigue life of solid specimens for the same strain range.

The susceptibility of the following austenitic stainless steels and nickel-base alloys to hydrogen embrittlement has been investigated:[37] Fe–18 Cr–11 Ni, Fe–18 Cr–14 Ni, Fe–20 Cr–25 Ni, Fe–20 Cr–35 Ni, and Fe–16 Cr–75 Ni. Notched specimens were tested in tension at −100 to 200°C after being charged with hydrogen. The only alloys that exhibited embrittlement were the low-nickel alloy 18 Cr–11 Ni and the high-nickel alloy 16 Cr–75 Ni. Sharp microcracks were found in the embrittled alloys after fracture. These cracks were preferentially formed in the twin boundaries of the austenite.

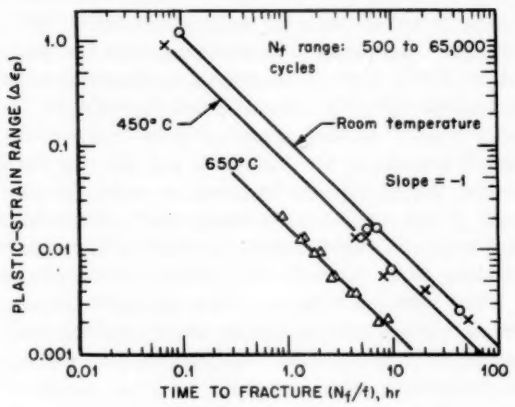

Fig. I-12 Plastic-strain range vs. N_f/f for 316 stainless steel at a strain rate[34] of 4×10^{-3} sec^{-1}.

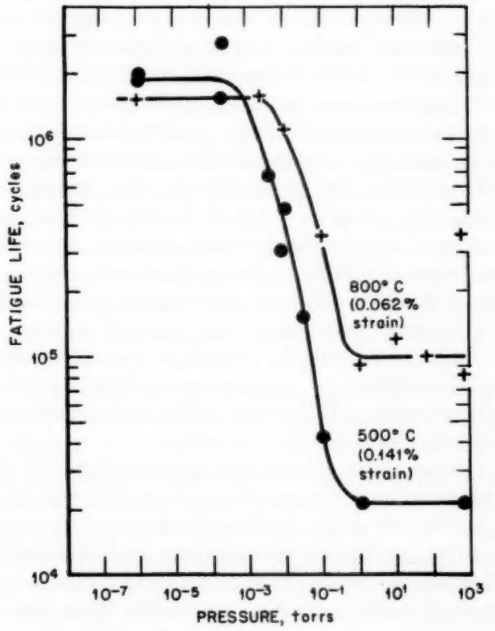

Fig. I-13 Effect of oxygen pressure on fatigue life of 316 stainless steel[35] at 500°C and 800°C.

SUPERALLOYS

In a study[38] of the effect of cold work before solution annealing (8 hr at 1080°C) on the mechanical properties of Nimonic 80A, it was found that excessive grain growth occurred if the amount of prior cold work was in the 0.5 to 2% range. The general stability and consistency of properties of the alloy are improved when it is cold rolled less than 8%. The tensile and creep properties are affected by the amount of cold work before annealing, since the final grain size is very sensitive to the amount of cold work. Figure I-14 shows the effect of grain size on the creep-rupture properties of Nimonic 80A at 750°C with a stress of 34,000 psi.

Twelve nickel-base superalloys were examined[39] utilizing microscopy and residue-analysis techniques to identify and determine the relative stability for long times (up to 5000 hr) of gamma prime and the minor phases in the 750 to 1150°C temperature range. The materials studied included seven cast alloys (IN-100, B-1900, Inco-713C, MAR-M200, MAR-M246, TRW-NASA IVY, and TRW-NASA VIA) and five wrought alloys (U-700, René 41, Inconel 718, Waspaloy, and Unitemp AF2-1D). Seven minor phases

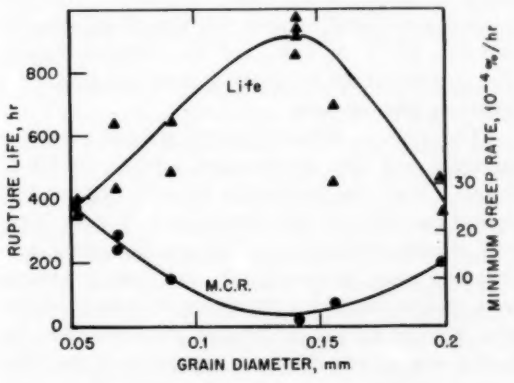

Fig. I-14 Effect of grain diameter on creep-rupture properties of Nimonic 80A at 750°C under 34 ksi stress.[38]

were identified: MC, $M_{23}C_6$, M_6C, M_3B_2, sigma, mu, and Ni_3Nb. The MC phase was found in all 12 alloys; $M_{23}C_6$ in all alloys except TRW-NASA IVY and Inconel 718; M_6C in B-1900, MAR-M200, MAR-M246, TRW-NASA VIA, René 41, and Unitemp AF2-1D; M_3B_2 in B-1900, Inco-713C, MAR-M200, MAR-M246, TRW-NASA IVY, TRW-NASA VIA, and U-700; sigma in IN-100, Inco-713C, U-700, René 41, and Inconel 718; mu in René 41 and Unitemp AF2-1D; and Ni_3Nb in Inconel 718. Complete solutioning of gamma prime did not occur in the seven cast alloys even at the highest exposure temperature studied, 1150°C. Complete solutioning of gamma prime occurred for the wrought alloys in the following temperature ranges: 980 to 1040°C for Waspaloy, 1040 to 1095°C for René 41, and 1095 to 1150°C for U-700 and Unitemp AF2-1D. Inconel 718 was an exception, in that gamma prime was not present at any of the temperatures studied after the long exposure times.

The effect of tungsten additions on the stability of precipitation-hardened nickel-base alloys at 850°C was investigated by Havalda in Czechoslovakia.[40] It was found that increasing the tungsten content resulted in retardation of transformation of the f_{cc} gamma prime (Ni_3Ti) to the hexagonal eta phase (Ni_3Ti). Therefore the loss of strength due to overaging occurs after longer times in alloys with higher tungsten contents. Increasing the tungsten content was also found to accelerate the Cr_7C_3-to-$Cr_{23}C_6$ transformation, provided that the Ti/Al atomic ratio was less than 1.

The influence of tungsten additions on the morphology of gamma prime in Ni–20 Cr alloys, with various Ti/Al ratios, was also studied by Havalda.[41] He found that increasing the tungsten content changes the particle morphology from cubic to spheroidal, especially in alloys having high Ti/Al ratios. No clear relation was found between the size of precipitating particles, the Ti/Al ratio, and the tungsten content. The quantity of the precipitating phase was greater at a higher tungsten content.

The effect of high-temperature aging on the microstructure and the precipitation kinetics of HS-25 (L-605) alloy was studied in Japan[42] by means of optical and electron microscopy, as well as by X-ray and electron-diffraction techniques. Specimens subjected to aging, stress rupture, and creep conditions were used to establish a correlation between precipitation phenomena and mechanical properties. The following seven kinds of phases precipitate in the alloy during aging: M_7C_3, $M_{23}C_6$, M_6C, α-Co_3W, β-Co_3W, Laves-Co_2W, and μ-Co_7W_6. The processes of precipitation are proposed as follows: $(M_7C_3) \rightarrow M_{23}C_6 \rightarrow M_6C \rightarrow (\alpha\text{-}Co_3W) \rightarrow \beta\text{-}Co_3W \rightarrow$ Laves-$Co_2W \rightarrow \mu$-Co_7W_6 at about 800°C, and $(M_7C_3) \rightarrow M_{23}C_6 \rightarrow M_6C \rightarrow (\alpha\text{-}Co_3W) \rightarrow \beta\text{-}Co_3W) \rightarrow$ Laves-Co_2W at about 700°C, where the phases parenthesized are considered to be metastable. In these processes the precipitation of α-Co_3W (ordered fcc), which is coherent to the matrix and transforms to β-Co_3W (ordered hexagonal) after aging for a long time, plays an important role in strengthening the alloy at temperatures below 700°C. On the other hand, age hardening at temperatures above 800°C is attributed mainly to the precipitation of carbides ($M_{23}C_6$ and M_6C) and Laves-Co_2W. The alloy is also hardened considerably by cold working, which introduces stacking faults and the hcp phase within the matrix. Furthermore, on aging the cold-worked specimen at lower temperatures, the carbides and α- and β-Co_3W precipitate preferentially on either stacking faults or in the hcp phase, causing a more marked subsequent age hardening. At higher temperatures, however, the disappearance of stacking faults and the recrystallization of the matrix result in softening of the alloy.

FERRITIC STEELS

A study was undertaken by the Japanese[43] to develop a ferritic steel that would not undergo losses in carbon when the ferritic steel was used together with an austenitic stainless steel in a sodium loop. Specimens of 2.25 Cr–1 Mo steel were alloyed with niobium, titanium, or tungsten and given different heat-treatments. Each sample was explosively welded to an austenitic stainless steel and heated in sodium at 600 to 700°C for 24 to 250 hr. After heating, the change in carbon content of the ferritic steel was measured, and tensile and creep fracture tests were performed at 550°C. It was found that the 2.25 Cr–1 Mo steel with a 1.0 to 1.5 wt.% niobium addition did not undergo any carbon loss, and its mechanical properties were markedly better than those of the alloy without niobium. It was concluded that this steel looks most promising for the tubes of the steam generator in a sodium-cooled fast breeder reactor.

An extensive program has been completed by the English Electric Company[44] to optimize the creep properties of large Cr–Mo–V steam-turbine rotor forgings. Improved creep properties were obtained by adjusting the composition so that upper bainite was obtained during quenching, and a fine dispersion of vanadium carbide was produced. The ideal alloy for rotors (Fe–0.25 C–0.25 Si–0.70 Mn–0.70 Ni–0.80 Cr–0.70 Mo–0.35 V) showed creep rates at 550°C as

small as one-tenth those of the preoptimized alloy under stresses of 10 to 20 ksi.

The plane-strain fracture toughness of ASTM A-533B, Class 1 steel was measured by Battelle–Northwest,[45] using double-cantilever-beam specimens. It was established that the K_{Ic} values increased as the specimen thickness was increased from 0.5 to 2.0 in. The plane-strain fracture toughness was 25 to 30% higher in specimens taken from the surface of 12-in.-thick A-533B quenched-and-tempered plate than in specimens from the interior.

Representative samples of 5 Ni–Cr–Mo–V steel in the product forms of plate and weld metal were investigated by the Naval Research Laboratory[46] with respect to fracture-toughness characterization features provided by the dynamic tear (DT) and Charpy V-notch (C_v) tests. The intrinsic fracture-propagation features were defined by the energy–temperature relations obtained with the DT test. The fracture modes of both base metal and weld metal as defined by the DT test demonstrated sharp changes in fracture toughness with test temperature. In contrast, the fracture modes of the C_v test remained essentially unchanged, and the energy curves had shallow, poorly defined slopes as shown in Fig. I-15. Therefore it is concluded that the DT test provides a better basis than regular impact tests for establishing the transition temperatures.

The effect of longtime heat-treatments on the mechanical properties of A-302B steel was determined by the Japanese.[47] Blocks of the steel were heated for 1000 hr at 300, 350, and 400°C, after which specimens were machined from the blocks. These specimens were tested in impact, fatigue, tension, and hardness at room temperature, 300, and 400°C. The longtime heat-treatments caused reductions in elongation as measured by tension tests, and the impact strength was reduced. However, significant improvements in fatigue occurred, with the largest improvement resulting from aging at 400°C.

The tempering characteristics of A-302B steel have also been studied by the Japanese.[48] It was found that tempering of quenched steel at 650°C for 1 hr resulted in the highest impact and strength properties. The normalized and tempered material exhibited the highest elongation values. However, in stress-relieving thick plates of A-302B steel, it was found[49] that deterioration of mechanical properties resulted from tempering at 625°C. This was attributed to spheroidizing and growth of complex carbides.

The effects of thermal cycling on the mechanical properties of A-302B, 18-8 stainless steels, and carbon

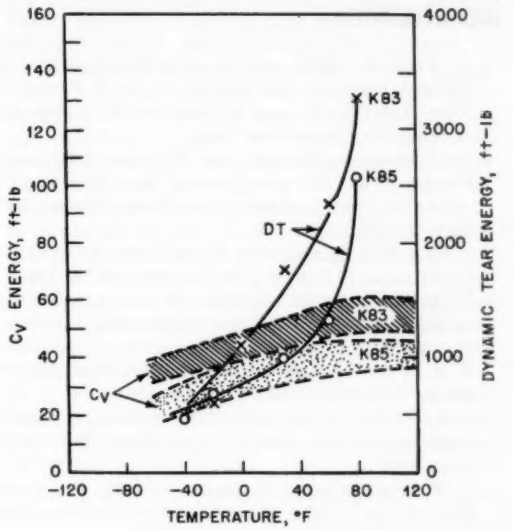

Fig. I-15 Dynamic tear (DT) and Charpy V energy–temperature relations for two 5 Ni–Cr–Mo–V weld metals.[46]

steels were investigated.[50] The temperature cycles utilized were 100 ⇌ 400°C, 400 ⇌ 700°C, and 100 ⇌ 900°C. It was found that cycling at 400 ⇌ 700°C and 100 ⇌ 900°C resulted in increases in elongation at fracture in subsequent tensile tests. The elongation resulting from thermal cycling increased with increasing number of cycles. Hardness showed a peak after 10 to 30 cycles and then diminished with continuing thermal cycling. The tensile strength declined, and the ratio of the yield stress to the tensile strength showed a rising trend with thermal cycling. In the 100 ⇌ 900°C tests, the amount of the initially precipitated ferrite increased with increasing number of cycles, and coarsening of the carbide particles was observed.

Fatigue-crack growth rates were determined at room temperature for ASTM A-302B and A-508, Class 2 steels in two characteristic plate and forging directions.[51] Tests were performed under zero-to-tension cyclic loading using both through-crack and part-through-crack specimens. Crack growth rates in the through-crack specimens, although affected by plate or forging directions, were found to correlate well upon the hypothesis that the crack extension per cycle is proportional to a positive power of the range of alternating-stress-intensity factor. In addition, the rate of crack extension through the plate thickness of the surface-crack specimens was successfully correlated with data from through-crack specimens.

REFERENCES

1. G. Beghi, B. Henry, and M. Nasi, Examination of the Thermal Resistance and Stability of Al–3 Percent Mg Alloy Tubes for Nuclear Applications (in Italian), *Met. Ital.*, 60: 883-890 (October 1968).
2. D. J. Boerman, M. Grin, and M. Veaux, Mechanical Properties of Al–Al_2O_3 Composites, Report EUR-4074e(Pts. 1 and 2), Joint Nuclear Research Center, Ispra, Italy, Nov. 29, 1968.
3. Nuclear Fuel Element Can, French Patent 1,511,641, to Commissariat à l'Energie Atomique, filed Dec. 20, 1966.
4. E. M. Savitskii (Ed.), *Diagrammy Sostoyaniya Metallischeskikh Sistem* (in Russian), published by Izdatel'stvo, Moscow, 1968.
5. E. D. Levine, Prismatic Slip in Zirconium, *Trans. Jap. Inst. Metals*, 9: 832-836 (1968).
6. C. Roy and J. G. Jacques, $\{10\bar{1}7\}$ Hydride Habit Planes in Single Crystal Zirconium, *J. Nucl. Mater*, 31: 233-237 (June 1969).
7. D. V. Edmonds and C. J. Beevers, Influence of a Second Phase on the Yielding Characteristics of Zirconium, *Met. Sci. J.*, 2: 228-232 (November 1968).
8. O. N. Carlson and F. A. Schmidt, Reactor Materials Development, Quarterly Report, April–June 1969, USAEC Report IS-RD-18, Ames Laboratory, June 1969.
9. O. K. Kallstrom, Closed End Burst Testing of Zircaloy Canning Tubes, *J. Nucl. Mater.*, 31: 111-113 (May 1969).
10. D. O. Hobson and P. L. Rittenhouse, Nonhomogeneous Deformation in Zircaloy Tubing, *Trans. AIME, Met. Soc.*, 245: 797-800 (April 1969).
11. L. A. James, Crack Propagation Behavior of Zircaloy-2, *Nucl. Appl.*, 6(4): 307-312 (April 1969).
12. R. F. Gessner, Effect of Thermal Treatment on the Alloy Distribution of Zircaloy-2, USAEC Report WAPD-TM-818, Westinghouse Electric Corp., Bettis Atomic Power Laboratory, March 1969.
13. G. Oestberg, Crack Propagation in Hydrided Zircaloy-2, *Int. J. Fracture Mech.*, 4: 95-99 (June 1968).
14. T. K. Sinha and V. S. Arunachalam, Influence of Texture on the Mechanical Properties of Zircaloy-2 Containing Stress-Oriented Hydrides, Indian Report BARC-367, 1968.
15. Y. Sasaki and H. Kimura, Resistometric Study of Hydride Precipitation in Zircaloy-2 (in Japanese), *Suiyokaishi*, 16: 462-465 (October 1968).
16. J. Boulton, Current Knowledge of Zirconium Alloys for Reactor Usage, Canadian Report AECL-3365, June 1969.
17. W. R. Thomas, Prospects for Zirconium Structural Alloys at High Temperatures, Canadian Report AECL-3362, May 1969.
18. W. Lehmann, Transformation Characteristics of a Zr–4 Wt.% Alloy, German Report BMwF-FBK-68-61, December 1968.
19. AECL progress report, unpublished, January–March 1969.
20. C. F. Slattery, The Terminal Solubility of Hydrogen in the Zirconium-2 At.% Chromium–0.16 At.% Iron Alloy, *J. Nucl. Mater.*, 32: 30-38 (August 1969).
21. C. N. Lovell, Zirconium-Base Alloy, U. S. Patent 3,431,104, to USAEC, Mar. 4, 1969.
22. Zirconium Base Alloys, British Patent 1,145,931, to Atomic Energy of Canada Limited, Mar. 19, 1969.
23. R. A. Murgatroyd and J. Winton, the Strength of Zr–$2\frac{1}{2}$ Percent Nb Alloy in the Annealed and Cold-Worked Condition, British TRG-Report-1786, Oct. 22, 1968.
24. P. J. Pankaskie, Creep of Zr–2.5 Wt.% Nb Alloy Pressure Tubes, USAEC Report BNWL-1077, Battelle–Northwest, June 1969.
25. E. F. Ibrahim, The Stress-Rupture Properties of Heat-Treated Zirconium–2.5 Percent Niobium Alloy, Canadian Report AECL-3361, May 1969.
26. P. J. Pankaskie, Fatigue Crack Growth and Propagation in Zr–2.5 Wt.% Nb Alloy Pressure Tubing, USAEC Report BNWL-1076, Battelle–Northwest, June 1969.
27. J. Irvine, T. Gladman, and F. B. Pickering, The Strength of Austenitic Stainless Steel, *J. Iron Steel Inst. (London)*, 207: 1017-1028 (July 1969).
28. G. P. Sanderson and D. T. Llewellyn, Mechanical Properties of Standard Austenitic Stainless Steels in the Temperature Range –196 to 800°C, *J. Iron Steel Inst. (London)*, 207: 1129-1140 (August 1969).
29. Argonne National Laboratory, Reactor Development Program, Progress Report, January 1969, USAEC Report ANL-7548, Feb. 28, 1969.
30. R. Yoda and H. Yoshida, Study on the Stainless Steels for Fast Reactors. 2. On the Creep Fatigue Strengths of Austenitic Steels of 304 and 316 Series with Different Carbon Concentrations (in Japanese), *Tetsu To Hagane*, 54: 289 (August 1968).
31. W. E. Ray, Stainless Steel Cladding Development, Quarterly Progress Report for Period Ending March 31, 1969, USAEC Report WARD-3791-35, Westinghouse Electric Corp., Advanced Reactors Division, May 1969.
32. G. V. Smith, An Evaluation of the Yield, Tensile, Creep and Rupture Strengths of Wrought 304, 316, 321, and 347 Stainless Steel at Elevated Temperatures, Report DS-5S2, American Society for Testing and Materials, February 1969.
33. General Electric Company, Missile and Space Division, AEC Fuels and Materials Development Program Progress Report No. 78, USAEC Report GEMP-1010, Dec. 31, 1968.
34. J. T. Berling and J. B. Conway, A Proposed Method for Predicting the Low-Cycle Fatigue Behavior of 304 and 316 Stainless Steel, *Trans. AIME, Met. Soc.*, 245(5): 1137-1140 (May 1969).
35. H. H. Smith, P. Shahinian, and M. R. Achter, Fatigue Crack Growth Rates in Type 316 Stainless Steel at Elevated Temperature as a Function of Oxygen Pressure, *Trans. AIME, Met. Soc.*, 245(5): 947-953 (May 1969).
36. W. E. Ray, Stainless Steel Cladding Development, Quarterly Progress Report for Period Ending June 30, 1969, USAEC Report WARD-3791-41, Westinghouse Electric Corp., Advanced Reactors Division, August 1969.
37. R. Lagneburg, Hydrogen Embrittlement in Austenitic Steels and Nickel-Base Alloys, *J. Iron Steel Inst. (London)*, 207: 363-366 (March 1969).
38. C. H. White, The Effect of Cold Work on the Grain Size and Properties of Nimonic Alloy 80A, *J. Inst. Metals*, 97: 215-220 (July 1969).
39. H. E. Collins, Relative Long-Time Stability of Carbide and Intermetallic Phases in Nickel-Base Superalloys, *Amer. Soc. Metals, Trans. Quart.*, 62: 82-104 (March 1969).

40. A. Havalda, Effect of Tungsten on Phase Transformation in Nickel-Base Alloys (in Czech), *Kovove Mater.*, **5**: 483-495 (1967).
41. A. Havalda, Effect of Tungsten on the Morphology of the Gamma-Prime Precipitate in Nickel-Base Alloys (in Czech), *Kovove Mater.*, **6**: 201-205 (1968).
42. N. Yukawa and K. Sato, Correlation Between Microstructure and Stress Rupture Properties of a Co–Cr–Ni–W (HS-25) Alloy, *Trans. Jap. Inst. Metals*, **9**: 680-686 (1968).
43. S. Yamamoto and T. Onishi, Study on Steel Tubes for Steam Generator of Fast Breeder Reactor (in Japanese), *Tetsu to Hagane*, **54**: 284 (August 1968).
44. J. F. Norton and A. Strang, Improvement of Creep and Rupture Properties of Large 1% Cr–Mo–V Steam-Turbine Rotor Forgings, *J. Iron Steel Inst. (London)*, **207**: 193-203 (February 1969).
45. T. T. Claudson, J. A. Williams, and J. A. DeMastry, Fracture Toughness of Irradiated and Unirradiated Heavy Section Pressure Vessel Material, USAEC Report BNWL-SA-1992, Battelle–Northwest, July 15, 1968.
46. R. W. Judy, Jr., P. P. Puzak, and E. A. Lange, Characterization of Fracture Toughness of 5 Ni–Cr–Mo–V Steel by Charpy V-Notch and Dynamic Tear Tests, USAEC Report NRL-6873, Naval Research Laboratory, Dec. 13, 1968.
47. M. Hasegawa and M. Sano, Study on the Steel for Pressure Vessel of Nuclear Reactor 2. The Effect of Many Hours Heating on Low Cycle Fatigue of A-302B Steel (in Japanese), *Tetsu To Hagane*, **54**: 210 (August 1968).
48. S. Nagashima and N. Mori, Tempering Characteristics of ASTM A-302B Steel for Atomic Pile Use (in Japanese), *Seitetsu Kenkya*, **258**: 7331-7342 (March 1967).
49. H. Gondo and M. Sato, Mechanical Properties of A-302B Plate for Nuclear Reactors (in Japanese), *Seitetsu Kenkyu*, **258**: 7343-7350 (March 1967).
50. M. Hasegawa and M. Sano, The Study on the Steels for Pressure Vessel of Nuclear Reactor. III. The Effect of Thermal Cycles on A-302B Steel (in Japanese), *Tetsu To Hagane*, **54**(10): 211 (August 1968).
51. D. F. Mowbray, W. R. Andrews, and A. J. Brothers, Fatigue-Crack Growth-Rate Studies of Low-Alloy Pressure-Vessel Steels, *J. Eng. Ind.*, **90**: 648-655 (November 1968).

Section II

Reactor Materials

Metallurgy of Refractory Metals

By J. H. Peterson

TUNGSTEN AND RHENIUM METAL AND ALLOYS

Properties of W–Re–Hf–C alloys were evaluated by NASA[1] to determine whether previously observed high-temperature strengthening effects of HfC in tungsten could be combined with the low-temperature ductilizing effect of dilute rhenium additions to tungsten. The general conclusion from this study was that these two effects can be combined without detrimental interaction. The optimum alloy, W–4 at.% Re–0.35 at.% Hf–0.35 at.% C, was found to have a tensile strength of 60 to 70 ksi at 3500°F (1955°C), Fig. II-1,

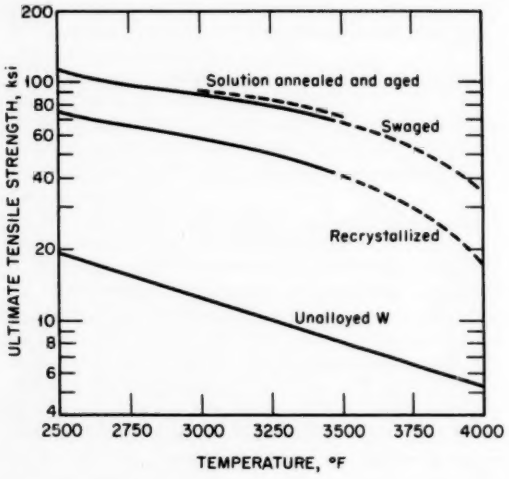

Fig. II-1 Tensile strength of optimum alloy composition W–4 Re–0.35 Hf–0.35 C (at.%) compared with strength of unalloyed tungsten at 2500 to 4000°F (Ref. 1).

and bend ductile-to-brittle transition temperatures of 200 and 540°F (95 and 285°C), Fig. II-2, in the as-rolled and solution-annealed conditions, respectively. The strength increment associated with HfC particles was found to be proportional to the square root of the mole % of HfC and to decrease with

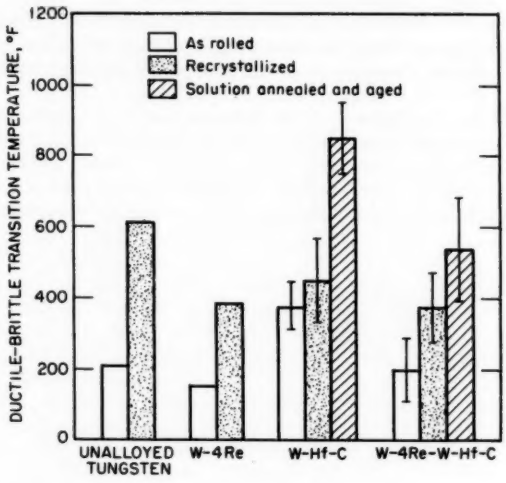

Fig. II-2 Ductile–brittle transition temperatures for arc-melted tungsten, W–4 Re, W–Hf–C (Ref. 1).

increasing HfC particle size, in accordance with recent dispersion-strengthening theory (Orowan mechanism). Growth of HfC particles was fairly rapid above 3500°F, limiting this alloy to short-time use at these temperatures. Calculations indicated that particle stability and high strengths should be maintained at lower temperatures for hundreds to thousands of hours.

Effects of the addition of 0.5 vol.% ThO_2 on the grain structure and texture of heavily rolled tungsten sheet were studied at the Research and Development Center of General Electric Company.[2] Powder-metallurgy ingots were rolled to sheet, 0.001 in. thick, and samples were annealed at temperatures from 1200 to 2500°C. The heating rate to the annealing temperature was varied from 3 to 6500°C/min. Orientations of the largest grains were determined by X-ray diffraction. Disposition and loss of the ThO_2 particles were determined by electron transmission microscopy, and the activation energy for removal of the thorium was measured by mass spectroscopy. Heating rates below about 800°C/min produced large, highly elongated

grains. Higher heating rates produced much smaller, less elongated grains. The grain structure and texture of the slowly heated samples were identical to the structures and textures of heavily rolled tungsten foil conventionally doped with aluminum, silicon, and potassium; but the recrystallization temperature for the thoria-doped material (about 1800°C) was about 200°C lower, even though the conventionally doped material contains a lower density of particles. There was stringerlike dispersion of larger ThO_2 particles, superimposed on a uniform dispersion of fine particles. The particles increased in size and decreased in number with time at temperature. The loss of particles was accompanied by formation of grain-boundary voids and surface pits. The activation energy for removal of the ThO_2 was about 40 kcal/mole.

Valentine and Hull at the University of Liverpool[3] have studied the effect of temperature on the tensile fracture stress of equiaxed-grain polycrystalline tungsten wire. This material had an average grain diameter of 0.03 mm and was investigated over the temperature range 77 to 480°K. The onset of the brittle-to-semibrittle transition occurred at 350°K. Below this transition the fracture stress increased with decreasing temperature. Above 473°K, grain-boundary cracking was observed on the specimen surface. Little mention has been made of this shallow cracking (< 0.005 mm deep) by other investigators. The presence of these cracks resulted in a reduction in fracture stress during retesting at lower temperatures. Fracture stresses at 77°K followed the Griffith relation, yielding a value of surface energy that was close to the theoretical value for the true surface energy.

At the Lawrence Radiation Laboratory,[4] tensile creep experiments have been conducted on high-purity polycrystalline rhenium. These experiments were conducted from 1500 to 2300°C at stresses from 1500 to 10,000 psi in a vacuum of 10^{-8} torr. The apparent activation energy for creep was 60 kcal/mole and was not a function of the applied stress. The steady-state creep rate varied directly with stress to the 3.4 power. No primary creep was evident during deformation under any conditions of temperature, stress, or grain size studied. Total dislocation densities in annealed and creep-tested specimens were nearly $10^9/cm^2$ and did not vary with temperature or stress. The creep behavior of polycrystalline rhenium is consistent with the dislocation glide mechanism, where the governing diffusion process was ascribed to dislocation core diffusion. A comparison of the creep data for tungsten and rhenium at 1500, 1800, and 2200°C is presented in Fig. II-3.

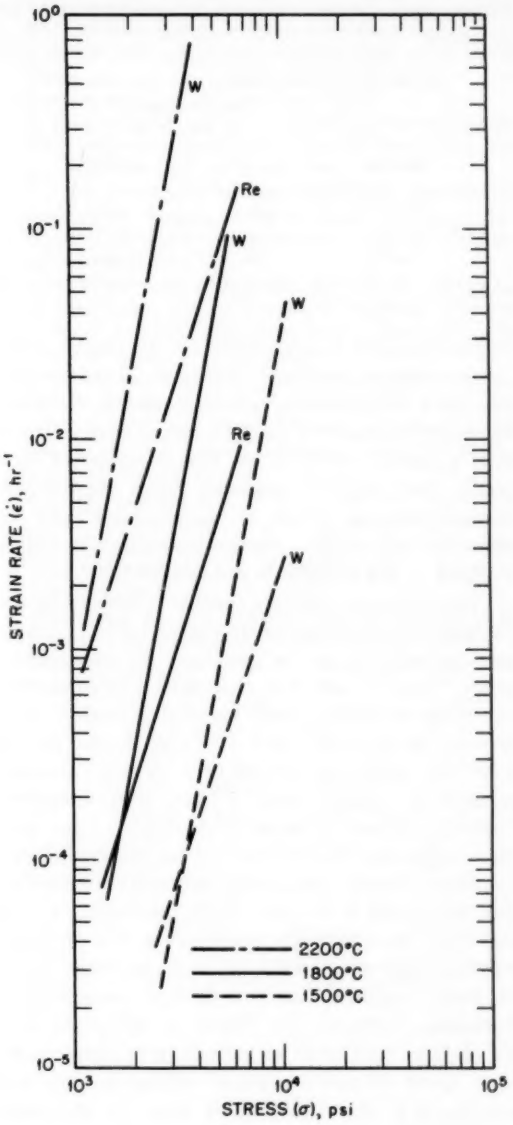

Fig. II-3 Comparison of creep data for tungsten and rhenium.[4]

PROPERTIES AND METALLURGY OF NIOBIUM AND TANTALUM ALLOYS

Creep- and stress-rupture properties have been determined at General Electric[5] on sheet samples of unalloyed niobium, tantalum, and the Cb-753 alloy (Nb-5 V-1.25 Zr) at 1200 and 1600°C in a vacuum of 1×10^{-6} torr over test times to 728 hr. Interpolated

100-hr stress-to-rupture times for these materials are as follows:

Material	Stress to rupture in 100 hr, psi	
	1200°C	1600°C
Nb	1050	350
Ta		850
Cb-753		1200

Posttest analyses showed essentially no change in the carbon, nitrogen, and hydrogen levels of these materials as a result of the test environment. However, significant increases in oxygen content were observed with increased testing time. This is consistent with results from other laboratories, which suggest that residual pressures of the order of 1×10^{-8} torr are necessary to avoid oxygen contamination during longtime testing of niobium and tantalum alloys.

The effects of internal oxidation treatments on the mechanical properties and structure of Nb-1 Zr have been investigated at the Lockheed Research Laboratory.[6] Internal oxidation treatments were performed on 0.040-in.-thick sheet material annealed in a vacuum between 10^{-5} and 10^{-6} torr. Under certain annealing conditions of temperature and pressure, pronounced strengthening effects were observed. Chemical analyses before and after treatment indicated that oxygen was the main interstitial absorbed during treatment. The temperature for optimum strengthening was determined to be near 800°C; treatments at 750 and 850°C were markedly less effective. The optimum pressure range was 4 to 8×10^{-6} torr, and much higher or lower pressures resulted in less strengthening. Annealing treatments for 240 hr at 800°C and 4 to 8×10^{-6} torr resulted in an increase in oxygen content from about 80 ppM to about 1500 ppM. This was accompanied by a fivefold increase in the yield strength and a fourfold increase in the ultimate strength at room temperature.

Similar internal oxidation treatments increased the stress-rupture life of Nb-1 Zr at 1200°C by a factor of 250 over that for the untreated alloy. The internal oxidation treatments resulted in a very uniform, extremely fine dispersion of particles. Strain contrast images indicate that these particles are coherent with the matrix and that they are disks approximately 35 Å in width and 10 Å in thickness. All the data suggest that the particles are clusters of zirconium and oxygen atoms. The fact that the strength of the alloy reaches a constant value at approximately 1600 ppM oxygen suggests that no additional zones are being formed as the oxygen content increases beyond this amount. That this occurs at an oxygen content of approximately 1 at.% suggests that the zones are composed of equal numbers of zirconium and oxygen atoms.

The effects of alloying additions of W, Re, Mo, Nb, Hf, V, and C on tantalum for the purpose of solid-solution strengthening and precipitation hardening have been investigated by Amra and Oxx.[7a] Ingots, which were triple electron-beam melted, were extruded to sheet bar and warm rolled to sheet less than 0.100 in. thick. Ease of fabrication, tensile strength, and ductility in the range -320 to 3550°F (-200 to 1955°C) were determined as a function of alloying additions. Some of the alloys after welding exhibited ductility at room temperature in a 2*t* bend test. Results showed that solid-solution additions of rhenium and tungsten in combination had the most potent effect on 3550°F strength. Substitution of as little as 1 wt.% rhenium for 1 wt.% tungsten in the basic Ta-10 W alloy raised the 3550°F strength by 50%. A Ta-10 W-5 Re alloy had an ultimate tensile strength of 19,400 psi at 3550°F. Considering the best physical properties attained, the optimum solid solution was a Ta-7 W-3 Re alloy which showed good ductility at -320°F, ductile welds in the recrystallized condition, and a high tensile strength at 3550°F. Chemical analyses showed that interstitial impurities, when not deliberately added, were below 50 ppM total in the cast material.

PROPERTIES OF CHROMIUM

Studies at Battelle-Columbus[7b] have been conducted to determine the effect of rhenium additions on the ductility of chromium. Tensile tests were made on recrystallized iodide chromium, Cr-1 at.% Re, and Cr-25 at.% Re over the temperature range -196 to 700°C. The pure chromium proved brittle at temperatures below 30°C, whereas the high-rhenium alloy retained some ductility down to -196°C, deforming by both slip and twinning prior to failure. The high-rhenium alloy also exhibited marked and unusual dynamic strain-aging behavior, suggesting that rhenium increases interstitial solubility between 300 and 600°C. The yield and flow data on pure chromium over the same temperature range indicated that interaction of dislocations with precipitates was the main source of strengthening rather than the classical picture of an interstitial drag on moving dislocations.

LITERATURE REVIEW

A comprehensive compilation[8] of available creep–rupture data for the refractory metals to 3000°C has been prepared by General Electric. In this 1000–page report, chapters are included to cover W, Re, Ta, Mo, and Nb, as well as alloys of these metals. In addition to the data for the refractory metals, chapters are devoted to mathematical techniques useful in the analysis of creep data and to parametric correlations of stress–rupture data. One chapter is also concerned with experimental procedures pertinent to the measurement of the creep–rupture behavior of refractory metals to elevated temperatures. Special attention is given to the data accumulated since 1962 in the AEC–sponsored refractory–metals evaluation program conducted at General Electric.

REFERENCES

1. W. D. Klopp and W. R. Witzke, Mechanical Properties of Arc-Melted Tungsten–Rhenium–Hafnium–Carbon Alloys, Report NASA-TN-D-5348, National Aeronautics and Space Administration, Lewis Research Center, July 1969.
2. J. L. Walter and A. U. Seybolt, Effect of ThO_2 Particles on Grain Growth and Preferred Orientation in Tungsten Sheet, *Trans. Met. Soc. AIME*, **245**: 1093-1099 (May 1969).
3. A. P. Valentine and D. Hull, Effect of Temperature on the Brittle Fracture of Polycrystalline Tungsten, *J. Less-Common Metals*, **17**: 353-361 (April 1969).
4. R. R. Vandervort and W. L. Barmore, High-Temperature Plastic Deformation of Polycrystalline Rhenium, *Trans. Met. Soc. AIME*, **245**: 825-829 (April 1969).
5. J. B. Conway and P. N. Flagella, AEC Fuels and Materials Development Program, Progress Report No. 78, USAEC Report GEMP-1010, General Electric Company, Missile and Space Division, Dec. 31, 1968.
6. R. M. Bonesteel, D. J. Rowcliffe, and T. E. Tietz, Mechanical Properties and Structure of Internally Oxidized Niobium–1 Percent Zirconium Alloy, *Trans. Jap. Inst. Metals*, 9(Suppl.): 597-602 (1968).
7. R. W. Fountain, J. Malt, and L. S. Richardson (Eds.), *High-Temperature Refractory Metals, New York, February 16–20, 1964. Part 2*, Metallurgical Society Conferences, Vol. 34, Gordon and Breach, Science Publishers, Inc., New York, 1966.
   a. L. H. Amra and G. D. Oxx, Jr., Tantalum Base Alloys with High Strength Above 3000°F, pp. 309-325.
   b. A. Gilbert, C. N. Reid, and G. T. Hahn, Tensile Properties of Chromium and Chromium–Rhenium Alloys, pp. 194-214.
8. J. B. Conway and P. N. Flagella, Creep-Rupture Data for the Refractory Metals to High Temperatures, USAEC Report GEMP-685, General Electric Company, Missile and Space Division, March 1969.

Section

III

Reactor Materials

Diffusion Studies

By A. N. Ashurst

SOLID-STATE DIFFUSION

Diffusion in Refractory Metals

An evaluation of diffusion-barrier effectiveness in preventing severe reactions between inner and outer claddings on isotope heat sources at 1100°C was undertaken by Battelle–Northwest.[1] Diffusion couples were assembled, each containing a refractory metal or alloy to represent the inner cladding (which must be compatible with the isotope fuel) and an oxidation-resistant outer cladding of 304L stainless steel, Haynes 25 cobalt-base superalloy, or Hastelloy X nickel-base superalloy. Two barrier materials that were evaluated are boron silicide (B_6Si) and aluminum oxide (Al_2O_3). These were applied to sheets or foils of the refractory-metal substrates by flame spraying. Cylindrical plugs of the oxidation-resistant materials were sandwiched between the coated foils, pneumatically impacted, and diffusion annealed at 1100°C for 1000 to 4000 hr. Couples with B_6Si showed as much or more reaction at the interface when compared to couples that had been assembled without diffusion barriers. Couples with Al_2O_3 showed reduced reaction zones when similarly compared. Reaction zones after 4000 hr with Al_2O_3 serving as the barrier were 2 mils or less in couples with tantalum and Mo–TZM and were 1 mil or less in couples with Re, W, and W–26 Re.

Interdiffusion of refractory bimetallic couples was studied[2] at temperatures of 1000 to 1500°C for times up to 500 hr. The four systems studied were W–Ir, W–Rh, Re–W, and Ta–W. Couples were prepared by vapor-depositing tungsten on iridium foil and on rhodium foil, rhenium on tungsten vapor deposits, and tantalum on tungsten vapor deposits. Iridium foils were 50 μ thick, and rhodium foils were 75 μ thick. The tungsten deposited onto these foils was, according to the author, "several microns in thickness," although it looked more like tens of microns thick in the metallographs. The tungsten vapor deposits used for substrates were applied to a thickness of about 5 μ on fluidized spherical magnesium particles that were about 150 to 250 μ in diameter. The magnesium was then removed by vaporizing during vacuum annealing. Rhenium and tantalum deposits on the tungsten shells were several microns thick. Diffusion anneals were conducted in vacuum at 10^{-4} torr. Interdiffusional thicknesses were measured optically and by microprobe tracings. The results are summarized in Table III-1. Voids were observed in all but the W–Re system, and the voids were attributed to the Kirkendall effect.

Table III-1 Interdiffusion in Refractory-Metal Couples[2]

Couple	Temp., °C	Time, hr	Interdiffusion zone, μ
CVD W on Ir foil	1200	101	8
	1200	501	12
	1500	99	14
CVD W on Rh foil	1000	105	8
	1200	101	30
	1200	501	47
	1500	99	>50
CVD Re on CVD W	1200	101	1
	1200	501	2
	1500	99	3
CVD Ta on CVD W	1200	101	1.5
	1500	99	3

The diffusion of ^{51}Cr into polycrystalline niobium was studied by Pelleg[3] in Canada over the temperature range 947 to 1493°C. The radioactive chromium was deposited by vacuum evaporation onto vacuum-annealed and electropolished niobium cylinders to a thickness of about 200 Å, then diffusion annealed in an inert atmosphere. Sections were taken by anodizing and stripping. Concentration–penetration plots (log activity against square of distance) were nonlinear at the lower temperatures. This behavior is attributed to rapid diffusion of ^{51}Cr along niobium lattice defects, rather than to grain-boundary diffusion. At the higher

temperatures, similar plots gave near linearity. The diffusivity of ^{51}Cr into niobium was expressed by the equation:

$$D_{Cr-Nb} = 0.13^{+0.12}_{-0.06} \times \exp\left[-(80.6 \pm 1.9 \text{ kcal/mole})/RT\right] \quad \text{cm}^2/\text{sec}$$

over the temperature range studied.

Japanese investigators[4] studied the diffusion of carbon in tantalum, niobium, and vanadium by serial sectioning, using ^{14}C as a tracer. The diffusion coefficients are described by the equations:

$$D_{C-Ta} = 1.2 \times 10^{-2} \times \exp\left[-(40.3 \text{ kcal/mole})/RT\right] \quad \text{cm}^2/\text{sec}$$

$$D_{C-Nb} = 3.3 \times 10^{-2} \times \exp\left[-(37.9 \text{ kcal/mole})/RT\right] \quad \text{cm}^2/\text{sec}$$

$$D_{C-V} = 4.9 \times 10^{-3} \times \exp\left[-(27.3 \text{ kcal/mole})/RT\right] \quad \text{cm}^2/\text{sec}$$

The diffusion of uranium in tungsten between 1970 and 2730°C was measured[5] by a mass-spectrometric technique. Thin ribbons of the solvent metals, each of which contained a low concentration of solute material as an impurity, were used as high-temperature ion sources in a mass spectrometer. Diffusion coefficients were calculated using the Fick's-law solution for impurity evaporation from a thin plate. The activation energies were found from plots of the natural logarithm of the diffusion coefficients against inverse temperature. The results yielded the relation:

$$D_{U-W} = (1.80 \pm 1.05) \times 10^{-2} \times \exp\left[-(93.0 \pm 6.0 \text{ kcal/mole})/RT\right] \quad \text{cm}^2/\text{sec}$$

Diffusion in Stainless Steel and Aluminum

Standard radiotracer techniques were used[6] to measure the volume-diffusion rates of chromium and nickel in a 20 Cr–25 Ni–Nb austenitic steel in the temperature range 840 to 1290°C. The results were described by the equations:

$$D_{Cr-SS} = 1.9 \times 10^{-1} \times \exp\left[-(58.8 \text{ kcal/mole})/RT\right] \quad \text{cm}^2/\text{sec}$$

$$D_{Ni-SS} = 4.06 \times \exp\left[-(67.5 \text{ kcal/mole})/RT\right] \quad \text{cm}^2/\text{sec}$$

Grain-boundary-diffusion measurements were made in the range 550 to 900°C. The diffusion rates of chromium and nickel isotopes were not significantly different from previously reported rates for iron.

An investigation of tracer diffusion of La, Ce, Pr, Nd, and Sm in aluminum was conducted in India[7] using the residual-activity technique to determine concentration–penetration curves. Plots of log D vs. $1/T$ in all cases were straight lines over the temperature range studied (450 to 630°C). Concentration–penetration curves show a sharp decrease in concentration of the diffusing material within 0.2 to 0.3 μ of the surface and a gradual decrease thereafter to a total penetration of from 4 to 20 μ. Diffusion coefficients were expressed by the following:

$$D_{La-Al} = 1.40 \times 10^{-6} \exp(-27{,}000/RT)$$

$$D_{Ce-Al} = 1.90 \times 10^{-6} \exp(-26{,}600/RT)$$

$$D_{Pr-Al} = 3.58 \times 10^{-7} \exp(-23{,}870/RT)$$

$$D_{Nd-Al} = 4.80 \times 10^{-7} \exp(-25{,}000/RT)$$

$$D_{Sm-Al} = 3.45 \times 10^{-7} \exp(-22{,}880/RT)$$

The authors discuss the low diffusivity of these tracer elements in aluminum in relation to the low solid solubility of the tracers. The activation energies are shown to be dependent on the ionic charge and atom-size difference, regardless of the solid solubility. However, the authors note that low solubility alone is not sufficient to predict low diffusivity and suggest that some constant factor, such as the electronic configuration, is probably responsible for the low diffusivities.

DIFFUSION OF GASES IN SOLIDS

Permeation constants were determined[8] for hydrogen in tungsten by mass-spectroscopic techniques at pressures between 600 and 10^{-8} torr at temperatures between 1100 and 2400°K. Diffusion and solubility constants were derived from degassing rates of a solid cylinder preloaded with hydrogen at 600 torrs. Attempts were made to measure hydrogen concentrations at low pressures using the flash-filament technique, by which the concentration is derived from pressure changes resulting from flashing the sample between selected high temperatures. The diffusivity of hydrogen in tungsten was expressed by the equation:

$$D_{H-W} = 4.1 \times 10^{-3} \times \exp\left[-(9000 \text{ cal/gram atom})/RT\right] \quad \text{cm}^2/\text{sec}$$

Solubility constants were given by the expression:

$$S_{H-W} = 2.9 \times 10^{-1} \times \exp\left[-(24{,}000 \text{ cal/gram atom})/RT\right] \text{ torr-liter}/(\text{cm}^3)(\text{torr}^{\frac{1}{2}})$$

These values indicate that hydrogen is interstitially dissolved. The concentration of interstitial hydrogen in tungsten is expressed as a function of pressure and temperature. Below 10^{-4} torr the total hydrogen concentration derived from the flash-filament experiments appeared to be orders of magnitude higher than the calculated concentration of hydrogen held at interstitial sites, suggesting to the author that the balance of hydrogen is held at a second site, called "residual site," of unknown nature.

The diffusion of ^{133}Xe in CsI was studied[9] at low gas concentrations and negligible radiation-damage levels by growing single crystals of CsI containing radioactive ^{133}I which decayed to ^{133}Xe ($T_{\frac{1}{2}}$ = 20.8 hr). Diffusion coefficients were described by the expression:

$$D_{Xe-CsI} = 5.7 \times 10^{-1} \times \exp\left[-(1.01 \text{ eV/atom})RT\right] \quad \text{cm}^2/\text{sec}$$

Crystals containing high concentrations of defects exhibited trapping of the rare gas and anomalous diffusion kinetics. Diffusion obeyed classical diffusion solutions at low fission-recoil concentrations, whereas at high concentrations radiation damage created traps that decreased gas diffusion rates. Increasing the gas concentration independent of radiation damage also lowered rare-gas diffusion coefficients, showing that formation of small gas-atom clusters also produced trapping.

REFERENCES

1. H. T. Fullam, The Use of Diffusion Barriers in Reducing Metal–Metal Interactions at 1100°C, USAEC Report BNWL-1015, Battelle–Northwest, May 1969.
2. J. M. Steichen, Interdiffusion Between Certain Vapor Deposited-Foil Refractory Metal Couples, USAEC Report BNWL-1071, Battelle–Northwest, June 1969.
3. J. Pelleg, Diffusion of ^{51}Cr into Polycrystalline Niobium, *J. Less Common Metals*, 17: 319-324 (1969).
4. P. Son, M. Miyake, and T. Sano, Diffusion of Carbon in Tantalum, Niobium, and Vanadium, *Technol. Rep. Osaka Univ.*, 18: 317-324 (October 1968).
5. E. C. Schwegler, Jr., and F. A. White, A Mass-Spectrometric Investigation of the High-Temperature Diffusion of Uranium in Tungsten and the Allotropic Phase Transition in Zirconium, *J. Mass Spectrom. Ion Phys.*, 1: 191-208 (June 1968).
6. A. F. Smith and G. B. Gibbs, Volume and Grain-Boundary Diffusion in 20 Cr/25 Ni/Nb Stainless Steel, *Metal Sci. J.*, 3: 93-94 (May 1969).
7. S. P. Murarka and R. P. Agarwala, Diffusion of Rare-Earth Elements in Aluminum, Indian Report BARC-368, 1968.
8. R. Frauenfelder, Solution and Diffusion of Hydrogen in Tungsten, *J. Vac. Sci. Technol.*, 6(3): 388-397 (May/June 1969).
9. T. S. Elleman, C. H. Fox, Jr., and L. D. Mears, Influence of Defects on Rare-Gas Diffusion in Solids, *J. Nucl. Mater.*, 30: 89-106 (April 1969).

Section

IV

Reactor Materials

Radiation Effects in Structural Materials

By M. Kangilaski

ZIRCONIUM AND ZIRCONIUM ALLOYS

A comprehensive model for the in-pile deformation of Zircaloy, either annealed or with varying degrees of cold work, at temperatures between 200 and 300°C was developed by Nichols[1] and shown to be in substantial agreement with all experimental results reported to date. These results employed different types of tests (fixed stress, fixed strain, and fixed strain rate) and different methods of loading (uniaxial and biaxial) and covered instantaneous flux levels from 5×10^{12} to 2×10^{14} neutrons/(cm^2)(sec) (>1 MeV) and strain rates from 10^{-6} to 10^{3} hr^{-1}.

Three basically different in-pile mechanisms have been proposed to account for the observations. At high stress levels the cutting of Seeger zones is proposed, and it is suggested that the properties in this region are identical to those obtainable by postirradiation testing at the same temperature and integrated exposure. Cold-worked material is stronger at low exposures, but it becomes comparable with annealed material at high exposures.

At intermediate stress levels, dislocations climb around the depleted zones at a rate set by the effective, radiation-enhanced diffusion coefficient. Here, the in-pile strength is less than that indicated by postirradiation testing, but no less than the intrinsic strength of unirradiated annealed Zircaloy at a low plastic-strain level. This mechanism operates as an alternative or parallel mechanism to the normal thermal mechanism. Annealed and cold-worked material behave similarly, with the cold-worked material possibly showing a slightly higher creep rate. Of larger significance is the superior strength of annealed material tested in the transverse direction compared with annealed material tested in the longitudinal direction, presumably due to differences in average resolved shear stress on active slip planes; comparable behavior is observed in out-of-pile testing.

In the low-stress region, point-defect loops are formed preferentially on particular planes to respond to the applied stress, thereby producing a "stress-directed growth" phenomenon (which in turn may cause some yielding creep) at a deformation rate directly proportional to both stress and flux level. This mechanism is intimately related to the free-growth mechanism that produces plastic strain even with no applied stress. This mechanism operates independently of the thermal creep, simply adding more strain to that obtainable out-of-pile at a rate essentially temperature independent for the temperatures of interest in reactor design. At very low temperatures (below 300°K), there are indications that this creep component actually increases somewhat, but not drastically. This irradiation creep is assumed to operate at all stresses, independently of the other mechanisms discussed above. However, because of its weak stress dependence, it dominates in the low-stress region and becomes completely negligible in the high-stress region.

British investigators[2] have found that the in-pile steady-state creep rate of cold-worked Zircaloy-2 is about 3×10^{-7} hr^{-1} at 300°C under a stress of 16,000 psi. At comparable temperature and stress, the out-of-pile steady-state creep rate was 3×10^{-8} hr^{-1}. Extensive studies are also under way to determine the postirradiation stress-rupture properties of cold-worked Zircaloy-2. The in-pile and out-of-pile creep histories and rupture strains of cold-worked Zircaloy-2 at 325°C are compared in Fig. IV-1. The unirradiated specimens all went into third-stage creep at 2.5 to 3.5% strain and failed at 10 to 12% strain, whereas both in-pile specimens were still in second-stage creep at 5 and 10% strain, respectively. These results suggest that creep-strain limits based on out-of-pile tests may be unduly pessimistic.

Piercy[3] suggested that rare-earth solutes added to zirconium may reduce its in-reactor creep by acting as vacancy-interstitial recombination centers. Further, he indicated that such rare-earth additives might also improve the high-temperature mechanical properties by forming stable precipitates.

Specimens of Zircaloy-2 were irradiated by the Canadians[5] at 300°C to fast fluences ranging from 4×10^{19} to 8×10^{21} neutrons/cm^2. Transmission

electron microscopy was performed on these specimens, and the size and distribution of defect clusters were established. The number of visible defect clusters and loops reached a saturation density of $3 \times 10^{16}/cm^3$ after a fast fluence of 5×10^{20} neutrons/cm^2, as illustrated in Fig. IV-2. With increasing fluence the average diameter of the visible defects increased slightly, the increase raising the volume fraction of the defects, i.e., the number of atom sites involved.

The effect of irradiation and annealing temperature on the hardness of cold-worked Zircaloy-2 is illustrated in Fig. IV-3. Irradiation of cold-worked Zircaloy-2 at 500°C to a fluence of 4×10^{21} neutrons/cm^2 in the Dounreay Fast Reactor (DFR) did not produce any three-dimensional voids like those observed in austenitic stainless steels, nickel-base alloys, and aluminum.

The response of the fracture toughness of Zircaloy-2 to various combinations of cold work, hydrogen content, and neutron fluence in hot pressurized water is characterized by embrittlement to a point where saturation in the fracture toughness is attained.[6] Further in-reactor exposure beyond this saturation point appears to have no effect on toughness, although other mechanical properties such as flow stress continue to change. In addition, anisotropy in the toughness of rolled plate material, evident in the unirradiated condition, is retained during in-reactor exposure and after increases in hydrogen content. Several processes are thought to be contributing to the toughness of Zircaloy-2 during irradiation. The reduction in toughness at low exposures must result from defect interactions with the deformation modes and the formation of the brittle hydride phase. However, the occurrence of saturation is not explained by these mechanisms, in view of data on other mechanical properties and corrosion rates. The difference in the

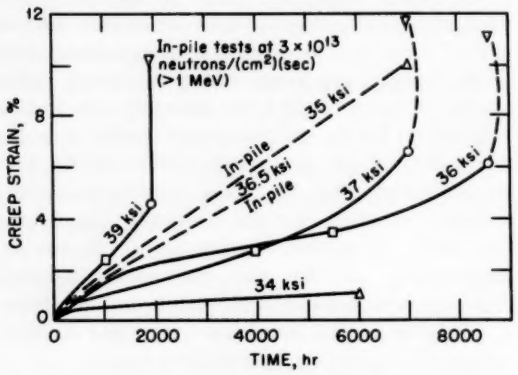

Fig. IV-1 Effect of irradiation on the stress-rupture behavior of cold-worked Zircaloy-2 at 325°C (Ref. 2). □, onset of accelerated creep; ▽, strain at failure; △, test terminated prior to failure; ○, last strain reading prior to failure.

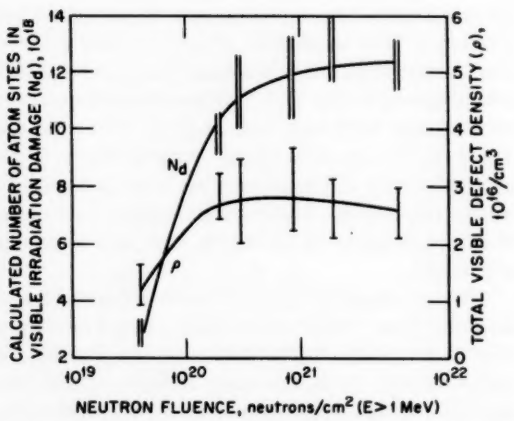
CALCULATED NUMBER OF ATOM SITES IN VISIBLE IRRADIATION DAMAGE (N_d), 10^{18}
TOTAL VISIBLE DEFECT DENSITY (ρ), $10^{16}/cm^3$
N_d
ρ
NEUTRON FLUENCE, neutrons/cm^2 (E>1 MeV)

Fig. IV-2 Damage accumulation in irradiated Zircaloy-2 (Ref. 5). ρ = volume density of visible defects; N_d = calculated number of atom sites involved in the visible damage, assuming that the defects are all monolayer planar loops on $\{1\bar{1}00\}$.

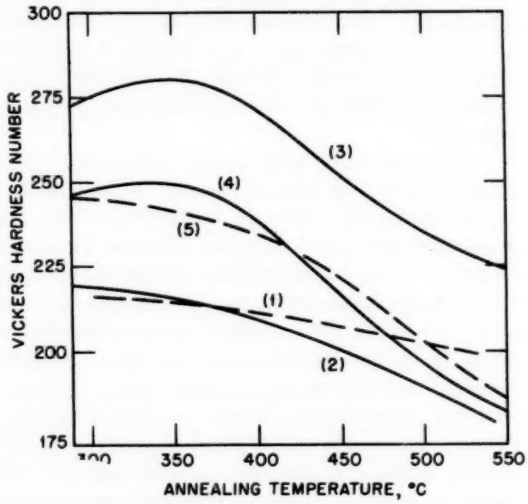

Fig. IV-3 Variation in hardness of cold-worked and irradiated Zircaloy after 1-hr anneals.[5] (1) 20% cold-worked Zircaloy-2, unirradiated; (2) annealed Zircaloy-2, irradiated to 7.9×10^{20} neutrons/cm^2 at 290°C; (3) 40% cold-worked Zircaloy-2 irradiated to 7.8×10^{21} neutrons/cm^2 at 290°C; (4) 30% cold-worked Zircaloy-2 irradiated to 2.0×10^{21} neutrons/cm^2 at ~500°C in the DFR; (5) 30% cold-worked Zircaloy-2 irradiated to 4×10^{21} neutrons/cm^2 at ~500°C in the DFR.

conditions needed to initiate slip and twinning indicates that the twinning component of deformation is not reduced as much as the slip component by radiation damage. Saturation is therefore interpretable on the basis that twinning plays a major role in the crack-tip plastic zone after irradiation. Additional study of the importance of twinning in determining the toughness of Zircaloy-2 was attempted by examining the relation between texture and the anisotropy in fracture toughness. A correlation exists between the crack-tip shear stresses resolved on the $\{11\bar{2}1\}\langle 11\bar{2}\bar{6}\rangle$ twin system and the toughness anisotropy.

General Electric[7] made a study to predict the behavior of irradiated Zircaloy-2 tubing in case of loss of coolant during shipping of spent fuel elements. The conditions of failure were expressed as a function of internal pressure, temperature, and heating rate. One important consideration in these predictions is the annealing out of radiation damage as the specimen temperature is increasing. Tests on irradiated Zircaloy-2 tubes gave failure temperatures that were generally lower than those predicted.

A group of specimens of Zr–1.2 Cr–0.1 Fe was irradiated by the Canadians[8] at 300°C to a fast fluence of 9.5×10^{19} neutrons/cm^2, and another group was autoclaved at the same temperature. All specimens had been water quenched and aged at different temperatures up to 850°C for 12 hr. Tensile tests showed that autoclaving reduced the strength, with little effect on ductility, whereas irradiation increased the strength and decreased the ductility to near zero in all the specimens.

The effect of temperature during neutron irradiation on postirradiation deformation behavior of Zr–2.5 Nb alloy was studied in Canada.[9] Tensile specimens, oriented for deformation by slip, were irradiated at 50 to 100°C and 250 to 325°C to neutron fluences of $\sim 5 \times 10^{19}$ neutrons/cm^2 ($E > 1.0$ MeV). Transmission electron microscopy revealed small clusters or loops ~25 Å in diameter in material irradiated in the higher temperature range. The defects generated at ~300°C were responsible for both a larger increment in yield stress and a higher rate of work hardening than were produced by the defects formed at the lower temperature. A reasonable correlation was obtained between the changes in deformation characteristics and the defects formed during irradiation.

STAINLESS STEELS AND SUPERALLOYS

To obtain a good comparison of the irradiation responses of different stainless steels, Oak Ridge workers[10] irradiated six types of stainless steels at temperatures of 350, 450, 550, and 650°C to thermal and fast (>1 MeV) fluences of 1.8×10^{21} and 1.4×10^{21} neutrons/cm^2, respectively. The stainless steels were 316, 316L, and titanium-modified (0.2 wt.%) 304, 304L, 316, and 316L. Results of postirradiation tensile tests at the same temperatures as the irradiation temperatures are summarized in Figs. IV-4 and IV-5.

A summary report[11] has been issued by Oak Ridge on the use of titanium additions to produce austenitic stainless steels that are resistant to irradiation embrittlement. It was originally thought that the improved resistance to radiation-induced embrittlement resulted from trapping of the helium atoms by fine precipitates of TiC. However, recent studies show that the titanium additions change the fracture mode of the unirradiated stainless steel from intergranular to transgranular, and materials that fail by transgranular fracture at elevated temperature are less susceptible to irradiation embrittlement.

Battelle–Columbus[12] performed tensile tests on 347 stainless steel that had been irradiated to a fast

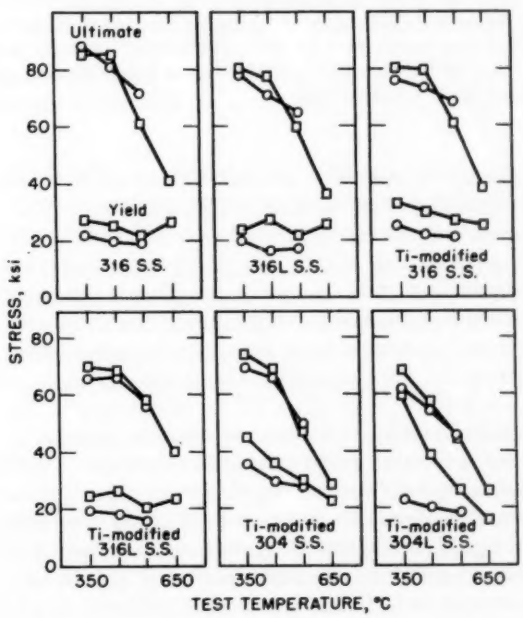

Fig. IV-4 Effect of irradiation on the yield and ultimate tensile strength of several austenitic stainless steels.[10] Specimens were irradiated at the test temperature to 1.8×10^{21} neutrons/cm^2 (thermal) and 1.4×10^{21} neutrons/cm^2 (>1 MeV); strain rate 0.002 min^{-1}; □, irradiated; ○, thermal controls.

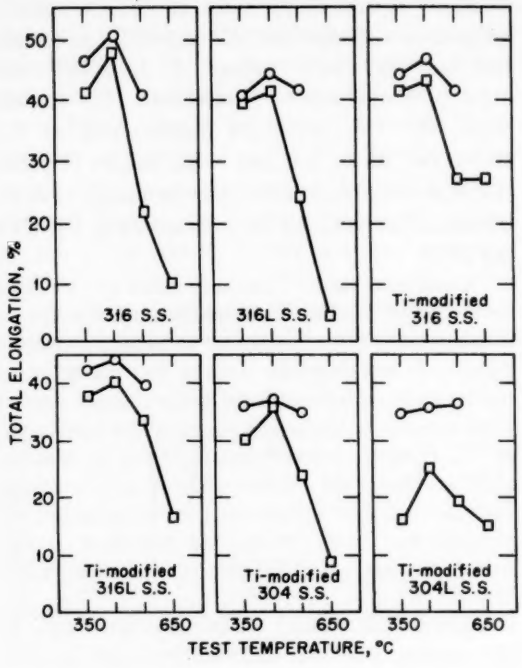

Fig. IV-5 Effect of irradiation on the ductility of several austenitic stainless steels.[10] Specimens were irradiated at the test temperature to 1.8×10^{21} neutrons/cm^2 (thermal) and 1.4×10^{21} neutrons/cm^2 (>1 MeV); strain rate 0.002 min^{-1}. □, irradiated; ○, thermal controls.

fluence of 3×10^{22} neutrons/cm^2 at 50°C in the Engineering Test Reactor (ETR). Results for these specimens and for those which had been tested earlier are summarized in Table IV-1. Previous test results had shown that, with increasing fast fluence, the yield strength and ultimate strength increased, with the yield strength increasing faster and approaching the ultimate strength. For example, after fast fluences of 1.6×10^{22} and 2.1×10^{22} neutrons/cm^2, the irradiation-induced increase in ultimate strength appeared to have reached a saturation level and the yield strength had become equivalent to the ultimate strength. Irradiation also caused reductions in uniform elongation and total elongation, which appeared to have reached a saturation level after 0.55×10^{22} neutrons/cm^2. Similar trends were exhibited by the irradiated specimens at both room temperature and 315°C. Therefore it was expected that irradiation of 347 stainless steel to a fast fluence of 3.0×10^{22} neutrons/cm^2 would impart tensile properties that were similar to those of specimens irradiated to 2.1×10^{22} neutrons/cm^2. Test results on specimens irradiated to 3.0×10^{22} neutrons/cm^2 showed that the ultimate strength was indeed at the same level as for specimens irradiated to 1.6×10^{22} and 2.1×10^{22} neutrons/cm^2. However, the yield strength was measurably lower. Values for both uniform elongation and total elongation were also higher after a fast fluence of 3.0×10^{22} neutrons/cm^2 than after a fast fluence of 2.1×10^{22} neutrons/cm^2. This apparent recovery of irradiation-induced tensile-property changes with irradiation beyond 2.1×10^{22} neutrons/cm^2 was observed in specimens tested at both room temperature and 315°C. It is suggested that the recovery in mechanical properties following exposure to large fast fluences is the result of agglomeration of small defects into larger defects that are not so effective in impeding dislocation movement.

The effects of irradiation on the yield strength and uniform elongation of 304 stainless steel at 450°C, as determined at Argonne,[13] are shown in Fig. IV-6. These results show that fluence level may have a stronger influence on mechanical properties than irradiation temperature does.

Battelle–Northwest[14] examined the effects of metallurgical condition on the response of 304 and 316 stainless-steel specimens to irradiation. The specimens were in the as-annealed condition, 20% cold worked at room temperature, 20% cold worked at 160°C, and 20% cold worked at 160°C followed by aging for 24 hr at 430°C. The specimens were irradiated in the ETR at temperatures of 375 and 625°C to a fast fluence of 7×10^{20} neutrons/cm^2. Preliminary conclusions from tensile tests on these specimens at 400, 650, and 750°C are as follows:

1. Martensitic structures formed by subzero deformation are effective contributors to postirradiation strengths.
2. None of the above preirradiation treatments resulted in significant improvement of postirradiation ductility relative to that of specimens in the solution-treated condition.
3. The steels that were annealed and those which were cold worked at room temperature show little or no sensitivity to irradiation temperature over the entire experimental range (375 to 625°C).
4. Residual yield-strength increases persist to a test temperature of 750°C for all cold-worked specimens.

A translation[15] of the proceedings of a Soviet symposium on fast reactor technology contains several papers pertaining to the effects of radiation on tensile properties of structural materials and on the stress-rupture properties of stainless steel. One paper[15a]

Table IV-1 Tensile Properties of Unirradiated and Irradiated 347 Stainless Steel[12]

Test temp., °C	Fast fluence, 10^{21} neutrons/cm^2	Yield strength (0.2% offset), ksi	Ultimate tensile strength, ksi	Elongation, %	
				Uniform	Total
25	0	36.9	90.2	52	65
	5.5	88.7	112	25.8	34.5
	9.2	109	113	24.7	32.7
	16	114	114	25.0	33.2
	21	113	113	24.3	34.5
	30	104	115	32.7	45.6
	16*	32.3	84.8	50.9	56.6
315	0	26.8	64.2	31.9	36.0
	5.5	80.0	84.0	13.2	16.4
	11.0	86.8	89.0	10.1	13.3
	16	86.2	86.2	8.0	13.7
	21	86.0	86.0	5.0	10.2
	30	78.7	83.4	9.0	15.7
	21*	33.0	61.0	26.8	32.6
600	0	23	40.5	17.8	22.5
	21	34.6	38.4	0.7	
	21†	36.7	42.3	3.2	3.6
	21*	22.3	33.1	5.2	5.8
750	0	22.0	25.5	16.0	26.0
	21	35.0	35.0	0.5	0.5
	30	‡	28.7	0.3	0.3
	30*	14.5	16.6	0.7	0.8

*Annealed for 1 hr at 980°C before testing.
†Annealed for 1 hr at a temperature somewhat lower than 980°C.
‡Specimen failed before the 0.2% offset yield strength was achieved.

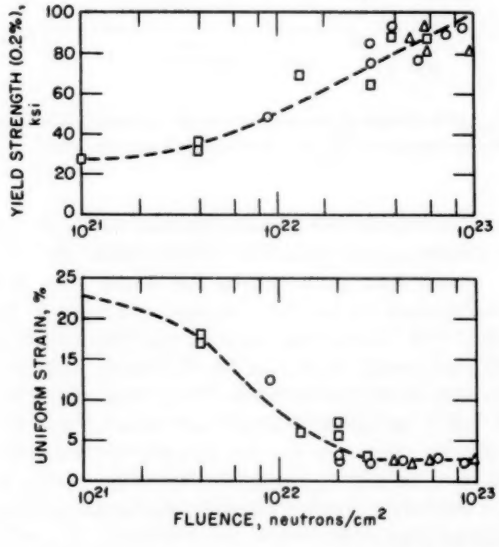

Fig. IV-6 Effects of fluence and irradiation temperature on the 450°C tensile properties of irradiated 304 stainless steel.[13] ○, 371 to 385°C; △, 400 to 425°C; □, 454 to 474°C.

discusses the response of different alloys to irradiation-induced elevated-temperature embrittlement. The types of alloys investigated are as follows:

1. Austenitic stainless steels with different C, Mo, Nb, B, and Ti contents.
2. Solid-solution-hardened nickel-base alloys.
3. Precipitation-hardened nickel-base alloys.
4. Duplex ferritic–martensitic steels.

The irradiations were carried out at 100°C with the fast fluences (>1 MeV) ranging from 4×10^{20} to 4×10^{21} neutrons/cm^2 and at 700°C with a fast fluence of 2×10^{20} neutrons/cm^2. Tensile-test results indicated that the elevated-temperature ductility of all the materials was reduced by irradiation. However, the degree of embrittlement was found to vary significantly. The two stainless steels (Fe–18 Cr–9 Ni–2.3 W and Fe–16 Cr–15 Ni–3 Mo–0.7 Nb) were affected the least by irradiation. The 200-hr stress-rupture strength of these materials at 650°C was not changed by irradiation. For Fe–Cr–Ni alloys without other alloying additions, the radiation-induced reduction of

ductility increases with increasing nickel content. On the basis of this study, it was concluded that helium is not the main source of high-temperature radiation embrittlement. The embrittlement phenomenon is believed to be associated with the preirradiation mechanical properties, especially with the minimum in plasticity that is exhibited by these alloys in the 500 to 800°C range. Another Soviet study[15b] suggests that the generation of hydrogen by (n,p) reactions plays a major role in causing elevated-temperature embrittlement in high-nickel alloys.

The Germans[16] have investigated the postirradiation tensile and creep-rupture properties of two types of austenitic stainless steels. These stainless steels were irradiated at 650°C to a fast fluence of 1.4×10^{20} neutrons/cm^2. One of the steels was similar to Incoloy 800 in composition (Fe–20 Cr–32 Ni), and the other was similar to 318 stainless steel (Fe–16 Cr–16 Ni–2 Mo–Nb stabilized). They found that, although irradiation caused a reduction of ductility at elevated temperatures for both of the alloys, the ductility loss was significantly smaller for the Fe–16 Cr–16 Ni–2 Mo–Nb stainless steel, as shown in Fig. IV-7. The better postirradiation ductility of the niobium-containing stainless steel is attributed to a dispersion of fine niobium carbide particles. These results confirm earlier British findings that showed that the British steel FV-548 (niobium-stabilized 316 stainless steel) underwent less radiation-induced embrittlement than regular 316 stainless steel. Similar conclusions have been reached by the Russians.[15] This German study also showed that the creep rates of these two steels were significantly increased by irradiation, presumably as a result of precipitation of carbide particles during the 650°C irradiation. Further, vacuum-melted heats showed larger radiation-induced losses of ductility than air-melted heats.

Postirradiation stress-rupture tests were run by Battelle–Northwest[17] at 540 and 595°C on 304 stainless steel that had been irradiated in Experimental Breeder Reactor II (EBR-II), with the results shown in Fig. IV-8. Similar tests of 316 stainless steel at temperatures up to 760°C showed similar trends, in that irradiation caused significant losses in rupture life.

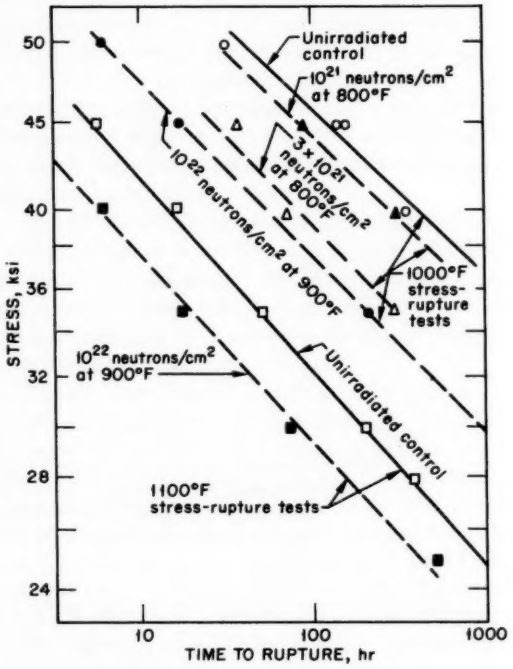

Fig. IV-8 Effect of irradiation on the postirradiation creep-rupture properties of solution-treated 304 stainless steel.[17]

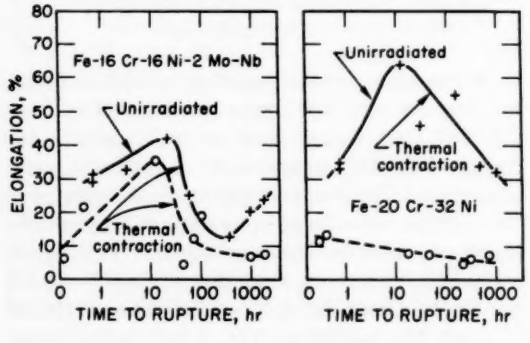

Fig. IV-7 Influence of rupture time and irradiation on rupture elongation of two austenitic alloys at 650°C (Ref. 16). ○- - -○, irradiated at 650°C to 1.4×10^{20} neutrons/cm^2 (fast).

Creep tests performed by the British[18] on 316 stainless-steel tubing that had been irradiated in the DFR gave results that were in line with previous findings, namely, that both the fracture ductility and the time to rupture were reduced by irradiation. Tests at 650°C on annealed specimens indicated that the minimum creep rate was not changed by irradiation. However, at 550°C, irradiated cold-worked 316 stainless steel crept about 10 times as fast as unirradiated material (Fig. IV-9).

In-reactor stress-rupture tests were performed by Russians[15c] on thin-wall tubes of Fe–18 Cr–10 Ni–1 Ti at 650°C. The tubes were about 4 in. long, were

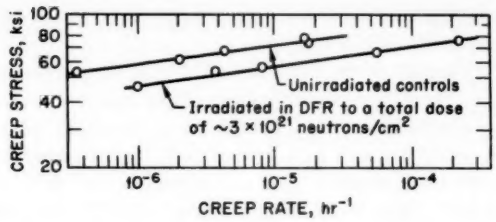

Fig. IV-9 550°C creep rates of cold-worked 316 stainless-steel tubing.[18]

0.55 in. in diameter, and had a wall thickness of 8 mils. Results of these tests are given in Fig. IV-10, which shows that irradiation causes a significant loss in rupture life.

British investigators have found[19] that Fe–15 Cr–4 Al alloy is embrittled by irradiation (6×10^{19} neutrons/cm^2 fission and 2×10^{20} neutrons/cm^2 thermal) when tested at temperatures above 750°C. The addition of 0.86 wt.% yttrium to the alloy was found to eliminate the radiation-induced ductility loss.

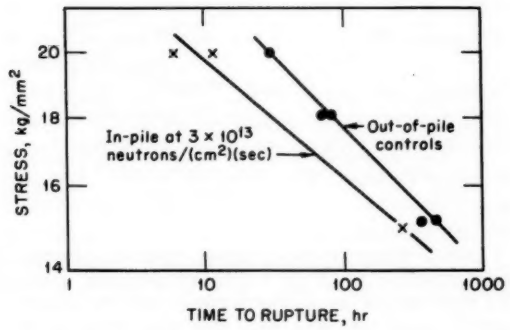

Fig. IV-10 Stress-rupture properties of tubular Fe–18 Cr–10 Ni–1 Ti specimens at 650°C (Ref. 15*c*).

It is postulated that yttrium removes the boron from the grain boundaries and ties it up within the YFe_9 particles. Therefore no helium is generated near the grain boundaries, and the radiation-induced embrittlement is eliminated.

Soviet investigators have found[15c] that a ferritic steel containing 12 wt.% chromium is embrittled very little by irradiation at temperatures up to 650°C (Fig. IV-11).

Cyclic-stress fatigue tests were performed by Battelle–Columbus[12] on irradiated 347 stainless steel

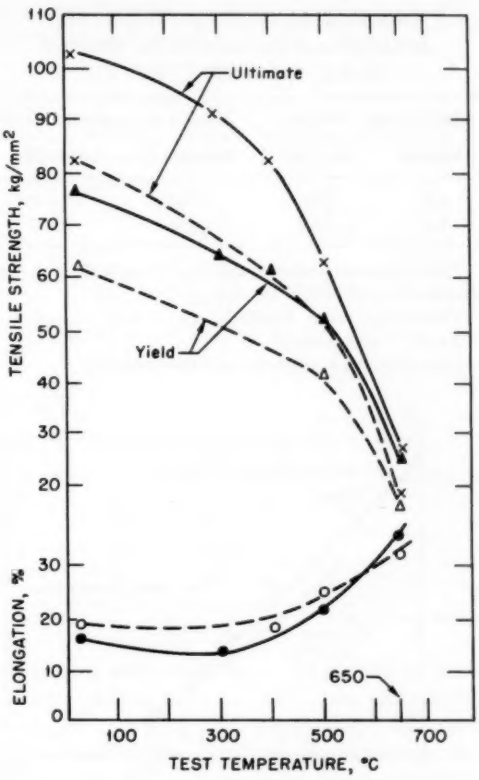

Fig. IV-11 Effect of radiation on tensile properties of 12% chromium steel as a function of test temperature.[15c] ---, unirradiated samples; ——, irradiated at 450 to 500°C to a fluence of 5×10^{21} neutrons/cm^2.

at 650°C. The stainless-steel specimens were irradiated at 50°C to a fast fluence of 2.2×10^{22} neutrons/cm^2 in the ETR. The results, summarized in Table IV-2, indicate that irradiation causes significant reductions in high-temperature fatigue life. The irradiated specimens elongated less than 1% at fracture, whereas the elongation was 18% for the unirradiated specimen that failed. The reduction in fatigue life was attributed to the radiation-induced loss of ductility.

Cyclic-strain fatigue tests on 316 stainless steel at 650°C by Berling and Conway[7] demonstrated that irradiation causes significant reductions in fatigue life, even for specimens irradiated in the Oak Ridge Research Reactor (ORR) at 70°C to a fast fluence of only 4.8×10^{18} neutrons/cm^2. Excellent agreement was obtained[20] by correlating the fatigue data for the irradiated specimens with the predicted curve obtained by the Berling–Conway equation. Figure IV-12 com-

Table IV-2 Cyclic Fatigue Properties of Irradiated and Unirradiated 347 Stainless Steel Tested at 650°C (Ref. 12)

Stress range, 1000 psi		Number of cycles to failure*	
Minimum	Maximum	Irradiated†	Unirradiated
2.0	22.0	2,368	15,324‡
2.0	27.0	1,496	7,485

*The specimens were cycled at 50 cycles/hr using a crosshead speed of 0.02 in./min.

†Specimens were irradiated to a fast fluence of 2.2×10^{22} neutrons/cm^2.

‡Specimen did not fail; test was discontinued.

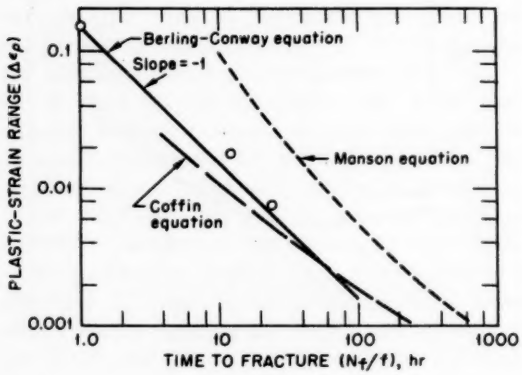

Fig. IV-12 Comparison of the effectiveness of various equations for predicting fatigue behavior of irradiated 316 stainless steel tested at 650°C and a strain rate of 4×10^{-5} sec^{-1} (Ref. 20).

pares the fatigue data with predictions based on various formulas.

Figure IV-13 illustrates the significant improvements in postirradiation ductility that can be obtained by the preirradiation aging of vacuum-melted Incoloy 800, as determined at Oak Ridge.[21] The improvements are especially significant in specimens irradiated at lower temperatures. It has been reported previously that the addition of titanium to Hastelloy N results in considerable improvement in postirradiation stress-rupture life at elevated temperatures. However, subsequent tests[21] indicate that there is no improvement if the irradiation temperature is above 700°C. Stress-rupture properties of standard Hastelloy N at 650°C are not affected by increasing the irradiation temperature to 760°C, but titanium-modified alloys undergo a 1000-fold reduction in rupture life. This large dependence on the irradiation temperature has not been explained satisfactorily.

German investigators found[22] that the postirradiation elongation of nickel-base alloys can be increased by preirradiation thermomechanical treatments. Specimens of Inconel 625, Hastelloy X, and Inconel 718 were cold worked 50% and annealed at 700°C for 400 hr. They were then irradiated at 50°C to a fast fluence of 2×10^{21} neutrons/cm^2. Tensile tests were performed on the irradiated specimens at temperatures ranging from 600 to 750°C. Compared with specimens that were only annealed prior to being irradiated, the cold-worked-and-annealed specimens showed not only improved postirradiation strength but also significantly smaller reductions in ductility, especially at the higher test temperatures.

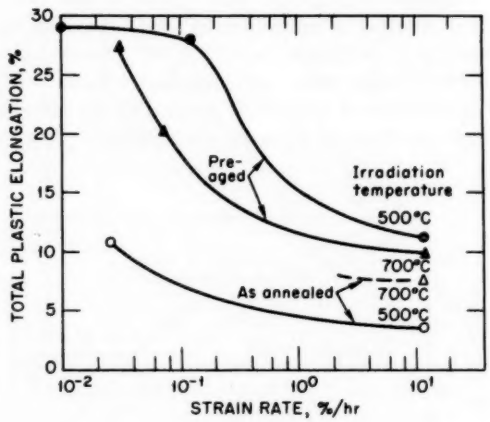

Fig. IV-13 Effect of preirradiation aging on ductility of Incoloy 800 at 650°C (Ref. 21). All specimens contained 0.1 wt.% titanium and 0.12 wt.% carbon and were annealed at 1150°C; some specimens were then aged 100 hr at 800°C before being irradiated at the indicated temperature to about 0.8×10^{21} neutrons/cm^2 (thermal and fast).

Studies are continuing on materials impregnated with helium in a cyclotron in order to simulate the helium-induced elevated-temperature embrittlement. Results of tensile tests performed by Atomics International[23] on the high-carbon 19-9DL stainless steel impregnated with helium are shown in Table IV-3. Note that considerably less embrittlement is caused by helium if the steel is annealed for 1 hr at 1100°C before the 100-hr treatment at 700°C.

The effect of helium on the stress-rupture properties of 304 stainless steel at 760°C is illustrated in Fig. IV-14. These results indicate that the presence of

Table IV-3 Influence of Helium on the Elevated-Temperature Tensile Properties of 19-9DL Stainless Steel[23]

Atom fraction helium	Test temp., °C	Yield strength, ksi	Tensile strength, ksi	Elongation, %	
				Uniform	Total
Cold rolled + 1 hr at 1100°C + 100 hr at 700°C					
0	800	18.5	25.3	8.8	58.9
3×10^{-5}	800	19.7	26.8	8.8	26.4
0	700	23.6	42.6	15.8	43.4
3×10^{-5}	700	22.4	39.2	14.6	30.1
0	600	26.1	60.4	25.0	28.2
3×10^{-5}	600	24.2	57.4	21.7	24.1
Cold rolled + 100 hr at 700°C					
0	800	24.6	28.7	3.1	39.0
3×10^{-5}	800	23.4	30.2	2.6	10.3
0	700	44.7	51.1	4.6	32.1
3×10^{-5}	700	41.5	50.6	3.8	10.9
0	600	58.5	75.4	7.6	10.7
3×10^{-5}	600	58.4	73.8	7.5	9.5

helium causes a reduction of rupture life, but increasing the helium content by a factor of 30 (from 1×10^{-6} atom fraction to 3×10^{-5}) does not result in further reductions.

Previous test results have shown that titanium-modified 304 stainless steel is not as susceptible to helium-induced embrittlement as regular 304 stainless steel. In an attempt to improve the resistance to helium embrittlement further, Oak Ridge workers[10] gave different heat-treatments to titanium-modified stainless steel. They then impregnated the specimens with 20 ppM helium and tested them in stress rupture at 600°C. One heat-treatment (10 hr at 700°C, ¼ hr at 925°C, and 10 hr more at 700°C) was superior to the others in improving the stress-rupture life of the unimpregnated alloy. However, the stress-rupture behavior of the helium-impregnated alloy was essentially independent of the annealing treatments tried and only slightly inferior to that of similarly treated steels without helium.

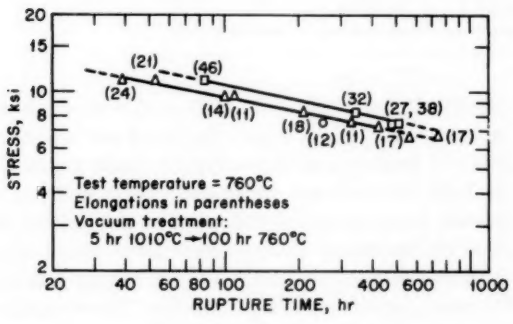

Fig. IV-14 Influence of helium on the stress rupture of 304 stainless steel at 760°C (Ref. 23). Atom fraction helium: □, zero; △, 1×10^{-6}; ○, 3×10^{-5}.

The effects of 24 ppM helium on the tensile properties of Inconel 102 and Inconel X-750 at elevated temperatures, as determined at Atomics International,[24] are shown in Tables IV-4 and IV-5. Just as it does in other materials, helium causes significant reductions in elongation of these alloys at elevated temperatures. Also, the formation of helium bubbles in helium-impregnated 405 stainless steel was found to be dependent on temperature of straining. Helium bubbles were formed by straining at 750°C, but no helium bubbles were formed when the straining was done at room temperature and the specimen was annealed at 750°C. These findings support the idea that bubble formation is the result of sweeping of helium atoms by moving dislocations.

Attempts have been made to correlate the change in ultrasonic shear velocity in irradiated 304 stainless steel with the postirradiation room-temperature ductility. Workers at Battelle–Northwest[25] found that both the postirradiation ductility and the shear veloc-

Table IV-4 Effect of Helium on the Elevated-Temperature Tensile Properties of Inconel X-750 (Ref. 24)

Atom fraction helium	Test temp., °C	Yield strength, ksi	Tensile strength, ksi	Elongation,%	
				Uniform	Total
Treated 1 hr 1100°C + 24 hr 800°C + 20 hr 700°C					
0	550	78.5	119	14	14
2.4×10^{-5}	550	75.0	105	9.4	9.7
0	650	79.7	114	9.7	9.9
2.4×10^{-5}	650	81.5	86.4		1.9
0	750	69.3	82.0	4.0	5.0
2.4×10^{-5}	750		61.3		1.2
Treated 24 hr 800°C + 20 hr 700°C					
0	550	128	150	4.9	5.2
2.4×10^{-5}	550	127	145	3.9	3.9
0	650	118	130	4.7	4.9
2.4×10^{-5}	650	114	114		2.2
0	750	76.0	85.7	3.8	5.1
2.4×10^{-5}	750		68.7		1.5

Table IV-5 Effect of Helium on the Elevated-Temperature Tensile Properties of Inconel 102 Treated 1 Hr at 1100°C + 100 Hr at 760°C (Ref. 24)

Atom fraction helium	Test temp., °C	Yield strength, ksi	Tensile strength, ksi	Elongation, %	
				Uniform	Total
0	550	30.4	86.1	47	48
2.4×10^{-5}	550	35.7	92.3	42	42
0	650	30.5	78.6	48	49
2.4×10^{-5}	650	32.8	66.1	24	25
0	750	29.4	57.8	17	52
2.4×10^{-5}	750	31.7	52.7	10	11

ity decrease with increasing fast fluence for material irradiated at temperatures below about 180°C. However, in specimens irradiated at about 320°C or higher, the shear velocity increases initially and then decreases with increasing fluence, whereas the elongation of the material irradiated at the higher temperature decreases continuously.

PRESSURE-VESSEL STEELS

The Naval Research Laboratory[26] has conducted cyclic annealing and irradiation tests on A-350LF1 (modified) steel. This is the same steel from which the pressure vessel of Stationary Medium Power Plant 1A (SM-1A) reactor was made. Typical results are shown in Table IV-6. It was noted that, for a given total fluence level, no overall reduction in the residual nil ductility transition (NDT) temperature [NDT temperature following 572°F (300°C) annealing] is gained by increasing the annealing frequency. Therefore there is no advantage in conducting annealing treatments more frequently than required to keep the vessel NDT temperature (or temperature for 30 ft-lb Charpy V-notch energy) below some preestablished limit.

Table IV-6 Effect of Irradiation and Annealing Cycles on Notch-Ductility Response of 2⅝-in. A-350LF1 (Modified) Ring Forging[26]

Condition of specimen	Temperature for Charpy V-notch energy of 30 ft-lb, °F
Unirradiated	−80
Irradiated (cycle 1) at 430°F to 1.3×10^{19} neutrons/cm^2 (>1 MeV)	+190
Annealed in reactor (cycle 1)	−10
Reirradiated (cycle 2) to 3.9×10^{19} neutrons/cm^2 (>1 MeV), cumulative	+320
Reannealed (cycle 2) 28 hr at 560°F + 144 hr at 572°F	+95

An excellent review article[27] on neutron-irradiation embrittlement of reactor pressure-vessel steels has been issued by the Naval Research Laboratory. The report discusses the aspects of fracture, irradiation effects on pressure-vessel steel as a function of microstructure, irradiation temperature, composition, and state of stress. The various pressure-vessel surveillance programs that have been completed and those which are presently in progress are also evaluated.

Factors influencing the performance of steel tendons during the 30-year life of a prestressed-concrete pressure vessel have been discussed in a book[28] published by the British Institute of Civil Engineers. These factors include the effects of irradiation on the mechanical properties of the steel tendons, relaxation of the prestressed tendons due to thermal effects, and relaxations due to the combined effects of temperature and irradiation.

EFFECTS OF RADIATION ON MISCELLANEOUS MATERIALS

To study the phenomenon of radiation-induced embrittlement at elevated temperatures, the Canadians[29] irradiated specimens of copper containing 0.8 at.% ^{11}B or 0.14 at.% ^{10}B. Since the specimens differed only in boron isotopic content, their preirradiation tensile properties were essentially the same. However, after irradiation the specimens had different helium contents, since the cross section for (n,α) reaction in ^{10}B is much larger than the cross section in ^{11}B. Results of postirradiation tensile tests, summarized in Table IV-7, indicate that the presence of 2.5 ppM helium has little influence on the ductility at temperatures up to 700°C. However, 330 ppM helium causes increasingly drastic reductions in ductility as the test temperature is raised from room temperature to 700°C. An increase in bubble size without changing the density of bubbles at grain boundaries was found to increase the extent of cavitation during testing. This suggests that a critical bubble size or stress is necessary for growth of bubbles.

Table IV-7 Postirradiation Tensile Properties of Cu–B Alloys Containing Various Amounts of Helium[29]

Composition	Fluence, neutrons/cm^2	Helium content, atomic ppM	Test temp., °C	Ultimate strength, ksi	Elongation, %
Cu–^{11}B	4.6×10^{17}	0.03	560*	3.2	17
Cu–^{10}B	4.6×10^{17}	2.5	560*	3.0	23
Cu–^{11}B	4.6×10^{17}	0.03	700†	4.0	28
Cu–^{10}B	4.6×10^{17}	2.5	700†	3.2	19
Cu–^{11}B	4.6×10^{17}	0.03	700‡	3.6	19
Cu–^{10}B	4.6×10^{17}	2.5	700‡	3.0	25
Cu–^{11}B	6×10^{19}	2.5	RT§	30.5	46
Cu–^{10}B	6×10^{19}	330	RT§	33.5	36
Cu–^{11}B	6×10^{19}	2.5	400§	11.0	32.5
Cu–^{10}B	6×10^{19}	330	400§	11.5	3.5
Cu–^{11}B	6×10^{19}	2.5	700§	3.6	20
Cu–^{10}B	6×10^{19}	330	700§	5.5	1.0

*Annealed 1 hr at 900°C before testing.
†Annealed 5 hr at 1000°C before testing.
‡Annealed 1 hr at 950°C before testing.
§Annealed 1 hr at 810°C before testing.

British investigators[30] have made calculations to predict compositional changes, due to neutron irradiation, in metals and alloys that are used as thermocouple materials. The metals include W, Re, Pt, Ru, Mo, Pd, Rh, and Ta. It is concluded that all of the materials investigated underwent sufficient compositional changes to cause significant drift in thermoelectric response.

The effect of fast-neutron irradiation on the properties of thermocouples was also investigated by the Russians.[31] Thermocouples of Cu, Fe, Constantan, Nichrome, Chromel, Alumel, Pt, Copel, Pt–13 Rh, Au, Au–40 Pd, and Mo were studied. The studies consisted in irradiating pairs of the above-mentioned materials to fast fluences of 10^{19} to 10^{20} neutrons/cm^2 and then determining their temperature–electromotive force curves. Irradiated thermocouples generally had lower thermoelectric power than their unirradiated counterparts. Pure gold and platinum were less affected than their alloys by irradiation. Postirradiation annealing was usually found to restore the preirradiation thermoelectric properties.

Stephen[32] reported on the effects of irradiation on the magnetic properties (coercivity, Curie point, saturation flux, and magnetic intensity) of a large number of magnetic alloys. He concluded that most ferritic magnets are satisfactory for low temperatures and low fluences but deteriorate at high fluences. The use of Si–Fe, Co–Fe, or Al–Fe is recommended for radiation environments in preference to the Ni–Fe and Ni–Co systems.

The effect of neutron irradiation on the silica-fiber-reinforced aluminum was investigated in Canada.[33] Irradiations were also carried out on silicon fibers. Results of tensile tests on irradiated (5×10^{20} fast neutrons/cm^2 at 25, 300, and 410°C) and unirradiated (heat-treated at 25, 300, and 410°C) composite materials indicate that irradiation causes only a small change in tensile properties. At the 25°C irradiation temperature, an increase in strength was observed and attributed to the radiation-induced increase in yield strength of the aluminum. However, the irradiation was found to cause a significant decrease in the strength of the silica fibers. Small density increases were noted for the composites that were irradiated, whereas the thermal controls underwent density decreases.

Effects of irradiation and postirradiation annealing on the cryogenic tensile properties of commercial titanium (55A) were investigated by Lockheed.[34] Measurements were made of the ultimate strength, yield strength, and ductility as a function of testing temperature for material irradiated at 17°K to a fast fluence of 6×10^{17} neutrons/cm^2. Modest increases in strength and decreases in ductility were produced by the irradiations. Tensile tests were also performed at 17°K after the irradiated specimens had been annealed for 1 hr at temperatures of 78 and 178°K. These test results show that the annealing caused measurable decreases in ultimate strength and that the yield strength and ductility were not significantly affected.

Tensile tests were performed by Westinghouse[35] on irradiated specimens of Ti–5 Al–2.5 Sn, ELI (extra-low interstitial). The specimens were irradiated to fluences ranging from 5.6 to 11×10^{17} neutrons/cm^2 at a temperature of 78°K. The ultimate and yield strengths were found to increase slightly, whereas the notched strength was unaffected by irradiation. The elongation was somewhat reduced by irradiation. About 60% of the radiation damage was annealed out in 1 hr at room temperature, and complete annealing occurred after 1 hr at 280°C.

Microhardness measurements were performed by Oak Ridge[10] at temperatures to 900°C on unirradiated vanadium specimens and on specimens that had been irradiated at 70°C to a fast fluence of 5×10^{19} neutrons/cm^2 ($E > 1$ MeV). It appears that the radiation-induced hardness increase in vanadium diminishes with increasing temperature and is essentially completely annealed out at about 500°C.

BASIC MECHANISMS OF RADIATION DAMAGE IN NONFUEL MATERIALS

A 1969 book entitled *Defects and Radiation Damage in Metals*[36] was published in England. It discusses point defects, extended defects, primary events, collision cascades, point defects in irradiated metals, point-defect clusters in irradiated metals, and impurity damage. A summary report[37] issued by Battelle–Northwest discusses the effect of irradiation on the substructure and its influence on mechanical properties of iron and steel. Of special interest is the theory that explains the mechanism of radiation-induced softening with further fluence after a maximum of radiation hardening has occurred. This softening is explained in terms of agglomeration of small defects into larger defects, which in turn offer less resistance to moving dislocations.

The British[38] have found that dislocation loops in irradiated or quenched metal crystals are swept out by the glide dislocations during deformation, leaving cleared channels. The removal of prismatic loops with the same Burgers vector as the glide dislocations can

occur by direct recombination, but the annihilation of loops with Burgers vector out of the glide plane has not been explained. It is proposed that their removal in face-centered cubic (fcc) crystals involves the formation of a junction around half the loop, followed by the gliding together and coalescence of this with the other half. Both steps are glissile and energetically favorable and give complete annihilation of the loop at the expense of a change in shape of the glide dislocation. Faulted loops may also be removed in this way if they first unfault in the presence of a glide dislocation. The mechanism is not diffusion controlled but requires a high loop mobility and may be affected by impurity pinning.

The effects of fast-neutron bombardment on the yield stress of fcc metals have been studied at Argonne.[39] The purpose was to resolve the controversy relating to the dose dependence of the yield stress, i.e., whether the yield stress (τ) increases as the fluence to the one-third power or whether the increase in yield stress ($\Delta\tau$) increases to the one-half power of the fluence, with a saturation term. A tensile machine was designed to operate in the CP-5 fast-flux facility in a bath of liquid helium so that yield stress could be determined at 4.2°K. The tensile machine had a strain sensitivity of 10^{-6}, so that microyield stresses could be observed. The macroyield stress of copper crystals, irradiated at 4.2°K, varied with the 0.333 power of the fluence for fluences ($E > 0.5$ MeV) ranging from 2.5×10^{14} (7-min full-power operating time) to 3.6×10^{17} neutrons/cm^2. Experiments at fluences between 7×10^{12} and 4×10^{13} neutrons/cm^2 showed that the change in yield stress ($\Delta\tau$) was not proportional to the fluence to the half power. But τ_{irrad} determined from the cube root of the difference between τ^3_{meas} and τ^3_0 shows a direct proportionality to the cube root of the fluence. The microyield stress of copper single crystals irradiated at 4.2°K shows a small, if any, increase for fluences less than 5×10^{15} neutrons/cm^2. For fluences from 5×10^{15} to 5×10^{16} neutrons/cm^2, the microyield stress increases as the cube of the fluence. Annealing experiments show that less than 1% yield-point recovery occurs between 4.2 and 100°K. It should be noted that about 50% of the radiation-induced resistivity recovers in this range.

Stress–strain characteristics, together with internal friction, were measured[40] on pure iron single crystals containing 0.1, 1, and 20 ppM carbon and irradiated to fluences of 0, 1.8×10^{17}, 1.3×10^{18}, and 1×10^{19} neutrons/cm^2 (>1 MeV) at ~70°C. Increases in yield stress and subsequent flow stress at larger strain were interpreted as having been caused mainly by barriers of irradiation defects against the movements of edge and screw dislocations, respectively, on the basis that the latter has a much larger Peierls stress than the former. Appreciable decreases in activation volume, associated with the flow stress observed in irradiated specimens, were attributed to the process of screw dislocation overcoming Peierls hill near the top of irradiation defects of sufficiently small size. The increase in the flow stress estimated from the present view coincides with the observed value. The carbon contents were found to have no large effects on hardening of iron crystals irradiated to less than 1.3×10^{18} neutrons/cm^2. However, they resulted in large effects in the course of recovery of yield stress and internal friction after anneals. These observations indicate that carbon atoms are first trapped and then detrapped by defect clusters during annealing.

Single crystals of iron with two different carbon concentrations (20 and <8 wppM) were deformed in tension[41] before and after neutron irradiation to a fast fluence of 2×10^{18} neutrons/cm^2. The dependence of the yield stress on neutron dose, deformation temperature, and strain rate was analyzed in detail. In unirradiated crystals the interaction of dislocations with carbon atoms in solution controls the temperature and strain-rate dependence of the yield stress. It can be concluded that, before irradiation in both types of samples, the same concentration of carbon is in solution, which is only a part of the total carbon content. Owing to the irradiation, it is suggested that the originally undissolved carbon becomes dispersed in the lattice and that complexes of carbon atoms and vacancies or iron interstitials are formed. These complex defect clusters act as the predominant dislocation obstacles.

The influence of nitrogen content on the irradiation response of iron has been investigated by workers at Oak Ridge.[42] The specimens were irradiated at 50°C to a fast fluence of 4×10^{17} neutrons/cm^2. The effects of irradiation on iron with 20 ppM nitrogen and no nitrogen added are compared in Fig. IV-15. The increase in yield strength upon annealing at 100°C and above indicates that nitrogen leaves the solid solution and becomes trapped by defect clusters. The defect-cluster–nitrogen complex then causes larger resistance to dislocation movement and thereby increases the flow stress.

Serrated yielding is found in unirradiated Cu–Ni alloys that are carburized. This effect is caused by the interstitial carbon atoms. Irradiation of a Cu–Ni alloy to a fast fluence of 2×10^{19} neutrons/cm^2 was found

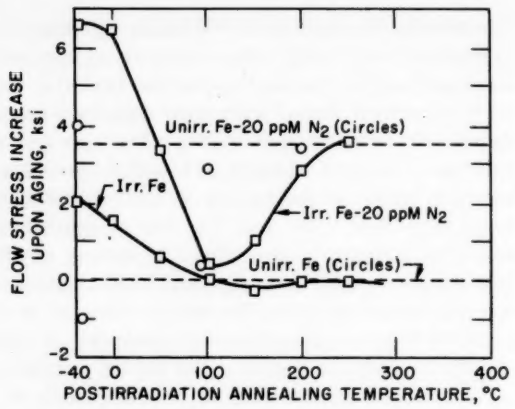

Fig. IV-15 Increase in flow stress for tensile specimens of fine-grain iron and iron containing 20 ppM nitrogen tested at −36°C (Ref. 42).

by the Australians[43] to cause substantial increases in yield strength and also to remove the serrated yielding. The removal of serrated yielding is attributed to trapping of the carbon atoms by the radiation-induced defect clusters.

The recovery in irradiated aluminum during annealing is influenced by small amounts of magnesium.[44] Stage II and stage III recovery are both increased by increasing magnesium content while the appearance of stage III prime is observed. The increase in stage II recovery results from the liberation of trapped interstitial faults by the magnesium during annealing.

An attempt has been made[45] to evaluate the amount of annealing that is occurring in a material while it is being irradiated at elevated temperature. The technique is to compare the results of high-temperature irradiations of low-alloy steels with the behavior of these steels irradiated at low temperatures and subjected to postirradiation anneals. On this basis, it is postulated that the variations in irradiation response of commercial low-alloy steels irradiated at temperatures above 200°C result from differences in the annealing characteristics of these steels during irradiation.

A phenomenological theory has been developed by the Japanese[46] for predicting the radiation-induced change of ductile-to-brittle transition temperature in ferritic steels. The theory predicts the change of neutron-irradiation sensitivity in terms of grain size, interstitial solute-atom concentration, spacing of precipitates, and dislocation density.

Postirradiation aging characteristics of a Cu–9.5 at.% Be–0.2 at.% Zn alloy were investigated by electrical-resistivity measurements.[47] The increase in resistivity caused by irradiation decreased with decreasing degree of supersaturation of beryllium in the matrix of the specimens. The isothermal aging curves of the resistivity of the irradiated specimens at 250°C showed two stages: an initial small decrease and a subsequent large decrease. The first stage was ascribed to the dissolution of Guinier–Preston zones formed during irradiation, and the early period of the second stage, to the precipitation of intermediate gamma-prime phase. The time needed for the initiation of the precipitation of gamma-prime phase was much shorter for the irradiated specimens than for the unirradiated specimens.

Considerable interest has developed in the phenomenon of void formation in materials during irradiation at elevated temperatures. If the fluence is sufficiently high and the temperature conditions ideal, enough voids are produced to result in volume changes of as much as a few percent. It is considered desirable to predict such volume changes so that they can be taken into account when designing components for fast breeder reactors which are expected to operate at high-temperature, high-flux irradiation conditions. Attempts have been made to develop formulas that will explain this radiation-induced volume change in stainless steel as a function of different variables. At present the irradiation temperature and the total fast fluence are believed to be the most important variables. Figure IV-16 shows Argonne's predicted volume change for

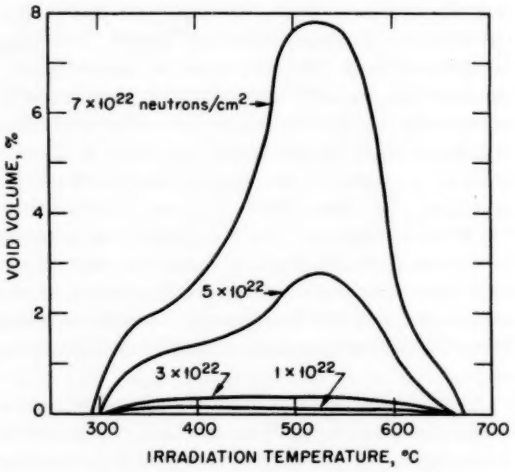

Fig. IV-16 Predicted effect of irradiation temperature and fluence on void volume in 304 stainless steel.[48]

304 stainless steel as a function of irradiation temperature and fluence.[48]

Although most of the data on radiation-induced swelling have been obtained from stainless-steel specimens, there is considerable effort to study the phenomenon in other materials so that a better understanding of the mechanism may be developed. In one study,[50] various fcc metals (nickel, copper, and aluminum) were irradiated at temperatures above $0.3T_m$ (T_m is the melting point in absolute temperature). The irradiated metals were examined by transmission electron microscopy, and all of them exhibited voids. Since similar voids have been reported in austenitic stainless steels, it appears that the formation of voids is characteristic of all fcc materials irradiated above $0.3T_m$.

Densities of nickel of various purities that had been irradiated at 430°C to a total fluence of 4.3×10^{22} neutrons/cm^2 have also been measured.[51] The samples consisted of Nickel 270 (99.98 wt.% nickel), Nickel 200 (99.6 wt.% nickel), and Inconel 600 (73 Ni–17 Cr–8 Fe) in the annealed and 50% cold-worked condition. Results of these density measurements, shown in Fig. IV-17, indicate that the amount of swelling increases with purity of the nickel but is independent of whether the material is annealed or cold worked.

The study of radiation-induced void formation has also been extended to body-centered cubic (bcc) materials. Commercially pure vanadium,[10,52] tungsten,[53] and molybdenum[53] have been irradiated at various conditions. Void densities in these samples, as determined by transmission electron microscopy, along with the irradiation conditions, are enumerated in Table IV-8. Voids were found in all cases except for the vanadium, which was irradiated at $0.32T_m$. As discussed earlier, a temperature of $0.3T_m$ appeared to be necessary for radiation-induced void formation in fcc materials. Annealing of the voids in irradiated vanadium is illustrated in Fig. IV-18, which shows that a temperature of 900°C is necessary to remove the voids.

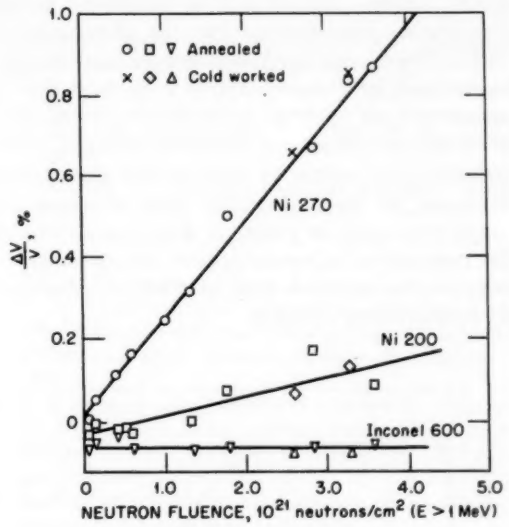

Fig. IV-17 Radiation-induced swelling in nickel-base alloys.[51]

The annealing of creep fracture damage in irradiated 20 Cr–25 Ni–Nb stainless steel has been investigated.[54] Both irradiated and unirradiated specimens were tested in creep at 750°C to establish their ductility at fracture. Then specimens were strained from 3 to 20% and annealed at 750°C for either 1 hr or 24 hr. For unirradiated specimens, very little recovery occurred if the prestrain was above 7%, no matter how long the specimens were annealed. However, when the prestrain was reduced to 3% for the unirradiated specimens, complete recovery in ductility occurred, even for the short annealing time of 1 hr. For irradiated specimens that were prestrained 3%, only

Table IV-8 Radiation-Induced Void Formation in Vanadium, Tungsten, and Molybdenum

Metal	Irradiation temp., °C	Irradiation temp., T/T_m	Fluence, 10^{20} neutrons/cm^2	Void diameter, Å	Void density, cm^{-3}	Vol. fraction, %	Ref.
Tungsten	1000	0.35	1.5	37	2×10^{16}	0.04	53
Tungsten	1300	0.43	1.6	100	1×10^{15}	0.05	53
Vanadium	430	0.32	2.5×10^{22}				52
Vanadium	690	0.44	1.7×10^{22}	NA	5×10^{15}	NA	10
Molybdenum	700	0.34	1.4	40	3×10^{16}	0.10	53
Molybdenum	1000	0.44	1.3	200	5×10^{14}	0.19	53

partial recovery occurred after an anneal of 1 hr, but complete recovery occurred after the 24-hr anneal at 750°C. The fracture mechanism in both irradiated and unirradiated specimens at 750°C is by formation of cavities at grain boundaries. The recovery of ductility in prestrained specimens is attributed to healing of the grain-boundary cavities by sintering during annealing. Therefore the longer annealing times necessary for complete recovery in irradiated specimens are due to the presence of helium in cavities. The presence of helium in the cavities is believed to hinder sintering of the cavities during annealing.

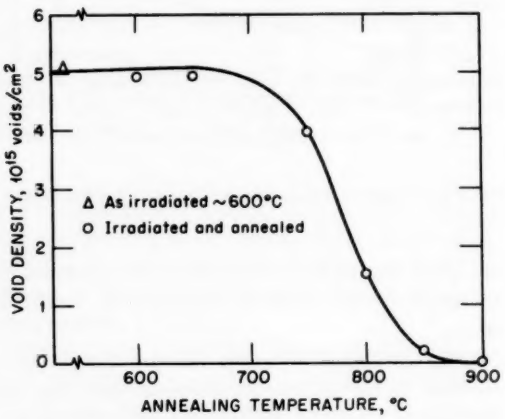

Fig. IV-18 Void density in vanadium as a function of postirradiation annealing temperature.[10] All anneals were for 1 hr at the temperature indicated. The segments of vanadium tubing were annealed before thinning for microscopic examination.

It has been suggested that preferential orientation of radiation-induced dislocation loops causes in-reactor creep of cold-worked Zircaloy. If the above hypothesis were true, one would expect the in-pile creep to be recovered when the irradiated sample is heated at a high enough temperature to anneal out the dislocation loops. Sections of cold-worked Zircaloy tubing which were used for in-pile creep tests at 260 to 290°C were annealed at 400 and 450°C (Ref. 55). The anneals did not result in recovery of the in-pile creep strain. However, these anneals were sufficient to restore the radiation-induced yield-strength increase, which is due to small dislocation loops. It was therefore concluded that the in-reactor creep of these cold-worked Zircaloy pressure tubes was not caused by the preferred alignment of those small damage regions which recover below 400°C.

REFERENCES

1. F. A. Nichols, Theory of the Creep of Zircaloy During Neutron Irradiation, *J. Nucl. Mater.*, 30: 249-270 (April 1969).
2. B. Watkins and D. S. Wood, The Significance of Irradiation-Induced Creep on Reactor Performance of a Zircaloy-2 Pressure Tube, paper presented at Philadelphia Zirconium Conference, October 1968 (to be published by ASTM).
3. G. R. Piercy, Physical Features in the Interactions of Point Defects in Metals with Special Reference to Zirconium, Canadian Report AECL-3227, November 1968.
4. Reference deleted.
5. C. D. Williams and R. W. Gilbert, Fast Neutron Damage in Zirconium-Based Structural Alloys, Canadian Report AECL-3308, June 1969.
6. R. G. Hoagland and R. G. Rowe, Fracture of Irradiated Zircaloy-2, *J. Nucl. Mater.*, 30: 179-195 (April 1969).
7. General Electric Company, Missile and Space Division, AEC Fuels and Materials Development Program Progress Report No. 78, USAEC Report GEMP-1010, Dec. 31, 1968.
8. Atomic Energy of Canada Limited, Fuels and Materials Division Progress Report, January 1–March 31, 1969, Canadian Report PR-FM-8, 1969.
9. C. E. Ells and C. D. Williams, Effect of Temperature During Neutron Irradiation on Subsequent Deformation in the Zr–2.5 Wt. Percent Nb Alloy, *Trans. Jap. Inst. Metals*, 9(Suppl): 214-219 (1968).
10. P. Patriarca and D. J. Rucker (Comp. and Ed.), Fuels and Materials Development Program, Quarterly Progress Report for Period Ending March 31, 1969, USAEC Report ORNL-4420, Oak Ridge National Laboratory, August 1969.
11. E. E. Bloom and J. R. Weir, Jr., Development of Austenitic Stainless Steels with Improved Resistance to Elevated-Temperature Irradiation Embrittlement, USAEC Report ORNL-TM-2328, Oak Ridge National Laboratory, December 1968.
12. D. L. Keller (Comp.), Progress on Development of Materials and Technology for Advanced Reactors During January Through March 1969, USAEC Report BMI-1862, Battelle–Columbus, April 1969.
13. Argonne National Laboratory, Reactor Development Program Progress Report, March 1969, USAEC Report ANL-7561, Apr. 22, 1969.
14. Battelle–Northwest, Reactor Fuels and Materials Development Programs for Fuels and Materials Branch of USAEC Division of Reactor Development and Technology, Quarterly Progress Report, January–March 1969, May 1969.
15. *CEMA Symposium: Status and Perspectives for Work on Atomic Power Stations with Fast Reactors, Collection of Reports,* Obninsk, 1967, Vol. II, USAEC Report JPRS-48331, July 1, 1969.
   a. V. D. Balashov, S. N. Votinov, P. P. Grinchuk, Z. Ye. Ostrovskiy, V. I. Prokhorov, V. K. Shamardin, N. P. Agapova, and T. A. Krasina, Effect of Radiation on Structure and Properties of Stainless Steels, pp. 553-575.
   b. N. P. Agapova, M. G. Bogolepov, F. P. Butra, V. P. Voyeykov, S. N. Votinov, Yu. M. Golovchenko, A. G.

Ioltukhovskiy, Yu. I. Kazennov, T. A. Krasina, N. Yu. Pal'chuk, V. I. Prokhorov, V. V. Romaneyev, V. G. Serbayev, D. D. Sokolov, Yu. N. Sokurskiy, and R. S. Sychev, Study of Stainless Steels Applicable to Core Conditions in Fast Reactors Developed in the USSR, pp. 512-552.

c. Sh. Sh. Ibragimov, V. N. Bykov, A. N. Vorob'yev, I. M. Voronin, and A. M. Veremeyev, Effect of Radiation on the Properties of Structural Materials, pp. 495-511.

16. F. Garzarolli, K. P. Francke, and J. Fisher, Neutron Embrittlement of Two Austenitic Iron-Base Alloys at Elevated Temperatures, *J. Nucl. Mater.*, **28**: 280-290 (1968).
17. Battelle–Northwest, May 7, 1969, unpublished.
18. J. Standring, I. P. Bell, H. Tickle, and A. Glendinning, The Effects of Neutron Irradiation on the Creep-Rupture Properties of Type 316 Stainless Steel Tubes, British Report TRG-Report-1789, Nov. 14, 1968.
19. A. C. Roberts, D. R. Harries, D. R. Arkell, and M. A. P. Dewey, Effects of Yttrium on the Structure and Postirradiation Tensile Properties of an Iron–Chromium–Aluminum Alloy, from Proceedings of the American Society for Testing and Materials Conference, June 1968, ASTM Special Publication No. 457, December 1969.
20. J. T. Berling and J. B. Conway, A Proposed Method for Predicting the Low-Cycle Fatigue Behavior of 304 and 316 Stainless Steel, *Trans. Met. Soc. AIME*, **245**: 1137-1140 (May 1969).
21. P. Patriarca and D. J. Rucker (Comp. and Ed.), Fuels and Materials Development Program, Quarterly Progress Report for Period Ending December 31, 1968, USAEC Report ORNL-4390, Oak Ridge National Laboratory, May 1969.
22. H. Boehm, H. Hauck, and H. J. Lane, Influence of Thermo Mechanical Treatment on High-Temperature Embrittlement of Nickel Alloys After Irradiation (in German), *Metall.*, **22**: 1192-1196 (December 1968).
23. Atomics International, AEC Unclassified Programs, Quarterly Technical Progress Report, July–September 1968, USAEC Report AI-AEC-12744, Jan. 13, 1969.
24. Atomics International, AEC Unclassified Programs, Quarterly Technical Progress Report, October–December 1968, USAEC Report AI-AEC-12777.
25. D. O. Hunter, Ultrasonic Velocities and Critical-Angle-Method Changes in Irradiated 304 Stainless Steel, USAEC Report BNWL-1012, Battelle–Northwest, March 1969.
26. L. E. Steele, J. R. Hawthorne, and C. Z. Serpan, Irradiation Effects on Reactor Structural Materials, Quarterly Progress Report, November 1 1968–January 31, 1969, USAEC Report NRL-Memo-1962(AD-685591), Naval Research Laboratory, Feb. 15, 1969.
27. L. E. Steele, Neutron Irradiation Embrittlement of Reactor Pressure Vessel Steels, *At. Energy Rev. (IAEA)*, **7**(2): 1-133 (1969).
28. M. S. Udall, *Prestressed Concrete Pressure Vessels*, pp. 219-228, 229-235, Institute of Civil Engineers, London, 1968.
29. G. J. C. Carpenter, and R. B. Nicholson, the High Temperature Embrittlement of Metals by Rare Gas Bubbles, Canadian Report AECL-3331, April 1969.
30. C. B. T. Braunton, D. N. Hall, and C. M. Ryall, Estimation of Compositional and Volume Changes in Noble and Refractory Metal Alloys Due to Neutron Irradiation, British Report AERE-R-5837, September 1968.
31. N. F. Pravdyuk, A. N. Ivanov, and K. P. Dubrovin, Effects of Reactor Irradiation on Thermocouple Materials (in Russian), *At. Energy. (USSR)*, **25**: 233-235 (September 1968).
32. J. Stephen, The Irradiation Properties of Magnetic Materials, *Nucl. Energy (U. K.)*, pp. 76-82 (May–June 1969).
33. M. R. Piggott and A. E. Hunton, Properties of Irradiated Silica Fibre Reinforced Aluminum, *J. Nucl. Mater.*, **29**: 334-344 (March 1969).
34. C. A. Schwanbeck, Low Temperature Annealing of Irradiated Commercially Pure Titanium, Report NASA-CR-72428(N68-33385), Lockheed Nuclear Products, May 1968.
35. R. P. Shogan, Tensile Properties of Irradiated Ti–5 Percent Al–2.5 Percent Sn ELI at Cryogenic Temperatures, Report WANL-TME-1860, Westinghouse Electric Corp., Astronuclear Laboratory, November 1968.
36. M. N. Thompson, *Defects and Radiation Damage in Metals*, Cambridge University Press, England, 1969.
37. F. A. Smidt, Jr., Dislocation Substructure Interactions in Irradiated Iron and Steel, USAEC Report BNWL-1045, Battelle–Northwest, June 1969.
38. A. J. E. Foreman and J. V. Sharp, Mechanism for Sweeping Up of Loops by Glide Dislocations During Deformation, *Phil. Mag.*, **19**: 931-938 (May 1969).
39. T. H. Blewitt and C. A. Arenberg, Irradiation Hardness in Copper, *Trans. Jap. Inst. Metals*, **9**(Suppl): 226-233 (1968).
40. K. Kitajima, Neutron Irradiation Effects on the Plastic Properties of Pure Iron, *Trans. Jap. Inst. Metals*, **9**(Suppl.): 182-186 (1968).
41. J. Diehl, Neutron Irradiation Hardening of Iron Single Crystals Containing Small Amounts of Carbon, *Trans. Jap. Inst. Metals*, **9**(Suppl.): 219-225 (1968).
42. Oak Ridge National Laboratory, Radiation Metallurgy Section, Solid State Division Progress Report for Period Ending October 1968, USAEC Report ORNL-4369, April 1969.
43. J. S. Blakemore and E. O. Hall, The Effects of Irradiation Damage on the Postevin–LeChatelier Effect in Carburized Nickel Copper Alloys, *J. Nucl. Mater.*, **29**: 238-240 (February 1969).
44. C. Dimitrov, L. Minel, and O. Dimitrov, Reaction Between Point Defects and Magnesium Atoms in Aluminum Irradiated by Neutrons at 78°K, *Compt. Rend., Ser. C.*, **267**: 1759-1762 (December 1968).
45. A. E. Powers, Postirradiation and Co-Irradiation Annealing of Iron and Steel, USAEC Report KAPL-3440, Knolls Atomic Power Laboratory, September 1968.
46. N. Igata and R. Hasiguti, A Phenomenological Theory of Neutron Irradiation Sensitivity of Ductile–Brittle Transition Temperature of Ferritic Steels, *Trans. Iron Steel Inst. Jap.*, **8**: 386-391 (November 1968).
47. H. Yashida, Aging Characteristics of Neutron Irradiated Copper–9.5 At. Percent Beryllium Alloy, *Phil. Mag.*, **19**: 987-992 (May 1969).
48. Argonne National Laboratory, Reactor Development Program Progress Report, July 1969, USAEC Report ANL-7595, Aug. 25, 1969.

49. Reference deleted.
50. J. L. Brimhall and B. Mastel, Voids in Neutron Irradiated Face Centered Cubic Metals, *J. Nucl. Mater.*, **29**: 123-125 (January 1969).
51. Battelle–Northwest, Apr. 7, 1969, unpublished.
52. Argonne National Laboratory, Reactor Development Program Progress Report, January 1969, USAEC Report ANL-7548, Feb. 28, 1969.
53. R. C. Rau, R. L. Ladd, and J. Moteff, Voids in Irradiated Tungsten and Molybdenum, USAEC Report GEMP-692, General Electric Company, Missile and Space Division, 1969.
54. H. E. Evans and J. S. Waddington, The Annealing of Creep Fracture Damage in a Stainless Steel, *J. Nucl. Mater.*, **30**: 337-339 (April 1969).
55. G. R. Piercy and J. Lori, Strain Caused by Recovery of Radiation Damage in Zircaloy Pressure Tube, Canadian Report AECL-3226, December 1968.

Section

V

Reactor Materials

Nonfueled Refractories

By D. E. Niesz

TRANSITION-METAL CARBIDES

Harrod and Fleischer[1a] studied the role of diffusion in the plastic deformation of transition-metal carbides. They discussed the relation between the general deformation behavior of carbides and diffusion data on selected Groups IVB and VB metals.

In an investigation of the plastic properties of WC, Pons[1b] subjected specimens to precise micrographic observations during tests for indentation, impact, and friction. These tests were made on large-grained sintered test specimens of recently manufactured industrial WC, with or without cobalt binders. The WC showed plasticity at ordinary temperatures, as revealed by the appearance of rectilinear slip lines in the vicinity of Vickers indentations or else during mechanical impact tests. X rays were used to determine the orientation of a WC crystal, and it was found that the slips occurred along the three prismatic planes $(10\bar{1}0)$. The slip directions were determined as being directions [0001] and $\langle 11\bar{2}0\rangle$, which correspond to the two more or less equivalent minimum Burgers vectors.

The recrystallization and sintering of WC at high temperatures, the morphology of WC crystals, and the growth of grains at high temperatures were studied. The brittleness of WC depends on the crystallographic orientations. The hardest planes (0001) offer the most possibilities of plastic deformation and are more easily fractured than prismatic planes. Intragranular fracture of WC is always accompanied by plastic deformation, the extent of which depends on the orientation of the crystals.

Hollox and Venables[2] studied the mechanical behavior of pure $VC_{0.85}$ doped with boron over the temperature range 1000 to 1700°C. The critical resolved shear stress for $VC_{0.85}$ was found to be about 25 kg/mm^2 at 1250°C, but it decreased rapidly with increasing temperature to about 3 kg/mm^2 at 1500°C. The strength of undoped $VC_{0.85}$ was anomalously high compared with that of other carbides, possibly because carbon vacancy ordering occurs in this material, and this phenomenon significantly influences dislocation mobility. It was found that the vacancy-disordering temperature coincides with the brittle-to-ductile transition temperature. In boron-doped $VC_{0.85}$, boride precipitates form on {111} and {100} planes, the plane of precipitation being dependent upon boron concentration. These precipitates increase the critical resolved shear stress at 1500°C from about 3 to 19 kg/mm^2.

Samsonov et al.[3] investigated the temperature dependence of the external friction of pairs of similar samples of NbC and TaC from room temperature to 1800°C in a vacuum of 10^{-5} torr. A minimum friction coefficient for NbC against itself was observed at 1200°C and for TaC at 1300°C. It was established that, in static contact under loading at high temperature, creep takes place, controlled by thermally activated dislocation slip. The energy of slip activation is 1.3 eV for NbC and 1.4 eV for TaC.

SILICON CARBIDE

In a study of the effect of multiaxial stresses on fracture strength at room temperature, Priddle[4] used combinations of stresses in the form of torsion, hoop, axial tension, and compression to determine the failure envelopes for silicon carbide. Current failure theories are not adequate for describing the results in both the tension-tension and tension-compression quadrants.

The influence of specimen geometry and structure on the impact resistance of silicon carbide between room temperature and 1000°C was studied by Ashford and Priddle.[5] They found that the impact resistance could be described in terms of two criteria: stored energy and Hertzian contact stress. The influence of microstructure on impact resistance is discussed, and equations are developed that describe the main impact-resistance criteria.

Marshall and Jones[6] studied the creep behavior of high-density SiC in air between 1000 and 1300°C using four-point bending. Behavior under stresses between 30,000 and 72,000 psi was investigated. The creep strain (Ep) was found to increase with time (t) according to $Ep = At^R$, where R is between 0.2 and 0.5. The dependence of A on stress (σ) and absolute

temperature (T) was found to be $A \propto \sigma^n \exp(-Q/RT)$, with n between 1 and 2 and $Q \approx 55$ kcal/mole. The results were compared with estimates of creep in SiC obtained by extrapolation of steady-state creep data from higher temperatures.

CERMETS

Kieffer et al.[7] investigated cermets containing NbC and HfC and found that NbC, which is relatively inexpensive and available, can be used in place of the more expensive TaC. Their conclusions were based on tests with the pseudoquaternary system TiC–TaC–NbC–WC and the pseudoternary system TiC–HfC–WC. These studies showed that NbC can replace TaC in WC–TiC–TaC up to 30 wt.%, and HfC can replace TaC completely. HfC–TaC solid solution showed the best behavior, but NbC–HfC instead of TaC also gave good results.

Nabarro and Luyckx[8] surveyed experimental data on the strength of WC–Co and derived the requirements for a satisfactory theory to describe the data. The volume fraction of cobalt (f_{Co}) and the tungsten carbide grain size (L_{WC}) were taken as the controlling variables. Their results showed that the mechanisms of fracture were different for high and low values of f_{Co}. Materials in which the fracture propagates along the interface between carbide and cobalt were not considered. The published models of the fracture process, and some new models, were discussed, and their predictions compared with experimental observations. Many of the observations were explained qualitatively. At low f_{Co} the strength was found to be controlled by the plasticity of the cobalt layers, which limits the ease of propagation of a crack. A relation describing the temperature dependence of the strength was not found.

The dependence of carbide–carbide particle contacts on the mechanical properties of WC–Co was studied by Doi.[9] Compressive tests and internal-friction measurements were made on several WC–Co alloy specimens with some critical structure, in which the carbide particles occupy 79 to 87 vol.%. It was found that yielding of the WC–Co alloy can be largely explained on the basis of Orowan's dislocation bypass model for alloys containing nondeforming particles, and strain hardening characteristics may also follow the model for the dispersion-hardened alloy. This concept is not compatible with the view that a continuous carbide skeleton has been formed within the alloy Because of the very large volume fraction of the carbide phase, however, movements of dislocations in the binder phase are greatly hindered, which results in a very rapid increase of dislocation density in the binder phase with increasing strain. Furthermore, a new concept of fracture of the alloy was proposed whereby the mode of fracture (intergranular or transgranular) is determined by competition between shear rupture along the intergranular regions and compressive rupture of the carbide particles. The binder content and the carbide particle size govern which type of rupture predominates.

Japanese investigators[10] have studied the fatigue behavior of WC–Co as a function of cobalt content, using a rotating-beam fatigue machine. The strength/number-of-cycles (S–N) curves did not show flat portions like those found for iron and steel. The fatigue strength (using 10^8 cycles as the fatigue limit) increased with cobalt content and was linearly related to the tensile strength. X-ray analysis showed that the cobalt phase was progressively transformed from γ (fcc) to ϵ (hcp) during fatigue.

ZIRCONIUM DIOXIDE

Hart and Chaklader[11] studied the enhanced plasticity in ZrO_2 during the monoclinic $\rightleftharpoons$ tetragonal transformation. They found that the plasticity was considerably enhanced during the inversion and that it was somewhat dependent on density of the material.

Soviet investigators[12] noted that the mechanical stability of ZrO_2 increases with the percentage of monoclinic phase up to 20 wt.%.

Garvie[13] investigated the improved thermal-shock resistance of partially stabilized ZrO_2 and observed that the decreased expansion obtained when the percentage of monoclinic phase is increased could not begin to account for the large improvement noted in the thermal-shock resistance. He concluded that the improved thermal-shock resistance was due to accommodation of thermal strain by the volume change associated with the monoclinic $\rightleftharpoons$ tetragonal transformation. Because of the pressure dependency of this transformation, it can be depressed to around room temperature under the high localized stresses that develop within the ZrO_2 during thermal shock.

A Soviet study[14] of the high-temperature erosion of ZrO_2 in gas streams revealed that separate grains as well as vapor species are removed from the ZrO_2. The erosion products were classified according to their geometric patterns. The effects of these erosion products on the durability of components downstream from the ZrO_2 were predicted from the data.

REFERENCES

1. F. W. Vahldiek and S. A. Mersol (Eds.), *Anisotropy in Single-Crystal Refractory Compounds*, Symposium Proceedings, Dayton, Ohio, June 13–15, 1967, Plenum Press, New York, 1968.
   a. D. L. Harrod and L. R. Fleischer, On the Role of Diffusion in the Plastic Deformation of Transition Metal Carbides, pp. 341-356 of Volume 1.
   b. L. Pons, Plastic Properties in Tungsten Monocarbide, pp. 393-444 of Volume 2.
2. G. E. Hollox and J. D. Venables, Microstructure and Mechanical Properties of Pure and Boron-Doped $VC_{0.85}$, *Trans. Jap. Inst. Metals*, 9(Suppl.): 295-300 (1968).
3. G. V. Samsonov, M. S. Kovalchenko, and Y. G. Tkachenko, Investigation of External Friction of Niobium and Tantalum Carbides at High Temperatures in a Vacuum (in Russian), *Porosh. Met., Akad. Nauk Ukr. SSR*, 2: 49-56 (February 1969).
4. E. K. Priddle, Effect of Multiaxial Stresses on Fracture Strength of Silicon Carbide, *J. Strain Anal.*, 4: 81-87 (April 1969).
5. J. P. Ashford and J. P. Priddle, Influence of Specimen Geometry and Structure on the Impact-Resistance of Silicon Carbide, *Powder Met.*, 12: 169-192 (April 1969).
6. P. Marshall and R. B. Jones, Creep of Silicon Carbide, *Powder Met.*, 12: 193-208 (April 1969).
7. R. Kieffer, G. Trabesinger, and N. Reiter, NbC- and HfC-Containing Cermets and Cemented Carbides, *Planseeber. Pulvermet.*, 17: 23-35 (April 1969).
8. F. R. N. Nabarro and S. B. Luyckx, Theory of the Strength of Tungsten Carbide–Cobalt Compacts, *Trans. Jap. Inst. Metals*, 9(Suppl.): 610-615 (1968).
9. H. Doi, On the Strengthening Mechanism of WC–Co Alloy, *Trans. Jap. Inst. Metals*, 9(Suppl.): 616-622 (1968).
10. K. Miyake, Y. Fujiwara, and K. Nishigaki, On the Fatigue of WC–Co Alloys (in Japanese), *Nippon Kinzoku Gakkaishi*, 32: 1128-1131 (1968).
11. J. L. Hart and A. C. D. Chaklader, Superplasticity in Pure ZrO_2, *Mater. Res. Bull.*, 2: 521-526 (1967).
12. Y. V. Klyucharov and V. I. Strakhov, Changes in the Engineering Properties of Zirconium Refractories in Relation to the Degree of Stabilization of ZrO_2 (in Russian), *Izv. Akad. Nauk SSSR, Neorg. Mater.*, 4: 1502-1506 (September 1968).
13. R. C. Garvie, A Theory of the Enhanced Thermal Shock Resistance of Partially Stabilized Zirconia Ceramics, paper presented at the Basic Science Meeting of the American Ceramic Society, Ottawa, September 29–30, 1969, abstracted in *Amer. Ceram. Soc. Bull.*, 48(8): 825 (Aug. 7, 1969).
14. R. I. Abraitis and I. S. Mayauskas, Erosion of the Refractory Zirconium Oxide Ceramics. 4. Some Peculiarities of Gas Erosion (in Russian), *Liet. TSR Mokslu Akad. Darbai, Ser. B*, No. 3: 103-108 (1968).

Section

VI

Reactor Materials

Concrete

By D. R. Lankard

CREEP OF CONCRETE

England and Phok[1] have discussed numerical techniques for estimating the redistribution of stresses due to creep in a cylindrical prestressed-concrete pressure vessel (PCPV) that is subjected to a radial temperature gradient and an internal pressure. For a model vessel with the inside face at 80°C and the outside face at 40°C, the effect of creep was a gradual transfer of stress from hot to cooler portions of the concrete. The authors point out that the redistribution of stress can produce undesirable reversals of stress when the vessel is cooled, which are accompanied by cracking on the inside face.

Several investigations[2-5] have demonstrated that the amount and rate of creep deformation in concrete sealed against moisture loss is increased as the temperature in the concrete is increased up to 212°F (100°C). Limited experimental data and the wide range of test procedures employed make it difficult to draw other than general conclusions regarding the nature of the phenomenon.

There appears to be some question as to whether or not the increase in creep and creep rate with increase in temperature is monotonic. In one series of investigations[2,3] the amount of creep in concrete under large compressive loads (60 or 70% of ultimate strength) for 15 months was greatest in specimens maintained at 160°F (70°C) relative to specimens maintained at 115 or 205°F (45 or 95°C). At lower stress levels (35% of ultimate strength), the creep increased monotonically with increasing temperature.

Other workers[4,5] observed that the creep of sealed concrete increases monotonically with increasing temperature up to 212°F. England[4] reported an increase in creep and creep rate in concrete loaded in compression at 1000 psi as the sustained temperature level was increased from 68, 127, and 171°F (20, 53, and 77°C) to 201°F (93°C). Similar results were reported by Browne[5a] for concrete loaded in compression (2116 psi) for up to 1000 days. The monotonic increase in creep and creep rate with increased temperature has also been reported for concrete subjected to multiaxial compressive loads.[5b,5c]

RADIOACTIVITY IN CONCRETES

Workers in the Health Physics Department at Lawrence Radiation Laboratory have described[6] their efforts in formulating low-radioactivity concretes for use in the construction of low-background counting facilities. In considering concrete for this application, the quantity of long-half-life radioactive elements (potassium, thorium, and uranium) in the cement and aggregate materials is of primary importance. Uranium and thorium contribute more radioactivity than does potassium in concrete raw materials in spite of their low concentrations, owing to their specific gamma radioactivity relative to potassium.

Serpentinized ultramafic rock (from California) was found suitable for use in construction of the low-background counting facility at LRL. Ultramafic rocks as a group are thought to be generally suitable for this application because of their inherent low concentrations of uranium, thorium, and potassium. Other potentially useful aggregates are barite, magnetite, hematite, ilmenite, steel-mill scale, and some silica sands.

The radioactivity of portland cements and their precursor raw materials was studied extensively. The gamma-ray counting rates of 12 commercial cements ranged from about 0.28 to 0.78 count/(min)(g). The primary source of radioactive contamination in the cement raw materials was shown to be the silica and alumina used. However, because of its high proportion in the raw cement mix, the calcium oxide exerts more control over the contamination of the cement. It was concluded that water and admixtures do not contribute significantly to the radioactivity of the concrete.

REFERENCES

1. G. L. England and M. Phok, Time-Dependent Stresses in a Long Thick Cylindrical Prestressed Concrete Vessel Subjected to Sustained Temperature Crossfall, *Nucl. Eng. Design*, 9(4): 488-495 (April 1969).
2. K. W. Nasser and A. M. Neville, Creep of Concrete at Elevated Temperature, *J. Amer. Concrete Inst.*, **62**(12): 1567-1579 (December 1965).
3. K. W. Nasser and A. M. Neville, Creep of Old Concrete at Normal and Elevated Temperatures, *J. Amer. Concrete Inst.*, **64**(2): 97-103 (February 1967).
4. G. L. England, A Study of Time-Dependent Strains in Concrete Maintained at Elevated Temperature and the Effect on Reinforced Concrete, Ph.D. Thesis, University of London, 1961.
5. *Prestressed Concrete Pressure Vessels*, published by the Institution of Civil Engineers, London, 1968.
   a. R. D. Browne, Properties of Concrete in Reactor Vessels, Paper C-13, pp. 131-151.
   b. N. T. Barrett and J. T. Murray, Creep in Pressure Vessels at Elevated Temperatures, Paper C-14, pp. 153-166.
   c. D. J. Hannant, Strain Behavior of Concrete Up to 95°C Under Compressive Stresses, Paper C-17, pp. 177-191.
6. H. A. Wollenberg and A. R. Smith, Low-Radioactivity Concrete *J. Mater.*, 3(4): 757-779 (December 1968).

Section
VII
Reactor Materials

Corrosion of Base-Metal Alloys in Aqueous and Gaseous Media

By W. E. Berry

CORROSION OF ZIRCONIUM ALLOYS

The long-term pretransition corrosion behavior of Zircaloy-2 and Zircaloy-4 in degassed deionized water at 232 to 316°C has been described by Bettis.[1] Exposures were for 1000 days at the lower temperatures and 500 days at the higher temperatures. The results indicate that the pretransition corrosion follows a cubic rate law with an Arrhenius temperature dependence, according to:

$$(\Delta W)^3 = 6.357 \times 10^{11} \exp(-13{,}640/T)t$$

where ΔW is the weight gain in milligrams per square decimeter, T is the absolute temperature in degrees Kelvin, and t is the time in days.

The oxidation and deuterium absorption of Zircaloys in steam (D_2O) at 300 and 340°C in the posttransition region (100 mg/dm^2) have been studied at Harwell.[2] Specimens were preoxidized in H_2O (steam) at 450°C to attain the posttransition region. Beta-quenched Zircaloy-2 and beta low-nickel Zircaloy-2 had lower deuterium-absorption rates but higher oxidation rates than beta-quenched Zircaloy-4, alpha-annealed Zircaloy-2, alpha low-nickel Zircaloy-2, and alpha Zircaloy-4.

The corrosion and hydriding behavior of Zircaloy-2 and Zircaloy-4 under heat transfer in aqueous solutions has been investigated at Babcock & Wilcox.[3] The surface heat flux was 600,000 Btu/(hr)(ft^2). Water temperature was 640°F (340°C), and flow rate was 13 ft/sec. Tests were conducted for periods up to 180 days in high-purity water and for 51 days in 13,000 ppM boric acid, 4 to 6 ppM potassium hydroxide, and 0.5 ppM lithium hydroxide. Both environments contained 20 to 40 cm^3 of hydrogen/kg of water. The results indicated that (1) corrosion rates under heat-transfer and isothermal conditions were the same, (2) more hydrogen was absorbed under heat-transfer conditions, and (3) the chemical shim solution (H_3BO_3) did not affect the corrosion rate or the hydrogen-absorption rate.

The morphology and mechanism of the growth of oxide films on zirconium and Zircaloy-2 have been discussed by Chalk River.[4] The proposed model indicates that amorphous oxide forms at the oxide–metal interface and subsequently crystallizes. This crystallization occurs homogeneously within the initial amorphous film, but, as the oxide film thickens, a cellular structure and a columnar growth pattern develop. Ionic transport (migration of oxygen ions) occurs via the columnar crystallite boundaries. Electron transport occurs via second-phase intermetallic particles (Zr–Fe–Cr or Zr–Fe–Ni) which are only partially oxidized and maintain electrical contact with the base metal while embedded in the oxide matrix. Electrons migrate laterally to oxygen-adsorption sites at the oxide–environment interface to complete the circuit.

The effect of changing the corrosive medium from 200 atm of steam to 1 atm of air and vice versa on the oxidation of Zr–1 Nb at 450 and 500°C has been studied in Egypt.[5] The corrosion rate was higher in steam than in air. An incubation period with no measurable oxidation was observed when the specimens were transferred from steam to air. This incubation period varied linearly with the square of the thickness of the steam-formed oxide. The activation energy obtained for calculations of the diffusion rates through this film was close to that reported for the diffusion of oxygen in zirconium oxide. There was no incubation period when specimens oxidized in air were transferred to steam. The results indicated that defects formed in the oxide during steam oxidation do not take part in the oxide-film growth upon subsequent exposure to air but that those formed in air do participate in the oxide-film growth upon subsequent exposure to steam.

CORROSION OF STAINLESS STEELS

An accelerated test procedure for studying the stress-corrosion cracking behavior of austenitic stainless

steels in high-temperature water has been described by General Electric.[6] Specimens were loaded in uniaxial tension and exposed in autoclaves to high-purity water containing 100 ppM dissolved oxygen at 289°C. Annealed 304 stainless steel did not crack under any conditions investigated. Sensitized or thick welded plates of 304 stainless steel exhibited intergranular stress-corrosion cracking. However, sensitized duplex alloys (austenite + ferrite), welded 304L stainless steel, and Uranus alloys (18 Cr–8 Ni–2 to 4 Si) did not crack in exposures of up to 300 hr.

The oxidation behavior of stainless steels and nickel-base alloys in steam has been studied in Sweden.[7] Alloys investigated were 15/15, 18/11, 20/25, 20/25 Nb, 20/35, Incoloy 800, 16/75, and 13 Cr/4 Al. In general, the oxidation rates were within the range of those reported by other investigators. The oxidation resistance did not show any simple relation to alloy composition but varied among alloys according to temperature and time of exposure. Ground specimens had lower oxidation rates than did pickled ones at temperatures up to 650°C. At 700°C the rates for the two surface conditions were about equal after long-term exposure, but at 800°C the rates became equal after short-term exposure. The improved oxidation resistance of ground surfaces at the lower temperatures was attributed to enhanced diffusion of chromium due to dislocations at the metal surface. Erosion in steam at 50 m/sec, 30 atm, and 310 and 640°C had little effect on the oxidation rates of 18/11, 20/25, 20/25 Nb, and 20/35 steels. After 2100 hr, the erosion–oxidation rates for these steels ranged from 0.01 to 1.0 mg/(dm^2)(month).

The reactions between oxides of the metallic components in 20/25 Nb stainless steel have been studied in England.[8] Oxides of Fe, Ni, Cr, Mn, and Si were studied at $\geqslant$1000°C in a vacuum of 10^{-5} torr. X-ray powder-diffraction techniques were used to identify the products. The reaction of MnO + FeO and MnO + NiO to form a solid solution went to completion quickly at 1000°C. However, FeO + NiO yielded $NiFe_2O_4$ + NiO + Ni, showing that FeO partially reduced the NiO. FeO + Cr_2O_3 and MnO + Cr_2O_3 readily combined to form MCr_2O_4 spinels at 1000°C. The reaction of NiO + Cr_2O_3 to form a spinel did not occur at all at 1000°C and required a temperature of 1350°C to go to completion. MnO and Fe_3O_4 reacted readily with SiO_2 at 1000°C, and NiO reacted only slightly at 1200°C. The resulting compounds were identified as M_2SiO_4 plus large amounts of an unidentified phase.

CORROSION OF NICKEL ALLOYS

The corrosion behavior of Inconel Alloy 600 in high-temperature borated water has been reported by the International Nickel Company.[9] Corrosion studies were run for periods up to 5000 hr at flow velocities of 20 ft/sec in 600°F (315°C) water containing 1500 ppM boron (as H_3BO_3), 0.7 ppM lithium (as LiOH), and 25 cm^3 of hydrogen/kg of water. Grit-blasted or surface-ground specimens exhibited higher initial rates of attack [22 to 35 mg/(dm^2)(month)] than did annealed specimens [14 mg/(dm^2)(month)]. However, in 1000 to 2000 hr, the corrosion rates of all samples decreased to about 1 mg/(dm^2)(month) regardless of surface preparation.

The Naval Radiological Defense Laboratory has studied the corrosion behavior of Hastelloy C in hot seawater vapor (200°C), under high hydrostatic pressure (7000 psi), or under ionizing radiation (2×10^5 R/hr), to predict the corrosion life of the SNAP-21 isotopic fuel container should an accident cause it to be contacted by seawater.[10] Compared with corrosion behavior in seawater at 23°C, the hot seawater vapor caused an increase in the corrosion rate of two orders of magnitude and the hydrostatic pressure caused an increase in rate of one order of magnitude. However, the maximum predicted corrosion rate was $\sim 7.4 \times 10^{-4}$ mil/year, which for a 0.25-in.-thick container shell extrapolated to a life of 3.2×10^5 years. On the basis of the relatively short half-life of 28 years for the radioisotopic fuel, it was concluded that this corrosion rate could easily be tolerated.

CORROSION OF MAGNESIUM ALLOYS

The expansion of Magnox alloy Mg–0.55 Zr in CO_2 at 20 atm and temperatures above 500°C has been studied at the Berkeley Nuclear Laboratory of England's Central Electricity Generating Board.[11] After exposures of ~500 hr, approximately 1% expansion was observed in nuclear grade CO_2 and about 10% expansion was observed in CO_2 contaminated with hydrocarbon vapors from heated pitch. A duplex microstructure was noted beneath black-gray deposits on the specimen surface. Narrow bands rich in zirconium precipitates separated the inner and outer zones in the microstructure. The outer zone contained networks of bands denuded in precipitate and aligned perpendicular to the surface of the strip. In the specimens exposed to hydrocarbon-contaminated CO_2, the width of these zones was about 10% of that of the

grain boundaries, which correlated well with the 10% strain observed in these specimens.

CORROSION OF COPPER ALLOYS

The corrosion behavior of copper-bearing feedwater-heater materials in low-oxygen (<10 ppB) flowing neutral water has been reported by General Electric.[12] Water temperature ranged from 150 to 400°F (65 to 205°C). Essentially 100% of the corrosion product formed on the alloys was released to the flowing stream. The release rate was linear with time. It varied from 1 mg/(dm^2)(month) at 150°F to 80 mg/(dm^2)(month) at 400°F for Monel. The release rate was much lower and essentially the same for admiralty brass, 90–10 copper nickel, 70–30 copper nickel, and iron-modified 70–30 copper nickel, ranging from 1 to 3 mg/(dm^2)(month) at 150°F to 8 to 12 mg/(dm^2)(month) at 400°F.

REFERENCES

1. S. Kass, Aqueous Corrosion of Zircaloy at Low Temperature, *J. Nucl. Mater.*, **29**(3): 315-321 (March 1969).
2. J. R. Findlay, C. F. Knights, and R. Perkins, Post-Transition Corrosion of Zircaloy-2, Low-Nickel Zircaloy-2, and Zircaloy-4 by Steam at 300°C and 340°C: Deuterium Absorption and the Influence of Heat Treatment, British Report AERE-R-5903, November 1968.
3. M. M. Rubright, D. W. Koch, and K. M. Ferguson, Corrosion and Hydriding of Zircaloy—Task 1 Final Report—Corrosion and Hydriding of Zircaloy Under Heat Transfer Conditions, USAEC–Euratom Report EURAEC-2016 (BAW-3765-7), The Babcock & Wilcox Co., January 1969.
4. B. Cox, The Morphology of Zirconia Films and Its Relation to the Oxidation Kinetics, Canadian Report AECL-3285, February 1969.
5. I. A. El-Shanshoury, V. A. Rudenko, M. E. El-Dashan, and F. H. Hammad, The Effect of Changing the Corrosive Medium on the Oxidation of Zr–1% Nb Alloy in Pressurized Steam and Air, *Corros. Sci.*, **9**: 315-322 (May 1969).
6. B. E. Wilde and J. E. Weber, Intergranular Stress-Corrosion Resistance of Austenitic Stainless Steels in Water/Oxygen Environments: Accelerated Test Procedure, *Brit. Corros. J.*, **4**(1): 42-46 (January 1969).
7. S. Jansson, W. Hubaer, G. Ostberg, and M. dePourbaix, Oxidation Resistance of Some Stainless Steels and Nickel-Based Alloys in High-Temperature Water and Steam, *Brit. Corros. J.*, **4**(1): 21-31 (January 1969).
8. W. H. Whitlow and J. H. Buddery, A Study of the Reactions Between Individual Oxides Formed During the Oxidation of Stainless Steels, British Report RD/B/N-1272, February 1969.
9. D. van Rooyen, H. R. Copson, and W. E. Berry, Corrosion Behavior of Nickel–Chromium–Iron Alloy 600 in Borated Pressurized Water Reactor Environments, *Corrosion*, **25**(5): 194-198 (May 1969).
10. D. A. Kubose, M. G. Lai, H. A. Goya, and H. I. Cordova, Seawater Corrosion Studies of SNAP-21 Materials, Report NRDL-TR-68-109, Naval Radiological Defense Laboratory, July 21, 1968.
11. J. C. Wood, Microstructural and Dimensional Changes in Strips of Magnox-Zr55 Exposed to CO_2 at Elevated Temperatures and Pressures, British Report RD/B/N-1286, January 1969.
12. E. G. Brush and W. L. Pearl, Corrosion Behavior of Nonferrous Alloy Feedwater-Heater Materials in Neutral Water with Low Oxygen Contents, *Corrosion*, **25**(3): 99-105 (March 1969).

Section

VIII

Reactor Materials

Corrosion of Refractory Metals in Aqueous and Gaseous Media

By B. C. Allen

CORROSION OF UNCOATED REFRACTORY METALS

The oxidation behavior of niobium containing 5 to 34 wt.% titanium was studied by United Aircraft[1-3] in air, oxygen, and nitrogen at 650 to 1000°C. In air and oxygen, Nb–25 Ti oxidized parabolically below 800°C. At higher temperatures, oxidation was linear in air and parabolic in oxygen. The higher oxidation rate in air was believed due to interaction of nitrogen during the conversion of metal to external oxide. A structural analysis of the scale was made. Five Nb–Ti alloys were nitrided at 1000°C in 0.1 atm nitrogen. A binary grain-boundary nitride, probably epsilon Ti_3N, was observed. The reaction with nitrogen involved both bulk and grain-boundary diffusion, the latter becoming more important as the titanium content of the alloy increased.

The oxidation of tantalum in CO_2 at 700 to 950°C was measured[4] using a quartz-spring thermobalance. Oxidation involved a surface-controlled reaction associated with the formation of a nonprotective Ta_2O_5 scale. Below 720°C there was a change in the rate-determining mechanisms, and above 830°C the linear rate was preceded by a complex region of nonlinear oxidation behavior. The linear rate has been explained quantitatively in terms of CO_2 adsorption, followed by a rate-controlling surface reaction.

The Soviets studied the oxidation resistance of binary and ternary tungsten alloys containing up to 50 wt.% niobium and/or titanium.[5] Niobium was found to be the more effective additive for increasing oxidation resistance, especially at levels up to 30 wt.%. Binary additions of up to 5 wt.% titanium were also beneficial. Above 5 wt.%, titanium was detrimental in both binary and ternary alloys, especially above 1200°C. Oxidation was found to occur by a two-way diffusion of oxygen and metal, with a preferred migration of niobium ions in W–Nb alloys and of titanium ions in the W–Nb–Ti alloys.

In other Russian work[6] the oxidation behavior of 99.9 Cr, Cr–0.5 Y, Cr–1.0 Y, and Cr–2.0 Y was studied at 1100 to 1450°C. Yttrium improved the oxidation resistance, especially at the 0.5 wt.% level, and resulted in a tightly adhering oxide layer. Oxygen and nitrogen penetration occurred along grain boundaries in unalloyed chromium, but no nitrides were found in the alloys. It was believed that yttrium improved the oxidation resistance of chromium primarily by a refining effect.

Oxidation of rhenium was studied in both France[7] and the United States.[8] The surface oxidation rate of tungsten and rhenium filaments was measured[7] between 1100 and 2200°C at oxygen pressures of 5×10^{-6} to 3×10^{-4} torr. The rates passed through a maximum that was dependent on pressure. This inversion was caused by the production of atomic oxygen above 1700°C. Aerochem Research Laboratories, Inc., has obtained oxidation kinetic data for the oxidation of rhenium in monatomic and diatomic oxygen at surface temperatures of 400 to 2900°C. There was an interval in which the oxidation rate decreased sharply with increasing temperature, followed by a range of appreciable rhenium loss by sublimation.

Corrosion of refractory metals in aqueous solutions up to 100°C has been reported in the USSR. The corrosion of binary Nb–Ta alloys was studied[9a] in H_2SO_4, HCl, and HNO_3. Alloys containing 5 to 30 wt.% tantalum were essentially resistant to 20 wt.% HCl. The resistance of binary Nb–Ti alloys (0 to 100 wt.% titanium) was determined[9b] in 20 to 40 wt.% KOH for times up to 100 hr. Titanium-rich alloys gave weight losses of 0.1 g/(m^2)(hr), whereas those of niobium-rich alloys fell in the range 55 to 105 g/(m^2)(hr). Electrochemical potentials were also measured. The corrosion rates and electrochemical behavior of rhenium in H_2SO_4, H_3PO_4, KOH, HNO_3, and NaCl were determined[9c] for times up to 200 days. Corrosion rates varied between 0.001 and 0.05 g/(m^2)(hr) except for HNO_3, which gave a rate of 200 g/(m^2)(hr) at 40 wt.% and above. As a result of electrochemical measurements, the author concluded that the passivation properties of rhenium are very weak.

PROTECTION OF REFRACTORY METALS BY COATING

A 3-year laboratory development program on improved fused-slurry silicide coatings for niobium

alloys has been completed by Sylvania Electric Products, Inc.[10] Silicide compositions involving various combinations of Cr, Ti, Fe, V, Mo, W, and Al were screened and optimized on the basis of slow-cycle oxidation tests. The more promising coatings were evaluated extensively. Structure and composition were characterized by X-ray diffraction and electron-microprobe analysis. Performance in hardware considerations was evaluated in terms of (1) wettability and faying surface penetration, (2) coating repair tests, (3) mechanical-property tests, (4) oxidation under furnace, slow-thermal, plasma-torch, and low-temperature cycling, (5) oxidation by simulated low-pressure and high-temperature reentry conditions, and (6) statistical reliability analysis. On the basis of the above criteria, the coating composition Si-20 Cr-20 Fe (R512E) was found to be optimum. As shown in Fig. VIII-1, this coating gave protection to D-43 alloy (Nb-10 W-1 Zr) substrates for fifty 1-hr 800 to 2500°F (425 to 1370°C) cycles at 99% reliability.

Less extensive effort was directed toward the demonstration of fused silicides as one-step braze coats useful to 3000°F (1650°C) and as coatings of threaded fasteners. Fused-slurry silicide compositions for tantalum and molybdenum alloys were also briefly investigated. Si-20 Ti-10 Mo (R512C) and Si-20 Cr-0.5 B_4Si were selected as better coatings for tantalum and molybdenum alloys, respectively, and indicated a maximum useful temperature of about 3200°F (1760°C).

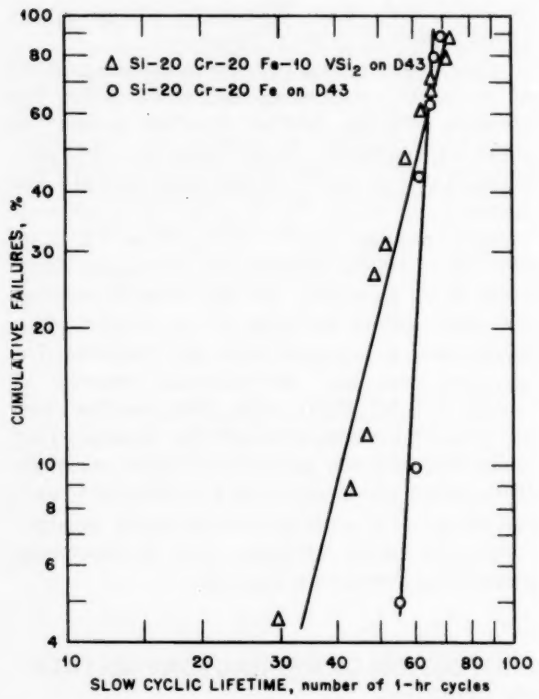

Fig. VIII-1 Weibull plots of slow cyclic (800 to 2500°F) oxidation performance of fused silicide coatings.[10]

REFERENCES

1. E. J. Felten, The Interaction of the Alloy Niobium–25 Titanium with Air, Oxygen, and Nitrogen. I. The Unusual Oxidation Behavior of Nb–25Ti at 1000°C, *J. Less-Common Metals*, 17: 185-197 (February 1969).
2. E. J. Felten, The Interaction of the Alloy Niobium–25 Titanium with Air, Oxygen, and Nitrogen. II. The Reaction of Nb–25Ti in Air and Oxygen Between 650 and 1000°C, *J. Less-Common Metals*, 17: 199-206 (February 1969).
3. E. J. Felten, The Interaction of the Alloy Niobium–25 Titanium with Air, Oxygen, and Nitrogen. III. The Products of the Nb–Ti–N Reaction at 1000°C, *J. Less-Common Metals*, 17: 207-213 (February 1969).
4. K. J. Richards and M. E. Wadsworth, The Oxidation of Tantalum Metal in CO_2 Atmospheres, in *High Temperature Refractory Metals*, Symposium, New York, February 1965, Metallurgical Society Conference, Vol. 34, Part I, pp. 291-304, Gordon and Breach, New York, 1968.
5. I. Yu. Lazareva, D. A. Prokoshkin, E. V. Vasil'eva, and S. B. Maslenkov, Investigation of the Oxidation Resistance of Tungsten–Niobium–Titanium Alloys, in *Svoystva i Primeneniye Zharoprochnykh Splavov* (in Russian), pp. 280-285, Izdatel'stvo, Moscow, 1966.
6. L. M. Kumok, L. N. Larikov, E. A. Maksimenko, and T. K. Yatsenko, Structural Changes Produced by Oxidation of Chromium–Yttrium Alloys, in *Struktura Metallicheskikh Splavov* (in Russian), pp. 99-104, Izdatel'stvo, Kiev, 1966.
7. A. Cassuto and J. Mihe, Oxidation of Tungsten and Rhenium at Low Pressure (in French), *Compt. Rend., Ser. C*, 266: 863-866 (1968).
8. D. E. Rocher and H. D. Allendorf, Kinetics of the Attack of Rhenium by Atomic and Diatomic Oxygen at High Temperatures, *J. Chem. Phys.*, 49: 5553-5555 (1968).
9. *Korroziya i Zashchita Konstruktsionnykh Splavov*, Izdatel'stvo, Moscow, 1966.
   a. V. V. Andreeva, A. I. Glukhova, S. N. Dontsov, I. S. Moiseeva, and L. V. Melnikova, Corrosion Resistance, Electrochemical and Mechanical Properties, and Microstructure of Niobium–Tantalum Alloys, pp. 178-190.
   b. A. I. Glukhova and V. V. Andreeva, Corrosion and Electrochemical Behavior of Niobium–Titanium Alloys in Alkali Solutions at Elevated Temperatures, pp. 191-198.
   c. N. D. Tomashov and T. V. Matveeva, Corrosion and Electrochemical Behavior of Rhenium, pp. 166-167.
10. S. Priceman and L. Sama, Development of Fused Slurry Silicide Coatings for the Elevated-Temperature Oxidation Protection of Columbium and Tantalum Alloys, Report AFML-TR-68-210, Sylvania Electric Products, Inc., December 1968.

Section
IX
Reactor Materials

Corrosion by Liquid Metals and Fused Salts

By E. M. Simons

SODIUM

Compatibility of Sodium with Austenitic Stainless Steels

It is generally agreed that sodium-cooled reactors will have to operate with relatively pure sodium (preferably <10 ppM oxygen) to limit corrosion of austenitic stainless-steel construction materials. In a clean system the stainless steel undergoes surface recession, as indicated by predictable weight losses of specimens. A surface layer of ferrite can form, and no oxidation products are evident either on the specimen surfaces or deposited downstream. In contrast, when oxygen is in excess of 20 ppM (either accidentally in service or purposely in the laboratory), surface scales appear, and specimens may undergo weight gains instead of losses.

A summary has been published[1] of the results of 5 years of corrosion studies by MSA Research Corp. using contaminated sodium (up to 300 ppM oxygen) in isothermal, low-velocity stainless-steel systems. At 1200°F (650°C), the 300-series stainless steels acquire a nonadherent gray surface scale in sodium with >20 ppM oxygen. The scale is interspersed with microscopic ferritic islands and has been identified as mainly sodium chromite ($Na_2Cr_2O_4$), containing very little iron or nickel (<0.3 wt.%). If the exposure temperature is raised to 1400°F (760°C), an unidentified green scale with a distinctive X-ray pattern is formed. This scale seems to be made up of two phases, both of which transform when the sodium temperature is lowered to 1200°F. The major phase reverts to sodium chromite.

Stress-rupture and stress-fatigue tests are being run at General Electric[2] on 304 and 316 stainless steels in clean sodium flowing at 17 ft/sec with a peak temperature of 1300°F (705°C). The stress-fatigue tests are run by low-frequency pressure cycling (essentially square wave), and the time at maximum stress (one-half of the total rupture life) is used for comparison with steady-state stress-rupture life. Preliminary results indicate that stress fatigue retards the long-term rupture of both 304 and 316 stainless steels, and the dynamic sodium environment may have a deleterious effect on the long-term stress-rupture life of these steels.

Experiments were also run to see how a carbide-agglomeration (CA) heat-treatment (900°C for 24 hr) affected the stress-rupture behavior, since Experimental Breeder Reactor II (EBR-II) exposure results had suggested that the CA structure has improved resistance to radiation embrittlement. The tests showed standard mill-annealed material to be slightly better than CA material, but the difference seems to be second order for rupture lives up to several thousand hours.

One drawback of normal austenitic stainless steels for sodium-heated steam generators is their susceptibility to stress-corrosion cracking on the water side of the boiler. Since 18-18-2 stainless steel (18 Cr–18 Ni–2 Si) has remarkable resistance to stress-corrosion cracking, MSA workers[3] exposed sheet tensile specimens at 1200°F (650°C) to helium (500 hr), flowing sodium containing <10 ppM oxygen (500 hr), sodium containing 20 ppM oxygen (500 hr), and carbon-contaminated sodium (750 hr) to ascertain the effects on strength, ductility, and microstructure. Postexposure tensile tests were run in air at room temperature, 1200°F (650°C), and 1400°F (760°C). The behavior of the 18-18-2 alloy was very similar to that of 304 and 316 stainless steels, in that neither the helium nor the clean sodium exposures altered the microstructure or produced significant embrittlement or strengthening effects. However, the high-carbon-sodium exposure resulted in noticeably less carburization and loss of ductility than occurred in comparably exposed 304 and 316 stainless steels. Also, the high-oxygen-sodium exposures produced only a faint greenish tinge on the 18-18-2 alloy, in place of the gray-oxide-scale buildup and penetration normally found on 304 and 316 stainless-steel surfaces in the same environment.

Concurrently with these MSA Research studies, workers at the Liquid Metal Engineering Center[4] were exposing 18 coupons of this same alloy (18-18-2) to 1200°F sodium containing 30 ppM oxygen for periods

up to 10 times as long (5060 hr). For the first 400 hr, the test coupons gained weight at almost the same rate as did comparable 304 stainless-steel coupons. Beyond this, they gained weight faster than did the 304 (5.61 mg/cm^2 vs. 4.00 mg/cm^2, total, after 3400 hr). Between 3400 and 5060 hr, however, the surface oxide film exfoliated, causing a marked decrease in the net weight gain of the silicon-bearing steel. Metallographic and microprobe studies revealed a chromium-rich green surface layer over an iron–nickel-rich chromium-depleted layer containing ferrite. The silicon was depleted from the entire reaction zone.

The investigators believe that the diffusion-limited silicon-depletion rate and other compositional changes in 18-18-2 steel exposed to lower-oxygen (<15 ppM) sodium would be slow enough to keep the steel resistant to stress corrosion for liquid-metal-cooled fast breeder reactor (LMFBR) target lifetimes. However, the early breakaway of nonadherent surface films might post an insurmountable barrier to the use of 18-18-2 steel. Further testing is recommended to see whether such films would really cause trouble in clean, high-velocity sodium over long periods of time.

An investigation was made by Argonne[5] to determine the cause of deep grain-boundary attack found in selective areas of the 304L stainless-steel cladding of a driver fuel element removed from the EBR-II. This was one of several elements that showed relatively high swelling; and, indeed, grain-boundary fissures originating at the outer surface were noted where maximum swelling occurred. Chemical and microprobe analyses revealed that a carbon-concentration increase was associated with the areas of attack. By streaking samples of 304L stainless steel with either Apiezon N grease or graphite aerosol and exposing them to circulating 550°C sodium for 1 week, the researchers were able to reproduce the same type of grain-boundary attack which occurred in the fuel-element cladding. It was concluded that the latter had been caused by localized surface contamination, either by grease left on the tube during manufacturing or by accidental contamination of the completed fuel element before it was inserted into the subassembly.

Atomics International[6] performed a series of tests to assess the effects of copper contamination of sodium (such as occurred in EBR-II) on the mechanical properties of 304 stainless steel. Biaxial stress-rupture tests on tubing specimens were conducted in copper-saturated sodium in static retorts at 950, 1100, and 1300°F (510, 595, and 705°C). Charpy impact specimens, exposed to the same environments, were subsequently tested at –75°C.

The presence of copper in the sodium had no measurable effect on either the stress-rupture behavior or the impact strength of the stainless steel up to the maximum test temperature. No serious penetration of copper into the stainless steel occurred. Copper precipitated from solution and deposited on the stainless steel in the isothermal region of the 950°F retort, but, in the higher-temperature retorts, deposits were found only in regions where the liquid sodium was cooler.

Compatibility of Sodium with Ferritic Steels

Portions of a sodium-cooled reactor where water is one of the environments operate at temperatures well below the maximum in the primary loop. Therefore certain low-alloy ferritic steels, which are not susceptible to stress-corrosion cracking, have sufficient strength and corrosion resistance to be considered for use. Unfortunately the carbon in such steels is transported by the sodium to any austenitic materials or other carbon sinks in the system. One suggested remedy for this carbon instability is to add a carbon stabilizer to the ferritic alloy.

MSA workers[7] evaluated a number of ferritic alloys to determine which, if any, are compatible with stainless steel in liquid-sodium service with respect to carbon content. These were exposed to static sodium and helium (controls) in 316 stainless-steel retorts at 1200°F (650°C) for periods up to 4000 hr, then tensile tested in air at room temperature and 1050°F (570°C) and analyzed for carbon and major alloying constituents. The alloys tested were 2.25 Cr–1 Mo (for reference); 2.25 Cr–1 Mo–V, Nb; 2.25 Cr–1 Mo–V, Ti, Zr; 3HK5S (2.25 Cr–1 Mo–Nb, Ta); Croloy 5 (5 Cr–0.5 Mo); and Croloy 5 Ti (5 Cr–0.5 Mo–0.5 Ti). Of these, the most promising for effective carbon stabilization and retention of good mechanical properties was the Croloy 5 Ti. A question of whether gross carbon losses might occur after longer exposures in the absence of a supplementary carbon source still exists.

The following observations were made by General Electric[8] from examinations of plain-carbon steels, low-alloy steels, ferritic stainless steels, and austenitic stainless steels that had been exposed simultaneously in an austenitic stainless-steel pot containing static sodium (100 ppM oxygen) at 1175°F (635°C) for 596 hr:

1. The plain-carbon steels were rapidly decarburized and suffered localized (intergranular) attack to a depth that was greater in steels with higher initial carbon contents.

2. The addition of chromium to plain-carbon steel produced stable carbides, decreasing the carbon activity and hence lowering the rates of decarburization and intergranular attack.

3. The high oxygen in the sodium promoted oxidation of the chromium in low-alloy ferritic steels, possibly by

$$6Fe_3C_{(\text{in steel})} + Cr_{(\text{in steel})} + 23Cr_{(\text{in Na})} + 2Na_2O_{(\text{in Na})} \rightarrow Cr_{23}C_{6(\text{in Na})} + NaCrO_{2(\text{in Na})} + 3Na_{(\text{liq})} + 18Fe$$

4. For steels with more chromium, the depth of intergranular attack by high-oxygen sodium increases and the mode of attack changes toward general oxidation of the chromium, possibly by

$$2(Fe,Cr)_7C_{3(\text{in steel})} + 10Cr_{(\text{in Na})} + 2Na_2O_{(\text{in Na})} \rightarrow (Fe,Cr)_{23}C_{6(\text{in Na})} + NaCrO_{2(\text{in Na})} + 3Na_{(\text{liq})}$$

5. Because of the greater chromium activity in ferrite, the ferritic stainless steels suffered greater general and grain-boundary attack than the austenitic stainless steels.

Compatibility of Sodium with FBR Fuels

Workers at Los Alamos[9] have been concerned with interactions among single-phase mixed (U,Pu)C, a sodium bond, and potential cladding materials (notably 316 stainless steel and vanadium-base alloys) for fast breeder reactor (FBR) fuels. Their analyses indicate that there is a strong thermodynamic potential for chromium to react with carbide fuels in the presence of sodium oxide to form chromium carbide, UO_2 and/or PuO_2, and free sodium. To examine the kinetics of such reactions, they exposed 316L stainless-steel tabs in zirconium-gettered sodium at 650°C for periods from 2 to 116 hr using an Fe–0.85 C alloy as the carbon source. As would be expected with diffusion-controlled processes, the rates of decarburization of the source and carburization of the stainless steel decreased exponentially with time. It is interesting to note that fresh cladding specimens immersed in sodium from which the carbon source had been removed were not carburized, which implies that the activity of the residual carbon in the sodium was insufficient to produce carburization.

Additional carburization experiments were run in magnesia crucibles with tabs of both the cladding material and an Fe_3C–graphite source immersed in sodium for 72 hr at 650°C. From metallographic data a diffusion constant of 1.96×10^{-10} cm²/sec was calculated for carbon in 316L stainless steel. From microhardness measurements the diffusion constant for carbon in the V–15 Cr–5 Ti alloy was determined to be an order of magnitude less (1.06×10^{-11} cm²/sec).

General Electric researchers made theoretical studies[10] of the analogous cladding–sodium bond–fuel compatibility situation with oxide fuels instead of carbides. They concluded that there is a much stronger tendency for sodium to react with uranium oxides to form one of several Na–U–O compounds than to form simply Na_2O. Such reactions occur at much lower oxygen-activity levels (O/U ratios) than suspected, and the presence of plutonium could further encourage the formation of the sodium–fuel compound and lead to greater swelling and transport of fuel.

Cavitation by Sodium

In an earlier review,[11] it was pointed out that increasing the pressure of the argon cover gas over sodium in a vibratory accelerated-cavitation apparatus at NASA–Lewis caused the cavitation damage to cobalt-base alloy L-605 in 800°F (427°C) sodium to increase exponentially. Parametric studies[12] showed that the damage was greater at 800°F than at either 400 or 1200°F (205 or 650°C). The combined effects of temperature and pressure of the sodium on cavitation damage are shown in Fig. IX-1, along with the solid–liquid and liquid–vapor lines that mark the

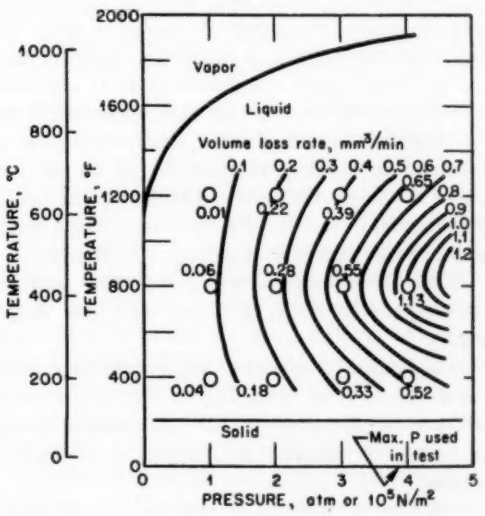

Fig. IX-1 Effect of temperature and pressure on normalized cavitation damage rate for L-605 tested in sodium.[12]

theoretical limits for zero cavitation-damage rate. The quantitative values of damage shown in Fig. IX-1 would be different for different test facilities, amplitudes, and frequencies.

In a program to study cavitation in an actual axial-flow sodium pump,[13] the NASA–Lewis workers ran a 200-hr cavitation test in 815°C sodium on a test rotor containing blades of 316 and 318 stainless steels and René 41, a Ni–Cr-base superalloy. At a constant tip speed of 75.5 ft/sec and a constant suction specific speed of 6500, the cavitation damage was concentrated near the tip leading edge of the suction surface. The René 41 blades sustained less cavitation damage than the stainless-steel blades. Roughening of the surfaces of all three materials was attributed to corrosive attack by the sodium.

Sodium Corrosion Reviews

Liquid Metals, a book published in Moscow in 1967, is now available from CFSTI in English translation.[14] It is a collection of Soviet papers on heat-transfer and component technology related to sodium-cooled fast reactors. A single paper on corrosion of structural materials reviews the general theories of corrosion by alkali metals and the role of oxygen impurities in the corrosion process. Evidence is presented that oxygen in liquid sodium at elevated temperatures exists in the very active ionic form, which the investigators suggest is the basis for the accelerating influence of oxygen on the corrosion of steels by sodium.

The results of Soviet loop tests on a large assortment of ferritic and austenitic steels, six nickel-base alloys, and two refractory metals are similar to those obtained from comparable studies in the United States and other countries. Representative observations are:

1. Unless a ferritic–pearlitic steel contains enough of the carbide-forming elements to tie up all of its carbon as stable carbides, it will be decarburized in the high-temperature zones of a dynamic sodium system and may suffer a significant reduction in strength.

2. Pearlitic steels show very low rates of weight loss in flowing sodium up to 12 m/sec, 700°C, and 50 ppM oxygen.

3. Austenitic steels are readily carburized (with consequent loss of ductility) if carbon steels or pearlitic steels are present in the same sodium system. They are also nitrided if a source of nitrogen is available.

4. Austenitic steels are more prone to mass transfer in sodium systems than ferritic steels, the tendency increasing sharply with peak temperature above 600°C.

5. Sodium attacks austenitic steels intergranularly with increasing severity as the temperature and oxygen levels are increased. However, most austenitic steels are sufficiently corrosion resistant up to 700°C if the sodium contains less than 50 ppM oxygen. (U. S. investigators would set the oxygen limit closer to 10 ppM.)

6. Nickel-base alloys are more prone to dissolution and mass transfer in flowing sodium than are steels. Mass-transfer rates increase with temperature, time, and nickel content of the alloy.

7. Molybdenum is highly resistant to flowing sodium containing 20 ppM oxygen, at temperatures to at least 1050°C, and flow velocity seems to have no effect.

8. Niobium is severely attacked by sodium at 600°C, unless the oxygen content of the sodium is kept below 10 ppM. The corrosion rate increases with increasing flow velocity.

Thorley and Bardsley[15] have drawn on the results of numerous past sodium corrosion studies to explain some of the structural changes that occur when various materials are exposed to flowing sodium. Some of their observations follow.

Niobium: Loses weight by formation and spalling of $Na_2Nb_2O_5$ at a rate depending on temperature, oxygen content, and velocity of the sodium.

Zirconium: Forms a black, adherent ZrO_2 film and gains weight at a rate that is independent of oxygen content (to 50 ppM) and velocity (to 25 ft/sec) of the sodium.

Stainless Steel: Loses nickel and chromium from surface, the losses resulting in the formation of an iron-rich ferritic layer that then corrodes at a rate governed by temperature and oxygen content of the sodium; also may be carburized so as to form $M_{23}C_6$ and M_6C in 650°C sodium containing carbon impurities.

Ferritic Steel: Becomes decarburized under the driving force of high-activity carbides such as Fe_3C, especially when stainless steels are present in the same circuit, resulting in increased ductility and grain size and decreased strength.

Braze Alloys: Undergo selective leaching (e.g., Nicrobraz 50 loses phosphorus, and Nicrobraz 30 loses silicon).

General Electric's updated evaluation of potential fuel-cladding materials for the LMFBR[16] contains a 68-page chapter on the corrosion of selected materials

by liquid sodium. This chapter constitutes a comprehensive state-of-the-art review of the general corrosion picture, as well as specific information on steels and alloys based on Ni, Co, V, Nb, Mo, Ta, and W. Alloys ranked as having "good" corrosion resistance are ferritic steels, austenitic stainless steels, Fe–Cr–Ni–Co alloys, cobalt alloys, and molybdenum. "Intermediate" ratings were given to vanadium and niobium alloys, as well as to nickel-base alloys with less than 50 wt.% nickel. Alloys with over 50 wt.% nickel were rated as "poor."

CORROSION IN RANKINE-CYCLE SPACE POWER SYSTEMS

Alkali-Metal Systems

The proceedings of a 1968 symposium on refractory-metal alloys[17] contains several papers dealing with their application as structural materials for liquid-metal Rankine-cycle space electric-power systems. The review by Hoffman and Harrison[17a] points out that refractory metals generally have excellent compatibility with liquid metals, but only if strict controls are exercised over impurities. Their discussion includes information from tests of refractory metals in contact with Hg, Cs, K, Na, and Li. Also described are the compatibility results obtained in a 5000-hr test of a two-loop Nb–1 Zr facility in which sodium was circulated in the heater circuit and potassium was boiled and circulated in a two-phase secondary loop containing turbine simulator test sections of Mo–TZM alloy.

A paper by Semmel[17b] reviews the status of refractory-alloy applications to alkali-metal Rankine-cycle systems for future power requirements above 100 kW. Niobium and tantalum alloys are considered for containment for over 10,000 hr at temperatures near 1100°C. Molybdenum alloys are considered for alkali-metal-vapor turbine wheel and blade applications where weldability is not essential.

The 5000-hr test mentioned above was conducted by General Electric.[18] The secondary loop was designed to simulate a Rankine-cycle space electric-power system. Maximum and minimum temperatures in the sodium circuit were 2150°F (1175°C) and 1960°F (1075°C), respectively, and temperatures in the two-phase potassium loop ranged from 2000°F (1090°C) for superheated vapor at the boiler outlet to 600°F (315°C) liquid.

The system was operated in a vacuum chamber at 2×10^{-8} torr with no significant contamination of the components by the vacuum-chamber environment. Extensive chemical, metallurgical, weight-change, and dimensional examinations indicated that the Nb–1 Zr structural alloy and the Mo–TZM turbine alloy have excellent compatibility with the alkali metals. No significant corrosion was found, and the substantial oxygen migration noted from the hotter to cooler regions of the sodium circuit had no detectable effect on the strength or the ductility of the Nb–1 Zr alloy.

Mercury Systems

Workers at NASA–Lewis[19] operated a two-phase, forced-convection mercury loop constructed of the cobalt-base alloy HS-25 (L-605) for 1147 hr with a liquid velocity of about 8 ft/sec. The peak temperature in the boiler was 1075°F (858°K), and the vapor reached 1300°F (977°K) in the superheater. Severe corrosion to a depth of about 10 mils was found near the boiler inlet where two-phase flow began. This penetration was much greater than had been expected from lower-velocity capsule and loop tests, indicating that liquid velocity is an important corrosion parameter.

A U. S. patent[20] has been granted on a technique for inhibiting the corrosion of an alloy containing Co, W, Cr, and Ni (which includes most cobalt-base superalloys) by hot liquid mercury. It involves soaking the alloy in high-temperature mercury long enough to leach chromium and nickel from the first several mils on the surface. The next step is to anneal the alloy in hydrogen to convert the surface layer to the intermetallic compound Co_2W, which is presumably highly resistant to attack by the molten mercury.

Capsule tests were run for 1000 hr at General Electric[21] to evaluate the resistance of Nb–1 Zr and T-111 (Ta–8 W–2 Hf) alloys to corrosion by 1200°F (650°C) liquid mercury. These alloys are being considered as possible replacements for the lower-strength unalloyed tantalum tubing presently specified for the NaK-heated mercury boiler in the SNAP-8 Rankine-cycle space power system. Specimens of tantalum and the two alloys were strained 5 and 20% by bending and tested in the as-bent and as-bent-and-annealed (8 hr at 870°C, 2 hr at 1040°C, or 2 hr at 1200°C) conditions. Although stress-corrosion cracking of these alloys under similar conditions had previously been reported by Brookhaven National Laboratory, neither cracking nor changes in weight or metallographic structure could be detected in any of the General Electric specimens.

CORROSION BY LITHIUM

The Soviets conducted a study[22] to determine the effect of molten lithium on the corrosion resistance and strength of welded joints in 1Kh18N10T (18 Cr, 10 Ni, 0.8 Ti, 0.8 Si, 0.12 C) and 2Kh13 (13 Cr, 0.2 C, up to 0.6 Ni, 0.7 Si, 0.5 Mn) steel tubing. Parameters were weld atmosphere (spectrographically pure argon and commercial argon), lithium purity (pure lithium and lithium contaminated with oxygen or nitrogen or both), and exposure temperature (700, 800, and 900°C).

Results for the 1Kh18N10T steel, shown in Table IX-1, indicate that neither lithium purity nor welding-atmosphere purity has a dramatic effect on short-time tensile properties within the range studied. However, the specimens were slightly weaker and less ductile when tested in pure lithium than when tested in argon; also, they were slightly weaker and less ductile when welded in commercial argon than when welded in spectrographically pure argon. These effects are attributed to intergranular penetration of the steel by the lithium. The penetration was noted to be shallower in the welds than in the base metal, suggesting that the welded material has better corrosion resistance to lithium than does the base metal.

Table IX-1 Effect of Welding Atmosphere on Elevated-Temperature Tensile Properties* of 18 Cr–10 Ni Steel Welds After 500-Hr Exposure to Various Environments[22]

Temp. of 500-hr soak and tensile test, °C	Purity of argon welding atmosphere	Tensile properties for indicated test environment									
		Li		Li + N_2		Li + O_2		Li + N_2 + O_2		Argon	
		UTS,† kg/mm^2	Elong.,† %	UTS, kg/mm^2	Elong., %	UTS, kg/mm^2	Elong., %	UTS, kg/mm^2	Elong., %	UTS, kg/mm^2	Elong., %
700	Spectrographic	24.8	16.0	21	16	24.2	14	24.8	14	27.5	22
800	Spectrographic	17.8	20.0	17	24	18	26	16.8	27	18.5	28
800	Commercial	16.5	17.0	15	21	16	18	16	23	17.6	24
900	Spectrographic	6.6	22	6.7	25	6.7	27	7.0	26	7.1	24

*All fractures occurred in weld zone.

†UTS = ultimate tensile strength; Elong. = elongation.

The as-welded ferritic steel 2Kh13 showed a marked loss of strength and ductility as a result of similar lithium exposures in the range 250 to 450°C; but between 450 and 800°C the properties of the lithium-exposed and argon-exposed specimens were the same. However, if the specimens were given a postweld heat-treatment prior to their exposures, their mechanical properties were unaffected by either the lithium or the purity of the welding atmosphere.

Workers at the Lawrence Radiation Laboratory[23] used microprobe analyses, along with optical and electron microscopy, to examine electropolished samples of a W–25 at.% Re–30 at.% Mo alloy that had been exposed for 1000 hr to flowing lithium in a 1400°C peak-temperature loop with a ΔT of about 200°C. Molybdenum was transported from the hot end to the cold end of the loop, the cold-leg samples showing almost 50 at.% Mo while the W/Re ratio remained essentially constant. In addition, there was evidence of etching at grain boundaries to depths as much as 1 mil at the hot end. Such etching, depending on its rate beyond 1000 hr and its effect on mechanical properties, could severely limit the use of W–Re–Mo alloys for containment of dynamic lithium above 1400°C. The 1000-hr exposure had no adverse effect on the room-temperature mechanical properties of the alloy.

CORROSION BY LEAD–BISMUTH ALLOYS

Ferritic steels are promising container materials for molten Bi–Pb alloys, although their use above about 450°C requires the addition of corrosion inhibitors (magnesium plus zirconium or titanium). Weeks and Romano[24] made detailed studies of the solubilities of iron and the inhibitors in Bi–Pb alloys in an attempt to estimate the relative aggressiveness of Bi–Pb alloys toward ferritic steels. At a given temperature the solubility of iron in liquid Bi–Pb alloys[24] increases with the bismuth content of the alloy, as shown in Fig. IX-2. The 20-fold greater solubility of iron in bismuth than in lead is reflected in a comparable ratio of

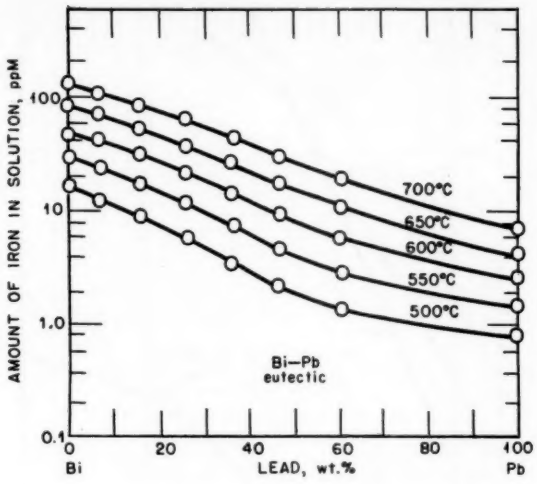

Fig. IX-2 Solubility of iron in Bi–Pb alloys.[24]

corrosion rates of steel loops in which pure bismuth and pure lead were circulated at 700 to 800°C. It is predicted that the corrosiveness of a Bi–Pb alloy would be proportional to its bismuth content.

The solubilities of titanium and zirconium in the eutectic alloy (55.5 wt.% Bi) are given by

$$\log (\text{ppM Ti}) = 4.95 - 2160/T(^\circ\text{K}) \quad \text{from 285 to 700°C}$$

$$\log (\text{ppM Zr}) = 6.15 - 3172/T(^\circ\text{K}) \quad \text{from 350 to 750°C}$$

As with iron, pure bismuth will dissolve substantially more titanium or zirconium than the Bi–Pb alloys will. However, the solubility of these inhibitors even in high-lead alloys appears to be adequate for the effective retardation of the corrosion of steels.

Tests carried out on various steels submerged in molten Pb–Bi alloy indicate that the liquid metal causes a substantial reduction in the fatigue limit of the steel, provided wetting of the specimen is ensured (by pretinning) before testing. This effect has been related to the stability and strength of oxide films, which presumably can inhibit the corrosive actions that weaken the steel.

A study by the Soviets[25] confirms these observations and sheds further light on them. The results of their fatigue tests on a 13 wt.% chromium steel, 4Kh13, at 500 and 600°C in air and in molten Pb–Bi eutectic are shown in Fig. IX-3. Note that the fatigue strength at 500°C in the liquid metal is much lower than in air, and at 600°C it was necessary to pretin the specimens before the fatigue-strength reduction

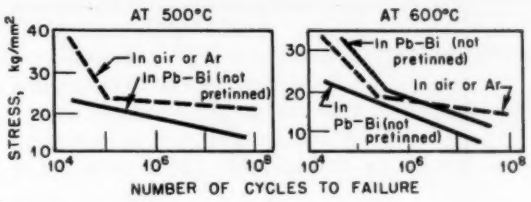

Fig. IX-3 Effect of environment on fatigue of 4Kh13 (13 wt.% chromium) steel in rotating bending.[25]

became significant. This is because the scale formed on the steel at 500°C is a brittle oxygen-rich Fe_2O_3, which is readily wet by the Pb–Bi. Raising the temperature to 600°C leads to the appearance of a chromium spinel, $FeOCr_2O_3$, which inhibits wetting by the molten alloy and its diffusion into the steel surface.

CORROSION BY MOLTEN URANIUM ALLOYS

The feasibility of a reactor concept using a molten-uranium-alloy fuel depends, among other things, on the ability of the container material to resist corrosive attack by the fuel at the operating temperatures. R. J. Cash, in his Ph.D. dissertation[26] at Iowa State University covering isothermal capsule corrosion tests, concluded that yttrium is not a satisfactory long-term container metal for the U–5 Cr eutectic at 950°C and above. Additions of iron to the U–Cr lowered the melting point but increased the corrosiveness of the fuel toward yttrium, particularly in amounts above 1 wt.%. No evidence of intergranular attack or intermetallic compound formation was found in any of the tests.

LIQUID-METAL CORROSION MECHANISMS

Nikitin[27] presented an interesting concept that the reduction in stress-rupture life of solid metals as a result of exposure to liquid metals can have various physical bases, depending on the materials involved. For example, the weakening effect of molten bismuth on copper (Fig. IX-4) is attributed to *adsorption* of the bismuth on the copper surface. This causes a reduction in the activation energy for fracture of the copper, as indicated by the lower slope of the Arrhenius line for the bismuth environment than for air in Fig. IX-4.

Diffusion is another possible cause for reduced stress-rupture life, as exemplified by the sharply

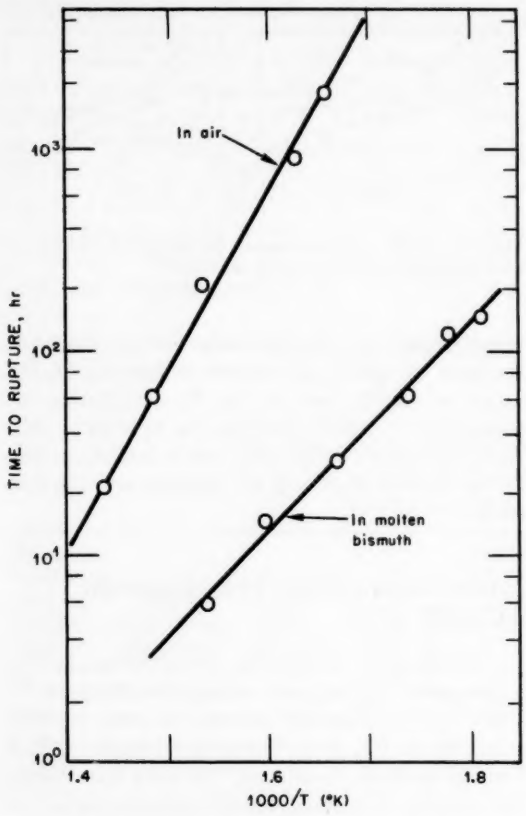

Fig. IX-4 Effect of environment on rupture life of copper at 4 kg/mm^2 stress.[27]

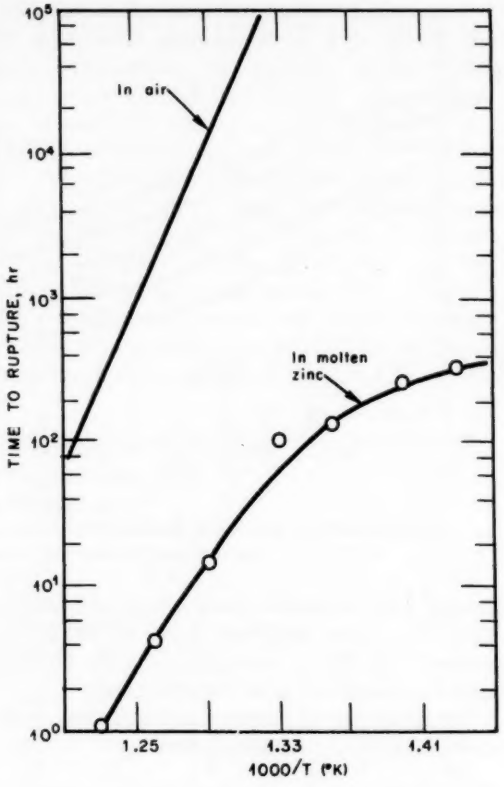

Fig. IX-5 Effect of environment on rupture life of Armco iron at 7 kg/mm^2 stress.[27]

reduced time to rupture of Armco iron in liquid zinc as compared with the time in air (Fig. IX-5). Nikitin attributes the nonlinearity of the zinc-atmosphere curve to the predominant weakening role played by diffusion. A third mechanism for reducing stress-rupture life is *corrosion*, as illustrated by the deleterious effect of molten sodium on the nickel-base alloy EI-872 (Fig. IX-6) at temperatures above 600°C. Unlike the other two phenomena, corrosion produces effects that get worse (relative to results in air) with increasing temperature, as a result of the faster dissolution rates on the specimen surface and at the tips of cracks.

CORROSION BY FUSED SALTS

Compatibility studies on structural materials with fused fluoride salts of interest for breeder reactors have been in progress at Oak Ridge for almost a decade.[28] In fact, one natural-circulation loop in this program has accumulated over 7 years of operating time at a peak temperature of 704°C. The four classes of salts being studied are (1) fuels, containing UF_4 but no ThF_4; (2) blanket salts, containing ThF_4 but no UF_4; (3) fertile–fissile salts, containing both UF_4 and ThF_4; and (4) coolant salts, containing neither UF_4 nor ThF_4.

Hastelloy N* and titanium-modified Hastelloy N* are alloys that were tailored specifically for use with

*Compositions:

Alloy	Content, wt.%						
	Ni	Mo	Cr	Fe	Si	Mn	Ti
Standard Hastelloy N	70	17.2	7.4	4.5	0.6	0.54	0.02
Titanium-modified Hastelloy N	78	13.6	7.3	<0.01	<0.01	0.14	0.5

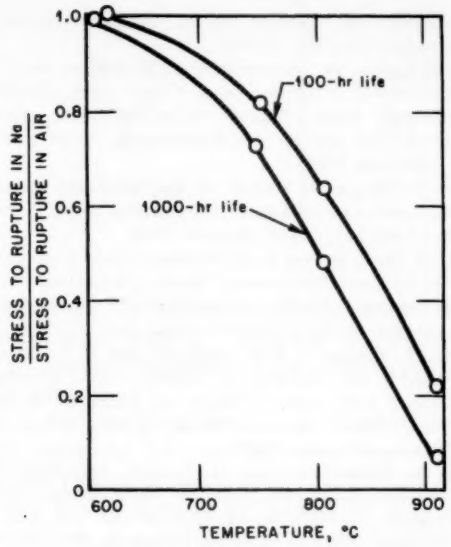

Fig. IX-6 Effect of exposure to sodium on the 100-hr and 1000-hr rupture stress of nickel-base alloy EI-872 (Ref. 27).

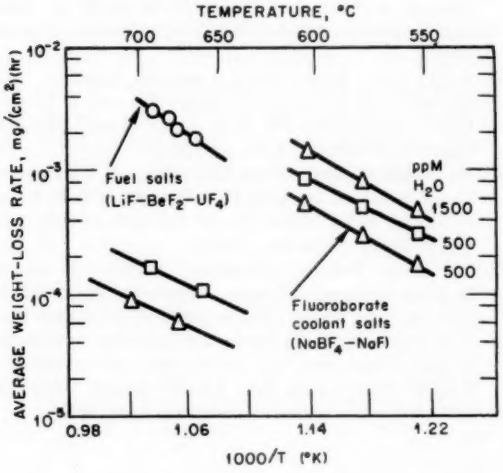

Fig. IX-7 Corrosion of materials by molten fluoride salts.[28] ○, 304L stainless steel; □, Hastelloy N; △, titanium-modified Hastelloy N.

fluoride salts. Their corrosion is generally manifested by weight losses in the hot zones and weight gains in the cooler regions, at rates which are sensitive to impurities in the salt (especially moisture) and decrease with time. Some typical average corrosion rates are plotted in Fig. IX-7, which reveals the following:

1. The corrosion of stainless steel and Hastelloy N follows an Arrhenius law.
2. Stainless steel is attacked at least an order of magnitude faster than Hastelloy N.
3. Titanium-modified Hastelloy N is more corrosion resistant than standard Hastelloy N.
4. Fluoroborate coolants salts are more corrosive than fuel salts.
5. Increasing the moisture content of fluoroborate salts causes them to be more corrosive.

Hastelloy N and Croloy 9M loops,[29] run with the relatively impure (>3000 ppM impurities) fluoroborate salt $NaBF_4$–NaF–KBF_4 (90–4–6 mole %) at a maximum temperature of 605°C, suffered severe mass transfer of all major alloying elements. The Hastelloy N loop was 75% plugged with deposits after 1 year of operation, and the Croloy 9M loop was completely plugged after 1440 hr.

REFERENCES

1. R. H. Hiltz, Oxidation of Stainless Steel in Oxygen-Contaminated High-Temperature Sodium, Topical Report No. 13, The Effect of High-Temperature Sodium on the Mechanical Properties of Candidate Alloys for the LMFBR Program, USAEC Report MSAR-69-91, MSA Research Corp., May 1969.
2. General Electric Company, Breeder Reactor Development Operation, Sodium Components Development Program, Mass Transfer Investigations in Liquid Metal Systems, Quarterly Progress Report No. 9, March–May 1969, USAEC Report GEAP-10036, June 1969.
3. MSA Research Corp., The Effect of High-Temperature Sodium on the Mechanical Properties of Candidate Alloys for the LMFBR Program, Quarterly Progress Report, October–December 1968, USAEC Report MSAR-69-42, April 1969.
4. W. T. Lee, Corrosion of Type 18-18-2 Stainless Steel in 1200°F Static Sodium, USAEC Report LMEC-69-11, Liquid Metal Engineering Center, May 15, 1969.
5. W. E. Ruther, T. D. Claar, and S. Matras, The Attack on the Cladding of EBR-II Driver Fuel Element C-249-16, USAEC Report ANL-7537, Argonne National Laboratory, March 1969.
6. D. F. Atkins, Mechanical Behavior of Type 304 Stainless Steel in Copper-Contaminated Sodium in the Range 950 to 1300°F, USAEC Report AI-AEC-12788, Atomics International, Apr. 1, 1969.
7. R. H. Hiltz and L. H. Kirschler, The Effect of High-Temperature Sodium on the Mechanical Properties of Candidate Alloys for the LMFBR Program, USAEC Report MSAR-69-139, MSA Research Corp., July 1969.
8. General Electric Company, Breeder Reactor Development Operation, Sodium Components Development Program, Mass Transfer Investigations in Liquid Metal Systems, Quarterly Progress Report No. 8, December 1968–February 1969, USAEC Report GEAP-10008, April 1969.

9. Los Alamos Scientific Laboratory, Quarterly Status Report on the Advanced Plutonium Fuels Program, January 1–March 31, 1969, USAEC Report LA-4193-MS, June 17, 1969.
10. E. A. Aitken, Thermodynamic Analysis of Possible Chemical Interactions in the System: UO_2–PuO_2 Fuel-Sodium-Stainless Steel, USAEC Report GEAP-5683, General Electric Company, Breeder Reactor Development Operation, July 1968.
11. E. M. Simons, Corrosion by Nonaqueous Liquids, *Reactor Mater.*, 11(3): 168 (Fall 1968).
12. S. G. Young and J. R. Johnston, Effect of Temperature and Pressure on Cavitation Damage to a Cobalt-Base Alloy in Sodium, Report NASA-TN-D-5273, National Aeronautics and Space Administration, Lewis Research Center, June 1969.
13. D. C. Reemsnyder, W. S. Cunnan, and C. Weigel, Performance and Cavitation Damage of an Axial-Flow Pump in 1500°F (1089°K) Sodium, Report NASA-TN-D-5138, National Aeronautics and Space Administration, Lewis Research Center, April 1969.
14. P. L. Kirillov, V. I. Subbotin, and P. A. Ushakov (Eds.), *Liquid Metals*, Report NASA-TT-F-522, May 1969 [translated from *Liquid Metals* (in Russian), Atomizdat, Moscow, 1967].
15. A. W. Thorley and J. A. Bardsley, Structural Changes in Materials Exposed to Liquid Sodium, *J. Roy. Microscop. Soc.*, 88(4): 431-447 (November 1968).
16. C. G. Collins, J. Moteff, and B. A. Chandler, Evaluation of the Potential of Selected Alloys for use as a Fuel Cladding Material in an LMFBR, USAEC Report GEMP-573(Rev.), General Electric Company, Missile and Space Division, June 1969.
17. I. Machlin, R. T. Begley, and E. D. Weisert (Eds.), *Refractory Metal Alloys. Metallurgy and Technology*, Proceedings of a Symposium held in Washington, D. C., April 25–26, 1968, a Publication of the Metallurgical Society of AIME, Plenum Press, New York, 1968.
    a. E. E. Hoffman and R. W. Harrison, Compatibility of Refractory Metals with Liquid Metals, pp. 251-287.
    b. J. W. Semmel, Jr., Refractory Metals in Space Electric Power Conversion Systems, pp. 289-324.
18. E. E. Hoffman and J. Holowach, Potassium Corrosion Test Loop Development, Topical Report No. 7, Cb–1Zr Rankine System Corrosion Test Loop, Report GESP-246 (R67SD3016), General Electric Company, Missile and Space Division, May 1, 1968.
19. A. Vary, C. M. Scheuermann, L. Rosenblum, and W. H. Lowdermilk, Corrosion in a Cobalt Alloy, Two-Phase Mercury Loop, Report NASA-TN-D-5326, National Aeronautics and Space Administration, Lewis Research Center, July 1969.
20. E. J. Vargo, A Method of Increasing the Corrosion Resistance of Cobalt-Based Alloys to Mercury, U. S. Patent No. 3,449,143, to AEC, June 10, 1969.
21. L. B. Engel, Jr., and R. W. Harrison, Topical Report No. 2, The Corrosion Resistance of Tantalum, T-111, and Cb–1Zr to Mercury at 1200°F, Report GESP-199, General Electric Company, Missile and Space Division, Apr. 17, 1969.
22. Ya. K. Bebkovich, V. F. Shatinskii, and M. I. Chaevskii, Strength and Ductility of Welded Joints Working in Contact with Liquid Lithium (in Russian), *Fiz.-Khim. Mekh. Mater. (Soviet Materials Science)*, 4(1): 3-12 (January–February 1968).
23. L. W. Roberts, Jr., and G. S. Root, Refractory Alloy Development for the Advanced Space Power Reactor Program, USAEC Report UCRL-50603, University of California Lawrence Radiation Laboratory, Mar.,17, 1969.
24. J. R. Weeks and A. J. Romano, Liquidus Curves and Corrosion of Fe, Ti, Zr, and Cu in Liquid Bi–Pb Alloys, *Corrosion*, 25(3): 131-136 (March 1969).
25. A. L. Bichuya, M. F. Zamora, V. F. Pikhel'son, and M. I. Chaevskii, Effect of Molten Pb–Bi Eutectic on the Fatigue Strength of Steel (in Russian), *Fiz.-Khim. Mekh. Mater. (Soviet Materials Science)*, 4(1): 19-22 (January–February 1968).
26. R. J. Cash, Liquid Metal Corrosion Effects of Iron Additions on Uranium–Chromium Eutectic in Yttrium, USAEC Report IS-T-299, Ph.D. Thesis, Ames Laboratory, Iowa State University, February 1969.
27. V. I. Nikitin, Temperature Dependence of the Effect of Liquid Metals on the Long-Time Strength of Solid Metals, *Fiz.-Khim. Mekh. Mater. (Soviet Materials Science)*, 4(1): 13-18 (January–February 1968).
28. Oak Ridge National Laboratory, Molten Salt Reactor Program Semiannual Progress Report for Period Ending Feb. 28, 1969, USAEC Report ORNL-4396, August 1969.
29. J. W. Koger and A. P. Litman, Compatibility of Hastelloy N and Croloy 9M with $NaBF_4$–NaF–KFB_4 (90–4–6 mole %) Fluoroborate Salt, USAEC Report ORNL-TM-2490, Oak Ridge National Laboratory, April 1969.

Section

X

Reactor Materials

Cladding Behavior in Loss-of-Coolant Accidents

By H. S. Rosenberg

H. A. McLain[1] has written an extensive review article on metal–water reactions in light-water-cooled power reactors, summarizing much of the previous work in the field.

Argonne[2] is doing small-scale experiments on steam explosions by injecting water into molten materials. Violent explosions were observed with AgCl at 600°C and with NaCl at 900 and 1000°C. A mild explosion was observed with yellow brass (63 Cu–37 Zn) at 1100°C. Experiments with molten aluminum at 800 and 1000°C and with silver at 1100 and 1200°C did not produce explosions.

Workers at General Electric[3] have studied the effect of steam oxidation on the mode of failure of internally pressurized Zircaloy-4 tubes under dynamic heating conditions. Zircaloy tubes that had a 5.1-cm length, a 0.076-cm wall thickness, and internal helium pressures of 70 to 150 psig were heated in steam at rates of 0.1 to 300°C/sec. They found that at internal pressures of 70 psig tubes will burst in steam at all heating rates. At pressures above about 115 psig, the tubes will expand 34% when heating rates exceed a few tenths of a degree per second. The tube failure temperature increases with increasing heating rates, and this fact indicates that steam oxidation generally increases the useful temperature range and leads to brittle tube failure.

References

1. H. A. McLain, Potential Metal-Water Reactions in Light-Water-Cooled Power Reactors, *Nucl. Safety*, **10**(5): 392-404 (September–October 1969).
2. Argonne National Laboratory, Reactor Development Program Progress Report, April–May 1969, USAEC Report ANL-7577, July 7, 1969.
3. J. F. White, AEC Fuels and Materials Development Program, Progress Report No. 76, USAEC Report GEMP-1008, General Electric Company, Missile and Space Division, Sept. 30, 1968.

LEGAL NOTICE

This journal was prepared under the sponsorship of the U. S. Atomic Energy Commission. Neither the United States, nor the Commission, nor any person acting on behalf of the Commission:

A. Makes any warranty or representation, expressed or implied, with respect to the accuracy, completeness, or usefulness of the information contained in this journal, or that the use of any information, apparatus, method, or process disclosed in this journal may not infringe privately owned rights; or

B. Assumes any liabilities with respect to the use of, or for damages resulting from the use of any information, apparatus, method, or process disclosed in this journal.

As used in the above, "person acting on behalf of the Commission" includes any employee or contractor of the Commission, or employee of such contractor, to the extent that such employee or contractor of the Commission, or employee of such contractor prepares, disseminates, or provides access to, any information pursuant to his employment or contract with the Commission, or his employment with such contractor.

Recent USAEC publication of special interest

UNIVERSITIES, NATIONAL LABORATORIES, AND MAN'S ENVIRONMENT

Argonne Universities Association Conference
July 27–29, 1969, Chicago, Illinois

The growing nationwide concern about environmental pollution prompted Argonne Universities Association, a group of 30 universities which is responsible for determining the policies of Argonne National Laboratory, to sponsor this conference. Some 300 participants from universities, government, and industry met to consider environmental problems and their solution under the conference's two subtitles: Is Man on His Way to Extinction—Is It a Natural Process and Organizing to Understand and Shape Man's Environmental Interactions.

In announcing the conference, Dr. Philip N. Powers of Purdue University, President of Argonne Universities Association, said: "There is an urgent need for all 'knowledge' institutions to seek the solution of environmental problems.... It is important that universities and national laboratories refashion themselves to attack these problems. We hope to learn how this can be done by exchanging ideas and by learning from the experiences of experts in academic planning and pollution control."

The major topic of discussion at the meeting was the desirability and feasibility of establishing a socio-technological research organization, utilizing the physical and intellectual resources of the universities and of Argonne National Laboratory, to study large-scale environmental problems.

The Atomic Energy Commission, keenly aware of the difficult decisions involved in exploiting technology to better human life while at the same time protecting the natural environment, published these proceedings as a manifestation of its concern that the public be well informed and decide wisely. (167 pages, 23 figures)

PRINCIPAL SPEAKERS

RENE DUBOS, Department of Environmental Biomedicine, Rockefeller University, and Pulitzer Prize winning author

ELVIS J. STAHR, President, National Audubon Society

MELVIN PRICE, Representative from Illinois; Chairman, Subcommittee on Research, Development, and Radiation, Joint Committee on Atomic Energy

JOHN L. BUCKLEY, Office of Science and Technology, Executive Office of the President

JAMES T. RAMEY, Commissioner, U. S. Atomic Energy Commission

LAURA FERMI, Author and cofounder of one of the first citizens' committees to fight air pollution

CHET HOLIFIELD, Representative from California; Chairman, Joint Committee on Atomic Energy

HENRY S. ROWEN, President, The Rand Corporation

FRED H. HARRINGTON, President, University of Wisconsin

LAWRENCE R. HAFSTAD, Member of the National Academy of Engineering

Available as CONF-690705 for $3.00 from

Clearinghouse for Federal Scientific and Technical Information
National Bureau of Standards, U. S. Department of Commerce
Springfield, Virginia 22151

AEC SYMPOSIUM SERIES

Available for $3.00 each from the Clearinghouse for Federal Scientific and Technical Information, National Bureau of Standards, U. S. Department of Commerce, Springfield, Virginia 22151

1 **Progress in Medical Radioisotope Scanning (TID-7673),**
Oak Ridge Institute of Nuclear Studies, 1963

2 **Reactor Kinetics and Control (TID-7662),**
The University of Arizona, 1964

3 **Dynamic Clinical Studies with Radioisotopes (TID-7678),**
Oak Ridge Institute of Nuclear Studies, 1964

4 **Noise Analysis in Nuclear Systems (TID-7679),**
University of Florida, 1964

5 **Radioactive Fallout from Nuclear Weapons Tests (CONF-765),**
U. S. Atomic Energy Commission, 1965

6 **Radioactive Pharmaceuticals (CONF-651111),**
Oak Ridge Institute of Nuclear Studies, 1966

7 **Neutron Dynamics and Control (CONF-650413),**
The University of Arizona, 1966

8 **Luminescence Dosimetry (CONF-650637),**
Stanford University, 1967

9 **Neutron Noise, Waves, and Pulse Propagation (CONF-660206),**
University of Florida, 1967

10 **Use of Computers in Analysis of Experimental Data and the Control of Nuclear Facilities (CONF-660527),**
Argonne National Laboratory, 1967

11 **Compartments, Pools, and Spaces in Medical Physiology (CONF-661010),**
Oak Ridge Associated Universities, 1967

12 **Thorium Fuel Cycle (CONF-660524),**
Oak Ridge National Laboratory, 1968

13 **Radioisotopes in Medicine: In Vitro Studies (CONF-671111),**
Oak Ridge Associated Universities, 1968

14 **Abundant Nuclear Energy (CONF-680810),**
Oak Ridge Associated Universities, 1969

15 **Fast Burst Reactors (CONF-690102),**
The University of New Mexico and American Nuclear Society, 1969

16 **Biological Implications of the Nuclear Age (CONF-690303),**
Lawrence Radiation Laboratory, 1969

17 **Radiation Biology of the Fetal and Juvenile Mammal (CONF-690501),**
Battelle Memorial Institute, 1969

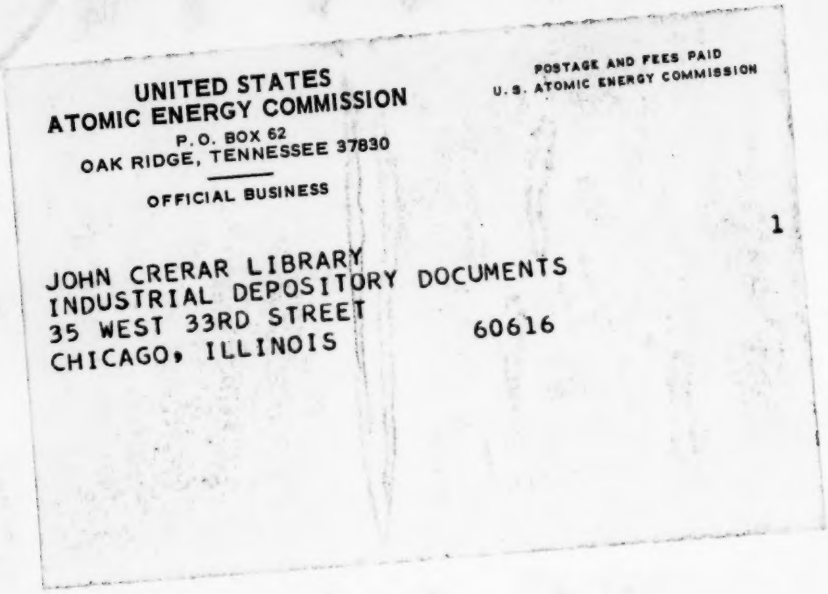

TECHNICAL PROGRESS REVIEWS may be purchased from Superintendent of Documents, U. S. Government Printing Office, Washington, D. C. 20402. *Nuclear Safety* at $3.50 per year (six issues) for each subscription or $0.60 per issue; *Reactor Technology* at $3.00 per year (four issues) for each subscription or $0.75 per issue; *Isotopes and Radiation Technology* at $2.50 per year (four issues) or $0.70 per issue. The use of the order form below will facilitate the handling of your order.

POSTAGE AND REMITTANCE: Postpaid within the United States, Canada, Mexico, and all Central and South American countries except Argentina, Brazil, Guyana, French Guiana, Surinam, and British Honduras. For these Central and South American countries and all other countries: add, for each annual subscription, $1.00 for *Nuclear Safety* and $0.75 for each of the other journals; for single issues, add one-fourth of the single-issue price. Payment should be by check, money order, or document coupons, and MUST accompany order. Remittances from foreign countries should be made by international money order or draft on an American bank payable to the Superintendent of Documents or by UNESCO book coupons.

order form

SUPERINTENDENT OF DOCUMENTS
U. S. GOVERNMENT PRINTING OFFICE
WASHINGTON, D. C. 20402

Please send — 1, 2, or 3 years

- ☐ Isotopes and Radiation Technology ____
- ☐ Nuclear Safety ____
- ☐ Reactor Technology ____

Enclosed: document coupons ☐ check ☐ money order ☐

Charge: Superintendent of Documents No. _____

SUPERINTENDENT OF DOCUMENTS
U. S. GOVERNMENT PRINTING OFFICE
WASHINGTON, D. C. 20402

(Print clearly)

_____
Name

_____
Street

_____
City, State, ZIP Code